Peninsula Technikon

Faculty of Engineering

Center for Research in Applied Technology

Simulation of Plasma Arc Cutting

Brian Reginald Hendricks

B.Tech. (Mech. Eng.)

Submitted towards the degree of
Master of Technology in Mechanical Engineering

Under Supervision of

Dr. G. Oliver (Internal)
Dr. J. Ronda (External)

CAPE TOWN, 1999

Acknowledgements

I would like to express my first words of gratitude to my advisor Dr. J. Ronda. Without his guidance and support this dissertation would never have materialized. Apart from support on technical issues he has provided an environment conducive to development of research in the area of virtual modelling in welding and cutting at the Peninsula Technikon.

I wish to thank Dr. G. Oliver, my internal supervisor, for his support and guidance.

Thank you to Dr. N. Mahomed for providing a dynamic learning environment. The international program that he had managed afforded me the opportunity to gain life long experiences.

I would like to express my thanks to my fellow colleagues: D. Huang, X. Li, A. Mennad, O. Philander, M. Riddels, M. Ludick, P. Simelane, M. Kekana and Dr. W. Cheng for all their support and hours of fun.

Thank you to W. Mead for his support during the write-up of the thesis.

Thank you to B. Gonzalves and E. Moosa for administrative support.

I wish to acknowledge the financial support provided by the NRF and Peninsula Technikon.

I would like to give a special acknowledgement to Ms. M. Ford for her support during the last three years of my studies.

A special thanks to my family for their never ending support and love. I hope that the result is worthy of their kindness.

Abstract

The simulation of Plasma Arc Cutting is presented in this study. The plasma arc cutting process employs a plasma torch with a very narrow bore to produce a transferred arc to the workpiece. A technique for modelling plasma arc cutting has been developed by applying the thermo-metallurgical model to the process and integrating a model of material removal to this model. The model is solved using the finite element method using the FE package SYSWORLD, more specifically SYSWELD. The objective is to determine the minimum energy required to cut a plate of some thickness using this virtual model. The characteristics of the cut need to exhibit the characteristics of a "high quality cut". The model presented can predict the kerf size given certain process variable settings. The numerical results obtained are assessed by conducting experiments.

By maintaining minimum energy input cost savings can be made through energy savings, limiting additional finishing processes and reducing expense of shortening the electrode and nozzle lifetimes. The modelling of the PAC process using virtual design techniques provides a cost-effective solution to the manufacturing industries with respect to process specification development. This plays an important role in South Africa's transition into a competitive global market. It is envisaged that the model will provide an alternative more efficient, non-destructive means of determining the optimum process variable settings for the plasma arc cutting process.

Table of Contents

Chapter 1

Introduction

1.1 Introduction

In this chapter, we review the different thermal cutting processes and highlight the significance of plasma arc cutting. The main content of this document focuses on the simulation of plasma arc cutting thus the advantages of the use of this cutting process compared to the other processes with regard to operational costs, cut quality and operational demands is discussed. No work has been done in the area of the virtual try-out space process design of the plasma arc cutting process. The most significant aspect of this project is the development of the heat source model and the kerf (removed material) model for this cutting process. The concept has been evolved from the latest development of virtual try-out space modelling of welding. The main source of research and development work, piloted by Ronda *et al.* [30] has been the foundation of this work.

The modelling of the PAC process using virtual design techniques provides a cost-effective solution to the manufacturing industries with respect to process specification development. This plays an important role in South Africa's transition into a competitive global market.

The main objective is to model the plasma arc cutting process taking into account the industrial demand on the economical performance. The added value of this project to industry lies in the evaluation of the extent of the latest relative technological development with respect to the physical process and to establish a model that provides a solution to a local industrial problem given the time limitations.

The focus is to establish the required parameter settings that govern the economics of the plasma arc cutting process to justify the capital expenditure to implement. Two criteria have been established. The minimum energy density required to cut a plate of a given thickness and the requirements to provide maximum production capacity for the process. This has been further extended to include the requirement to adhere to "good quality cut" classification ie. a narrow heat affected zone, parallel sides, small kerf width and no dross. To ensure adherence to this requirement, theory that has been qualitatively proven (referred to elsewhere) has been taken into account.

An automated procedure has been developed during this study to increase the computational efficiency with regard to the simulations. This was particularly helpful in the determination of the applicable arc shape variables as discussed in Chapter 5.1 as well as the execution of the variable sensitivity analysis.

Thermal cutting processes consist of oxygen, arc and other cutting processes. Some of these processes, such as oxygen arc, lance carbon arc, shielded arc, gas metal arc and

gas tungsten arc are only used in special applications since these processes are either difficult to regulate or are not capable of concentrating sufficient energy to make accurate, quality cuts. The most important cutting techniques are oxyfuel (OFC), plasma arc (PAC) and laser beam (LBC). Primarily the former two aforementioned have been classified as such due to the fact that they provide a solution in the form of low cost precision cuts of high quality in a variety of metals. LBC provides a solution to more specialised requirements such as the automotive industry but presents a higher operational cost.

1.2 Review of cutting processes

1.2.1 Oxygen Gas Cutting

Oxyfuel Gas Cutting (OFC) [1] is a process whereby metal is removed or severed by the chemical reaction of oxygen with the metal at elevated temperatures. The metal is heated to it's ignition temperature by a fuel-oxygen mixture, at this point a high velocity stream of oxygen is introduced to produce a chemical reaction and to blow the molten reaction products through the thickness. The OFC process employs a torch with a nozzle. These are designed to provide a small diameter high velocity stream of oxygen to oxidize and remove metal from a narrow section and produce a ring of flame to ignite the metal to it's ignition temperature. The torch is moved to act at a speed that will maintain a cutting action. The jet and the flame are symmetrical thus cutting in more than one place can be achieved. The cut quality depends on the torch tip, size, type, distance from the plate, the oxygen and pre-heat gas rates, and the cutting speeds. All of these are related to the material type and thickness.

There are advantages and disadvantages associated with this process:

Some of the advantages are as follows:

- Section shapes and thickness that are difficult to produce by mechanical means can be produced economically by OFC.
- Large plates can be cut in place by moving the OFC torch instead of the plate.
- Cutting direction can be changed rapidly.
- OFC is an economical method of plate edge preparation for bevel and groove weld joint design.

Several important disadvantages are as follows:

- The process is limited commercially to cutting steels and cast iron, though other easily oxidized metal can be cut.
- Process modifications are needed to cut high alloy steals and cast irons.
- Preheating and post heating may be required by hardened steel to control metallurgical and mechanical properties adjacent to edges.

1.2.2 Laser Beam Cutting

The source of heat for laser beam cutting (LBC) [1] is a concentrated coherent light beam that impinges on the work piece. The mechanism in laser cutting is the thermal

heating and consequently a combination of melting and vaporising of material from the kerf. The power input for this technique needs to exceed the thermal losses. In the LBC process both the highest quality and highest cutting rates are obtained when temperature gradients in the cut kerf are very large. It is thus necessary for the intensity of the energy in the front of the cut kerf to be maximized. The intensity of the energy absorbed is dependent on the laser output power, beam diameter and the fraction of incident light that is absorbed in the cut.

High Power lasers exhibit unique advantages for cutting applications:

- The ability to cut any metal and many non- metals regardless of hardness.
- Narrower kerf and heat affected zone than those produced by other thermal cutting processes.
- High cutting speeds.
- Ready adaptability to computer controlled contour cutting.

These advantages are a result of the high power densities that can be obtained and the ease at which the beam can be transmitted through the atmosphere. Typically a power density can be obtained which is sufficient to vaporize all materials.

One of the principle current disadvantages of LBC is the high capital cost of laser beam equipment. Also cutting speeds decrease as the metal thickness increase. These two factors limit the cost effectiveness of LBC to metals of approximately 13mm in thickness and less.

1.2.3 Plasma Arc Cutting

Plasma arc cutting (PAC) [1] is accomplished with an extremely hot, high velocity plasma gas jet formed by an arc and inert gas flowing from a small diameter orifice. The constricted arc is used to melt a localized area of a workpiece and the jet of hot plasma gas forces the molten metal through the kerf and out the back side. Plasma arc operates at temperatures ranging from $10\,000\,^{\circ}C$ to $14\,000\,^{\circ}C$ [1].

An arc plasma is a gas which has been heated by an arc to a partially ionized condition thus enabling it to conduct an electric current. The term plasma arc is associated with torch design which clearly distinguishes plasma arc torches from other thermal cutting torches. Specifically for a given current and gas flow rate the arc voltage is higher in the constricted arc torch. The arc is constricted by passing it through an orifice downstream of the electrode. As plasma gas passes through the arc, it is heated to a high temperature rapidly, expands and is accelerated as it passes through the constricting orifice towards the workpiece. Different gases are used in PAC these include nitrogen, argon, air, oxygen and mixtures of nitrogen / hydrogen and argon/ hydrogen [4].

Carbon steel is one of the most common materials to be cut with a manual plasma system, the process offers considerable advantages over other cutting methods for this material. For example, often there is a need for cutting unique or low production shapes, doing prototype work, or modifying a part in the field or in the shop. The following outlines several methods whereby such tasks can be accomplished and the drawbacks to each method:

- Shears leave a smooth edge and are quick, but can only cut straight edges.
- Nibblers are relatively inexpensive and can cut shapes and contours. However, they are comparatively slow, particularly on thicker materials, and can cause distortion on metals. They also generally leave a poor edge.
- Oxyfuel cutting is very difficult on gauge thickness materials, and is limited mainly to carbon steel.

In comparison, an appropriately sized manual plasma cutting unit offers the versatility to handle most of the same cutting chores and circumvents most of the drawbacks. The PAC unit can cut contours and straight lines. Most PAC units offer the ability to follow a template or a straight edge so cutting does not have to be done completely freehand. PAC operates at much higher energy levels thus resulting in high cutting speeds. Instantaneous start-up without any preheating is possible. The HAZ (heat affected zone) is relatively narrow and induces only insignificant distortion. There are no demands on the conditions of the plate surface before cutting proceeds. Air is generally used as a plasma to cut carbon steel, aluminium and stainless steel. In the case of aluminium and stainless steel, some oxidation of the edge occurs, aluminium will have a rough appearance and stainless steel will be somewhat discoloured. If this appearance is objectionable, a PAC system that uses an inert gas should be considered.

Some of the new, smaller portable PAC systems work well off the auxiliary output of an engine driven welding machine, making them convenient for field work. Formally, this type of cutting was almost exclusively the domain of oxyfuel cutting but with the increased use of materials such as aluminium, stainless steel and lighter gauge sheet metal the use of a PAC system is the logical solution.

The important dates in the development of plasma arc cutting technology has been listed below and a more detailed description is given in Chapter 2

- 1950 - TIG welding (Tungsten Inert Gas)
- 1957 - Conventional plasma arc cutting, using "dry" arc constriction techniques.
- 1962 - Dual flow plasma arc, incorporating a secondary gas shield around the nozzle.
- 1963 - Air plasma cutting.
  1965 - Water shield plasma cutting, substituting water as the shield gas.
- 1968 - Water injection plasma cutting, using water to increase arc constriction.
- 1972 - Water Muffler and Water Table, reducing noise, smoke and fumes during plasma Cutting.
- 1977 - Underwater cutting, further decreasing noise and pollution.
- 1980 - Low amp air plasma cutting, introducing plasma arc cutting to a new market.
- 1983 - Oxygen plasma cutting, increasing cut speed and quality on carbon steel.
- 1985 - Oxygen injected plasma cutting, using nitrogen as the plasma gas and injecting oxygen downstream in the nozzle.
- 1989 - Deep-water plasma cutting, allowing cuts in 1015 meters of water.
- 1990 - High density plasma cutting, rivaling laser cutting for cut quality and speed.

From this review, it is clear that the plasma process has made astonishing progress in the last thirty-five years, particularly in the last five years. Today, three pronounced trends can be detected:

- The market for light hand-cutting units with current levels below 200 amps will continue to expand. This expanding market will attract more competitors which will produce improved products and broaden the market for low-amp air plasma.
- The market for cutting machines and robots will continue to seek high quality, close tolerance cutting from plasma cutting systems. Attractively priced oxygen plasma and simpler and lighter low-amp units will compete favorably with laser-cutting equipment. Research and development on consumable parts and cutting torches will continue, constantly extending the life of consumables and improving cut quality.
- As plasma cutting approaches it's mature stage, the industry is challenged to provide more accurate torches and consumable parts and power sources of advanced technology. In general, it is expected that the plasma cutting market will continue along a high growth trend for the forseeable future.

1.3 Statement of the Problem

The modern approach to the modeling of cutting leads to the phenomenological description of a Thermo-Metallurgical process and finite element solution of this problem. The objective of this project is to develop a model and simulate a thermal cutting process specifically the plasma arc technique.

The formulation of the thermo problem appropriate for this simulation entails:

- The design of a model of the heat source representing the flux of the arc of the PAC process into the work piece.
- The implementation of the thermal model using SYSTUS/SYSWELD.
- The verification of the thermal model using the available data.
- Extension of the thermal model to include metallurgical phase changes to determine the width and depth of the kerf (material removed).
- Process variable sensitivity analysis.

1.4 Previous Related Studies

Plasma arc cutting, similar to welding, is a complex thermal-metallurgical-mechanical problem and involves four disciplines: thermodynamics, material science, continuum mechanics and production engineering.

Rosenthal [35] using Fourier's analysis first studied the phenomenon of heat transfer in welded structures as a steady state heat transfer process. The modelling of welding was further refined by works done by Hibbit and Marcal [12], Friedmann [7], Ueda and Yamakawa [38] and Masubuchi [18].

Since the 1980's investigators have succeeded in coupling the thermal and metallurgical phenomena occurring during welding. The evolution of thermal and metallurgical material characteristics due to welding can be applied to the cutting process.

Ronda, Oliver and Meinart 1993 [34] presented a simulation of welding with phase transformations. Oliver 1994 [23] presented the modeling of welding with various thermo-visco-plastic constitutive models for steel. The mathematical model presented in Chapter 3 is based on work done by Ronda and Oliver [23] and [29]. The material model is based on work by Bergheau and Leblond [3], [14], [15], [16], and [17].

Ramakrishnan and Rogozinski [28] have investigated the properties of plasmas generated for the air plasma cutting process. An approximate two zone arc model has been developed to estimate arc radius, voltage and pressure of the arc at the nozzle exit as a function of the current.

Nemchinski [20] investigated the dross formation (the resolidified metal that adheres to the bottom edge of the plasma cut) and heat transfer during plasma arc cutting. It was found that plasma arc cutting can be characterized in terms of two distinct speeds. At cutting speeds above some maximum the plasma jet does not cut through the metal plate and at speeds below some minimum, the molten metal from the kerf sticks to the bottom of the plate. Models by which to calculate these maximum and minimum velocities have been determined. It was also suggested that the speed separating dross producing and dross-free models of cutting correspond to a specific Weber number. The Weber number describes the comparative role of the surface tension and the opposing impulse of the molten metal emerging from the cut.

Nemchinski, 1996 [20] in which the main focus being aerodynamic drag and surface tensions are highlighted, has discussed liquid moving during plasma arc cutting.

1.5 Content of the Dissertation

In this dissertation a model for the plasma arc cutting process is presented. The objective is to determine the minimum energy required to cut a plate of some thickness. The quality of the cut is taken into consideration by determining the range of velocities, used in the sensitivity analysis, using models based on experimentally verified data.

In Chapter 2, a detailed discussion of the technological development of the plasma arc cutting process is presented. The fundamental process variables can be highlighted from this information and has been for the purpose of this study. The extent of the scope of the modelling of plasma arc cutting can be determined.

In Chapter 3, the formulation of the mathematical model is presented. Fundamentally the coupled thermo-mechano-metallurgical model as proposed by Ronda and Oliver [32] has been used and narrowed to a thermo-metallurgical framework for the modelling of plasma arc cutting. Phase transformations and stress distributions after the cutting have not been taken into account in this project since the objective is to determine the minimum energy required to cut a plate. This would result in the narrowest HAZ. Consequently, if necessary, the least amount of machining would be required to remove the HAZ.

In Chapter 4, the characteristics of a "high quality" cut are discussed and the factors affecting the quality are highlighted. A model is presented based on qualitative work done by Nemchinski [20]. The model describing the lower and upper cutting speed limits for dross free cuts have been incorporated into the simulations to ensure that the dross free criteria is satisfied.

In Chapter 5, the boundary conditions and the benchmark problem is presented. All the assumptions are discussed. An overview of the finite element package SYSTUS/SYSWELD is given. Flow charts representing the simulation procedures are included to enhance understanding of a new method controlling the automated creation of input files, execution of run command and management of output which previously required intensive operator attention. This script has been developed by the author and another member of the welding group and is a very powerful tool that can be used to optimize the simulation process.

The numerical results are presented in Chapter 6. The outputs from the simulations is shown in Appendix A. The results have been extracted from the simulation output and presented in graphical form in this chapter.

In Chapter 7, the experimental setup and results are presented. The same input parameters have been used and the kerf widths obtained have been compared with the simulated process. The quality of the cut (dross formation) have also been assessed and discussed

The flow chart Fig 1.1 gives a representation of the development of the plasma arc cutting model.

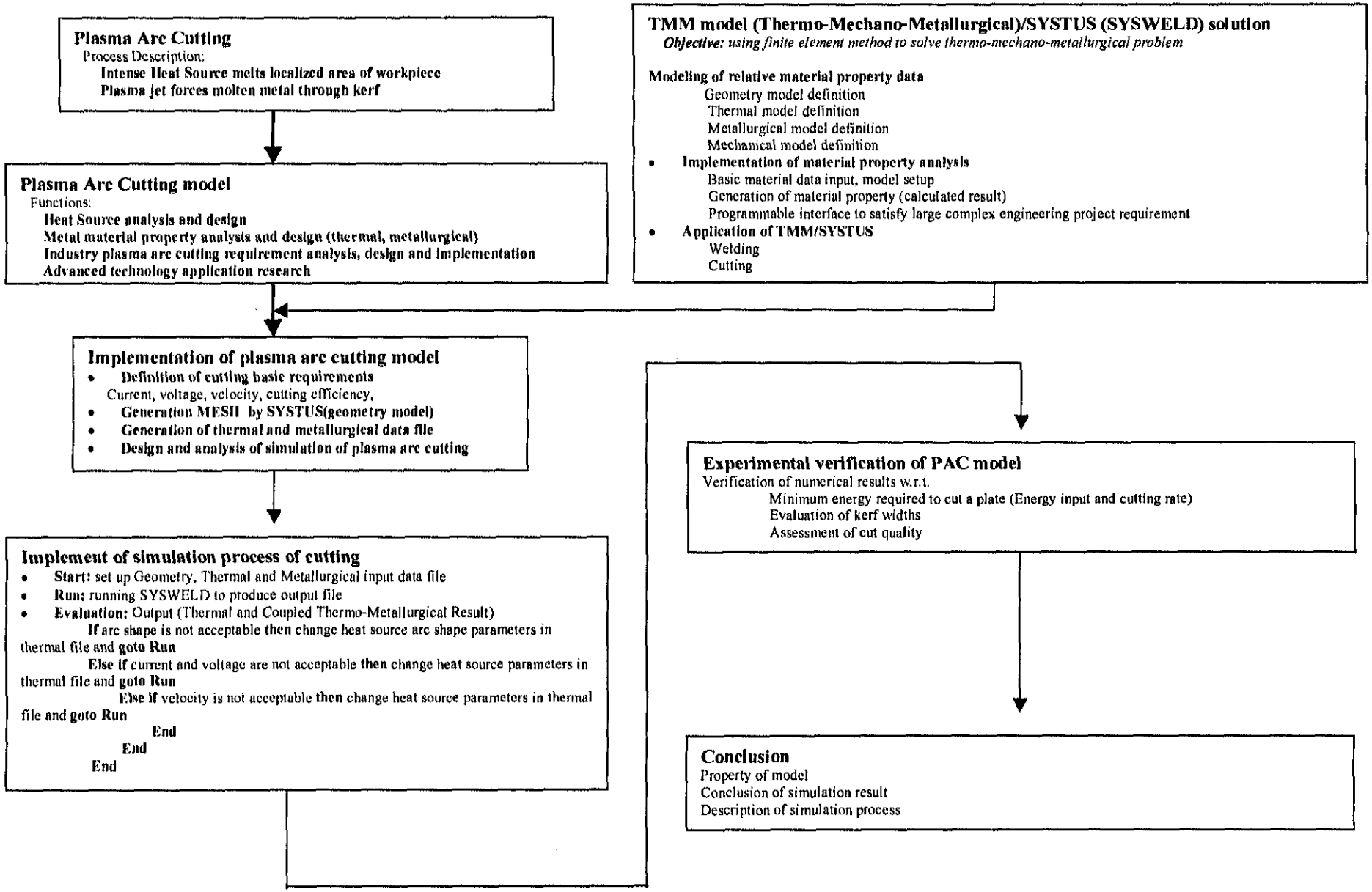

Figure 1.1 Flow Chart of Development of Plasma Arc Cutting Model

Chapter 2

Development of The Plasma Arc Cutting Process

By adding even more energy to a gas, we find that its characteristics are modified substantially in terms of temperature and electrical characteristics. This process is called ionization, the creation of free electrons and ions among the gas atoms. When this happens, the gas, which has now become a plasma, is electrically conductive because free electrons are available to carry current. Many principles that apply to current conduction through metals also apply to plasmas. For example, if the current-carrying cross-section of a metal is reduced, the resistance increases. A higher voltage is needed to force the same amount of electrons through this cross-section and the metal heats up. The same is true for a plasma gas; the more we reduce the cross-section, the hotter it gets. In this historic review of the plasma arc process, we will follow the development of a plasma arc with high speed gas flow which is, essentially, the "plasma cutting process.".

2.1 Development of the Plasma Arc Process

During 1941 the U.S. defense industry was looking for better ways of joining light metal together for the war effort and, more specifically, for the production of airplanes. Out of this effort, a new welding process was born. An electric arc was used to melt the metal, and an inert gas shield around the arc and the pool of molten metal was used to displace the air, preventing the molten metal from picking up oxygen from the air. This new process "TIG" (Tungsten Inert Gas), seemed to be a perfect solution for the very specific requirement of high-quality welding. Since this welding process became a substantial user of such gases as argon and helium, the industry that had the most interest in this new application turned out to be the industrial gas manufacturers. These industrial gas companies became active and successful with the TIG process, also known as "Argonarc" or "Heliarc." Today, this process is referred to as "GTAW" (Gas Tungsten Arc Welding).

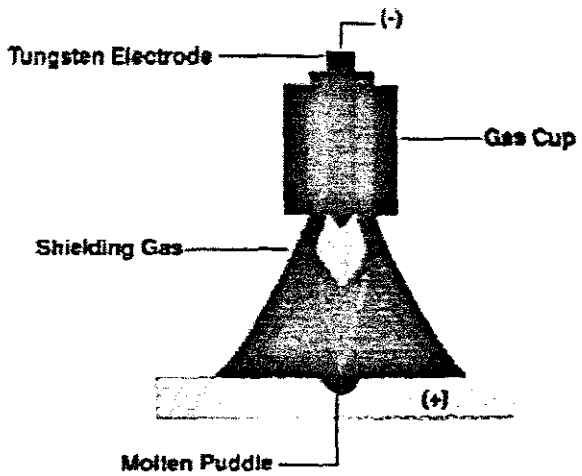

Figure 2.1 TIG Welding Arc

By 1950, TIG had firmly established itself as a new welding method for high-quality welds on exotic materials. While doing further development work on the TIG process, scientists at Union Carbide's welding laboratory discovered that when they reduced the gas nozzle opening that directed the inert gas from the TIG torch electrode (cathode) to the workpiece (anode), the properties of the open TIG arc could be greatly altered. The reduced nozzle opening constricted the electric arc and gas and increased its speed and its resistive heat. The arc temperature and voltage rose dramatically, and the momentum of the ionized and non-ionized gas removed the molten puddle due to the higher velocity. Instead of welding, the metal was cut by the plasma jet

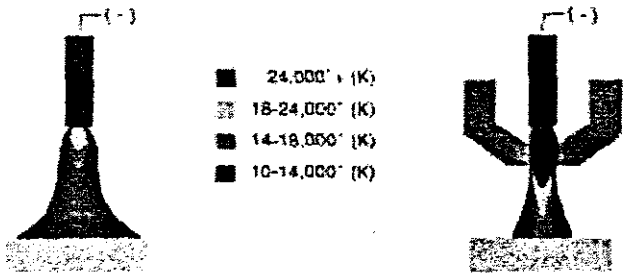

Figure 2.2 Temperature – TIG Arc and Plasma Jet

In Figure 2.2, both arcs are operating in argon at 200 amps. The plasma jet is only moderately constricted by the 3/16 inch (4.8 mm) diameter of the nozzle orifice, but it operates at twice the voltage and produces a much hotter plasma arc than the corresponding TIG arc. If the same current is forced through a nozzle with an even smaller opening, the temperature and voltage rise. At the same time, the higher kinetic energy of the gas leaving the nozzle ejects the molten metal, creating a cut.

The plasma cutting arc was considerably hotter than the TIG arc shown in Figure 2.1. These greater temperatures were possible because the high gas flow in the plasma torch nozzle formed a relatively cool boundary layer of un-ionized gas along the nozzle wall, allowing a higher degree of arc constriction. Swirling the cutting gas could farther increase the thickness of this boundary layer. The swirling action forced the heavier, cooler, un-ionized gas to move radially outward and form a thicker boundary layer. Most plasma cutting torches swirled the cutting gas to attain maximum arc constriction.

2.2 Transferred and Non-Transferred Modes

A plasma jet can be operated in the transferred mode, where the electric current flows between the plasma torch electrode (cathode) and the workpiece (anode). It can also be operated in the non-transferred mode where the electric current flows between the electrode and the torch nozzle. Both modes of operation are illustrated in Figure 2.3.

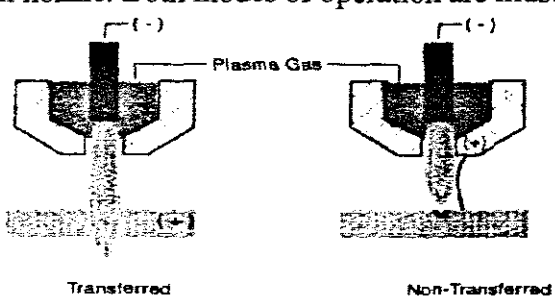

Figure 2.3 Transfered vs Non-transfered Arc

Although a stream of hot plasma emerges from the nozzle in both modes of operation, the transferred mode is invariably used in plasma cutting because the usable heat input to the workpiece is more efficiently applied when the arc is in electrical contact with the workpiece.

The characteristics of the plasma jet can be altered greatly by changing the gas type, gas flow rate, arc current, arc voltage and nozzle size. For example, if low gas flow rates are used, the plasma jet becomes a highly concentrated heat source ideal for welding. Conversely, if the gas flow rate is increased sufficiently, the velocity of the plasma jet is so great that it ejects molten metal created by the hot plasma arc and cuts through the back of the workpiece.

2.3 Plasma Cutting Technological Advancements

2.3.1 Conventional Plasma Arc Cutting (1957)

Union Carbide's Linde Division introduced the plasma jet generated by conventional "dry" arc constriction techniques in 1957. In the same year. Dr. Robert Gage obtained a patent, which for 17 years gave Union Carbide a virtual monopoly. This technique could be used to sever any metal at relatively high cutting speeds. The thickness of a plate could range from thin sheet metal to plates as thick as 250 mm. The cut thickness was ultimately dependent on the current-carrying capacity of the torch and the physical properties of the metal A heavy duty mechanized torch with a current capacity of 1000 amps could cut through 250 mm thick stainless steel and aluminum. However, in most industrial applications, plate thickness seldom exceeded 50 mm. In this thickness range, conventional plasma cuts were usually beveled and had a rounded top edge. Beveled cuts were a result of an imbalance in the heat input into the cut face. A positive cut angle resulted because the heat energy at the top of the cut dissipated as the arc progressed through the cut.

This heat imbalance was reduced by placing the torch as close as possible to the workpiece and applying the arc constriction principle, as shown in Figure 2.4. Increased arc constriction caused the temperature profile of the electric arc to become extended and more uniform. Correspondingly, the cut became more square. Unfortunately, the constriction of the conventional nozzle was limited by the tendency of increased constriction to develop two arcs in series, one arc between the electrode and nozzle and a second arc between the nozzle and, workpiece.

This phenomenon was known as "double arcing" and damaged both the electrode and nozzle. Double arcing severely limited the extent to which plasma cut quality could be improved. Since the introduction of the plasma arc process in the mid-50's, considerable research has focused on increasing arc constriction without creating double arcing. Plasma arc cutting as performed then is now referred to as "conventional plasma cutting." It can be cumbersome to apply if the user is cutting a wide variety of metals and different plate thicknesses. For example, if the conventional plasma process is used to cut stainless steel, mild steel, and aluminum, it is necessary to use different gases and gas flows for optimum cut quality on all three metals.

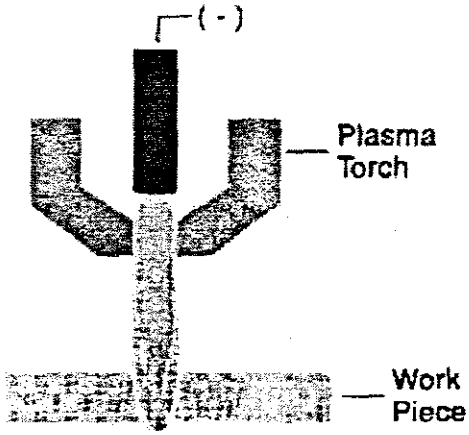

Figure 2.4 Conventional Plasma Arc Cutting

Conventional plasma cutting predominated from 1957 to 1970, and often required very expensive gas mixtures of argon and hydrogen.

2.3.2 Dual Flow Plasma Arc (1962)

The dual flow technique was developed and patented by Thermal Dynamics Corporation and James Browning, President of TDC, in 1963. It involved a slight modification of the conventional plasma cutting process. Essentially, it incorporated the same features as conventional plasma cutting, except that a secondary gas shield was added around the plasma nozzle. Usually, in dual flow operation the cutting, or plasma, gas was nitrogen and the secondary shielding gas was selected according to the metal to be cut. Secondary shield gases typically used were air or oxygen for mild steel, carbon dioxide for stainless steel, and an argon/hydrogen mixture for aluminum.

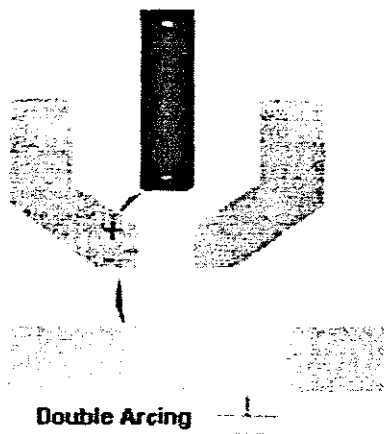

Figure 2.5 Double Arcing

Cutting speeds were still better than with conventional cutting on mild steel; however, cut quality was inadequate for many applications. Cutting speeds and quality on stainless steel and aluminum were essentially the same as with the conventional process.

The major advantage of this approach was that the nozzle could be recessed within a ceramic gas cup or shield cup as shown in Figure 2.6, preventing the nozzle from

shorting with the workpiece, and reducing the tendency for double arcing. The shield gas also covered the cutting zone, improving cut quality and speeds as well as cooling the nozzle and shield cap.

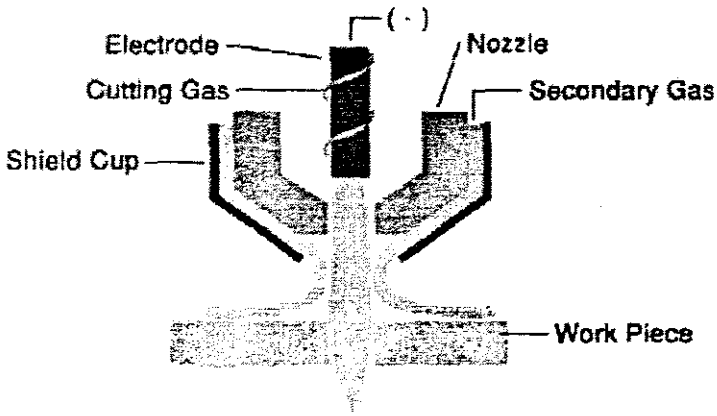

Figure 2.6 Dual Flow Plasma Cutting

2.3.3 Air Plasma Cutting (Since 1963)

Air cutting was introduced in the early 1960s for cutting mild steel. The oxygen in the air provided additional energy from the exothermic reaction with molten steel. This additional energy increased cutting speeds by about 25% over plasma cutting with nitrogen. Although the process could be used to cut stainless steel and aluminum, the cut surface on these materials was heavily oxidized and unacceptable for many applications.

The biggest problem with air cutting has always been the rapid erosion of the plasma torch electrode. Special electrodes, made of zirconium, hafaium, or hafnium alloy, were needed since tungsten eroded in seconds if the cutting gas contained oxygen. Even with these special materials, electrode life using air plasma was much less than the electrode life associated with conventional plasma.

Although air cutting was not pursued in the late 1960s in the United States and the western world, steady progress was made in eastern Europe with the introduction of the "Feinstrahl Brenner" (torch producing a restricted arc), developed by Manfred van Ardenne. This technology was adopted in Russia and eventually in Japan. The major supplier became Mansfeld of East Germany. Several shipyards in Japan were early users of air plasma cutting equipment. However, the electrode life was relatively short and studies disclosed that the cut face of the workpiece had a high percentage of nitrogen in solution which could cause porosity when subsequently welded.

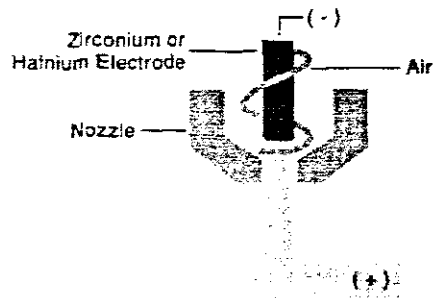

Figure 2.7 Air Plasma Cutting

2.3.4 Water Shield Plasma Cutting (1965)

Water shield plasma cutting was similar to dual flow except that water was substituted for the shield gas Cut appearance and nozzle life were improved because of the cooling effect provided by the water. Cut squareness, cutting speed and dross accumulation were not measurably improved over dual flow plasma cutting because the water did not provide additional arc constriction.

2.3.5 Water Injection Plasma Cutting (1968)

Earlier, it was stated that the key to improving cut quality was increasing arc constriction while preventing double arcing. In the water injection plasma cutting process, water was radially injected into the arc in a uniform manner as shown in Figure 2.9. The radial impingement of the water at the arc provided a higher degree of arc constriction than could be achieved by just the copper nozzle alone. Arc temperatures in this region are estimated to approach 50,000°K or roughly nine times the surface temperature of the sun and more than twice the temperature of the conventional plasma arc. The net result was improved cut squareness, increased cutting speeds and the elimination of dross when cutting mild steel. Radial water injection arc constriction was developed and patented in 1968 by Richard W. Couch Jr., President of Hypertherm, Inc.

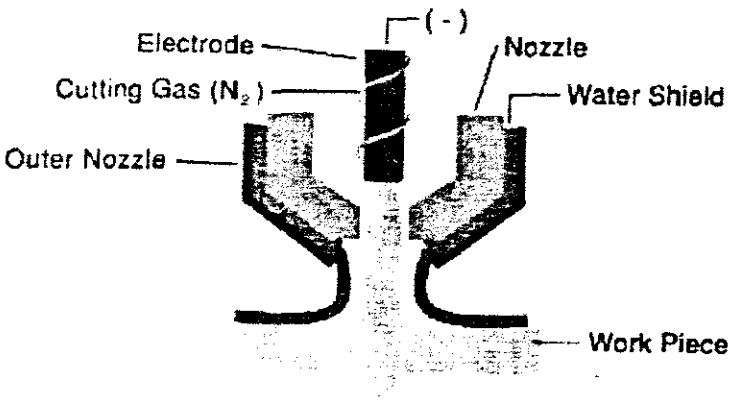

Figure 2.8 Water Shield Plasma Cutting

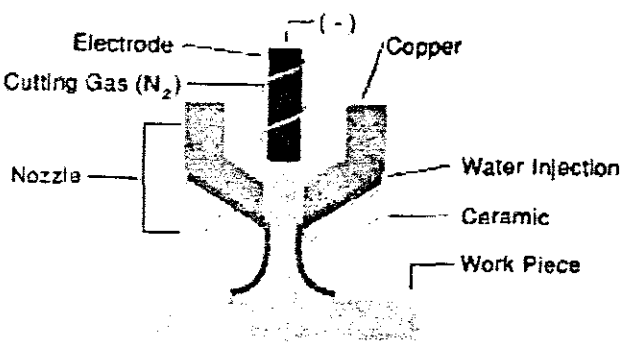

Figure 2.9 Water Injection Plasma Cutting

Another approach taken to constrict the arc with water was to develop a swirling vortex of water around the arc. With this technique, the arc constriction was dependent on the swirl velocity needed to produce a stable water vortex. The centrifugal force created by the high swirl velocity tended to flatten the annular film of water against the arc and, therefore, achieved less of a constricting effect than with radial water injection.

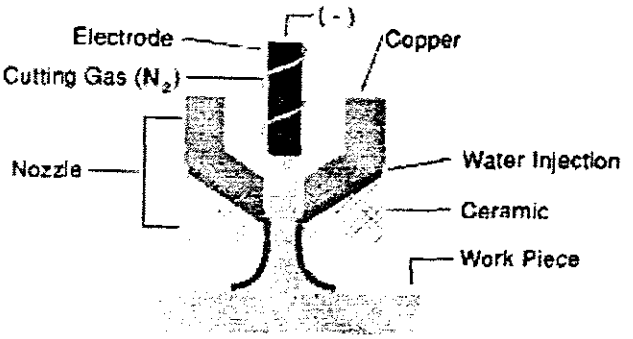

Figure 2.10 Water Injection Direction

Unlike the conventional process described earlier, optimum cut quality with water injection plasma was obtained on all metals with just one gas: nitrogen. This single gas requirement made the process more economical and easier to use. Physically, nitrogen was ideal because of its superior ability to transfer heat from the arc to the workpiece. The heat energy absorbed by nitrogen when it dissociated was relinquished when it recombined at the workpiece. Despite the extremely high temperatures at the point where the water impinged the arc, less than 10% of the water was vaporized. The remaining water exited from the nozzle in the form of a conical spray, which cooled the top surface of the workpiece. This additional cooling prevented the formation of oxides on the cut surface and efficiently cooled the nozzle at the point of maximum heat load.

The reason for arc constriction at the zone of water injection was the formation of an insulating boundary layer of steam between the plasma jet and the injected water. (This steam boundary layer, the "Linden Frost Layer," is the same principle that allows a drop of water to dance around on a hot metal plate rather than immediately vaporizing.)

Nozzle life was greatly increased with the water injection technique because the steam boundary layer insulated the nozzle from the intense heat of the arc, and the water cooled and protected the nozzle at the point of maximum arc constriction and maximum arc heat. The protection afforded by the water steam boundary layer also allowed a unique design innovation: the entire lower portion of the nozzle could be ceramic. Consequently, double arcing, a major cause of the nozzle destruction, was virtually eliminated.

An important characteristic of the cut edges was that the right side of the kerf was square and the left side of the kerf was slightly beveled. This was not caused by water injection but rather it resulted from the clockwise swirl of the plasma gas. This swirl caused more arc energy to be expended on the right side of the kerf. This same cut asymmetry existed using the conventional "dry" cutting when the cutting gas was swirled. This meant that the direction of travel needed to be properly selected to produce a square cut on the correct side of the workpiece.

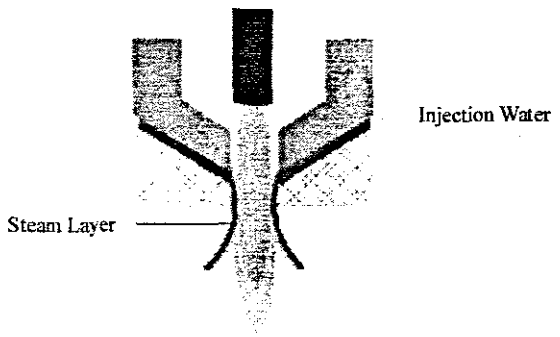

Figure 2.11 Steam Layer

2.3.6 Water Muffler and Water Table (1972)

Since the plasma arc process was a highly concentrated heat source of up to 50,000°K, there were some negative side effects with which to contend:

- At highest arc current, plasma cutting generated an intense noise level well over that normally allowed at work areas, requiring ear protection.
- Smoke and potentially toxic gas developed at the work area, requiring good ventilation. Ultraviolet radiation, which could potentially lead to skin and eye burns, required protective clothing and dark glasses.

These side effects opened the plasma arc process to criticism on the environmental front. Something had to be found to deal with these problem areas.

2.3.7 Underwater Cutting (1977)

Further attempts in Europe to decrease the noise level of the plasma arc and to eliminate smoke development as much as possible led to underwater cutting. This method for high power plasma cutting with cutting currents above 100 amps has become so popular that today, many high power plasma cutting systems cut under water.

For underwater plasma cutting, the workpiece is immersed about 50 to 75 mm under water and plasma torch cut while immersed in the water. The smoke and noise level as well as the arc glare are reduced dramatically. One negative effect of this cutting method is that the workpiece can not be observed while cutting and the cutting speed is reduced by 10-20%. Further, the operator can no longer determine from the arc sound whether the cutting process is proceeding correctly and whether the consumables are producing a good quality cut.

Finally, when cutting in water, some water surrounding the cut zone is disassociated into oxygen and hydrogen, and the freed oxygen has a tendency to combine with the molten metal from the cut (especially aluminum and other light metals) to form metal oxide, which leaves free hydrogen gas in the water. When this hydrogen collects in a pocket under the workpiece, it creates small explosions when reignited with the plasma jet. Therefore, the water needs to be constantly agitated while cutting such metals.

2.3.8 Underwater Water Muffler

Based on the popularity of underwater cutting, the design of an underwater Water Muffler which injected air around the torch, establishing an air bubble in which cutting could proceed originated. This became the air injected underwater cutting process which is most often used with oxygen cutting up to 260 amps. Use of this process increased cut quality and produced normal high cutting speeds achieved by water-line and "in-air" plasma cutting techniques.

2.3.9 Low-Amp Air Plasma Cutting (1980)

In 1980, plasma arc cutting equipment manufacturers in the Western hemisphere introduced equipment using air as the plasma gas, particularly for low-amp plasma systems. By early 1983, Thermal Dynamics launched the PAK3 and SAF introduced the ZIP-CUT. Both units were immensely successful, one in the USA and the other in Europe. This opened a new era for plasma arc cutting which increased the world market size about 50 times in the 1980s and created many new manufacturers. Plasma arc cutting was finally accepted as the new method for metal cutting and considered a valuable tool in all segments of the modern metalworking industry.

With the new thrust given to the plasma arc cutting industry through increased competition, many new improvements were introduced which made the process easy to use. The process was much more reliable and required less skill to operate. Power supply designs using solid state primary and secondary converter technology improved arc characteristics and reduced the size and weight of the systems.

2.3.10 Oxygen Plasma Cutting (1983)

Since the traditional method of cutting steel was the oxyfuel process, it was logical that engineers that developed plasma arc cutting tried from the very beginning to use oxygen as the plasma gas. However, the very high temperatures at the tip of the electrode and the presence of pure oxygen caused all known electrode materials to rapidly deteriorate, so either no cuts could be made or only cuts of a very short duration This rendered oxygen and air unacceptable as plasma gases. Oxygen cutting therefore was abandoned in the early years of plasma cutting technology development. In early 1970, it was found that hafnium and zirconium in an industrially available form did resist the rapid deterioration, which occurred with oxygen plasma arc cutting. Air and oxygen as plasma gases again became of extreme interest.

Oxygen plasma cutting offered a wide range of dross-free cutting speed conditions, increased cutting speed by up to 30%, while operating at lower current levels, and produced smooth, square, and softer edges. The resulting cut edge was easier to fabricate by bending or welding. All steels, including high strength, low alloy steels, were now cut dross free with this new process.

The critical part continued to be electrode life, which, even when using hafriium, remained limited. However, the cut quality of steel cut with oxygen was superb, and most end users found the tradeoff of much higher speed and cut quality in the face of shorter electrode life to be acceptable. Costly post-cut dross removal operations often associated with nitrogen cutting were virtually eliminated with oxygen plasma.

2.3.11 Oxygen Injection Plasma Cutting (1985)

Oxygen injection plasma cutting circumvented the electrode life problem by using nitrogen as the plasma gas and injecting oxygen downstream at the exit of the nozzle as shown in Figure 2.12.

This process was used exclusively on mild steel and slightly increased the cutting speeds. However, major disadvantages were lack of cut squareness, excessive kerf removal, short nozzle life, and limited versatility (mild steel). While this process is still being used at some locations, the limited increase in performance associated with it does not justify the extra expense of this rather complicated and delicate torch design.

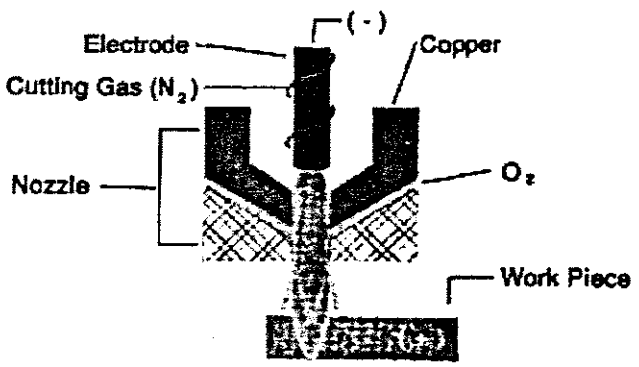

Figure 2.12 Oxygen Injection Plasma Cutting

2.3.12 Deep Water Plasma Cutting (1989)

In the 1990s, the atomic power industry was faced with two major challenges:

- How to extend the life of existing nuclear plants
- How to dismantle non-operational plants.

While the power industry is working hard to develop procedures for repairing components in the reactor pool, the atomic commissions of several countries are searching for methods to cut the expended reactors and other components into small pieces for disposal.

Since the reactor and auxiliary components must be kept in a pool of water, all repair and dismantling must also he done underwater. Since a major part of the components are made of stainless steel, plasma cutting is a desired method.

2.3.13 High Density Plasma Cutting (1990)

Laser cutting has become an important competitor in the metal-cutting industry because of its ability to produce high quality cuts with precise accuracy. To assume a place in the precision metal-cutting market plasma equipment manufacturers have increased their design efforts to further improve the cut quality of their equipment.

In the early 1990s we saw the first high quality plasma installation of 40 to 90 amps, which produced a squarer cut and reduced kerf width with increased cutting speed. Some units have come from Japanese manufacturers. The expectations are that a plasma cut will soon be of the same quality as a laser cut. Since plasma equipment is much

lower in capital cost than a laser unit, it is expected that this type of plasma cutting will become a major competitor in today's laser cutting market.

2.3.14 Longer Lasting Consumable Parts (1990)

Since air and oxygen plasma cutting have become more popular, the major issue has become the short life cycle of their consumable parts. The major manufacturers of plasma cutting systems are working on this issue. It is expected in the near future that the lifetime of air/oxygen electrodes will be extended substantially, reducing the cost of plasma cutting, and thereby making this process much more widely used for cutting steels.

CHAPTER 3

MATHEMATICAL MODEL OF PLASMA CUTTING

3.1 Introduction

The plasma arc cutting process is formulated as a coupled thermo-mechanical problem with solid phase transitions and interactions with environment. The formulation of the mathematical and finite element models for the cutting process is based on the thermo-mechano-metallurgical model [30] with enhancements for plasma cutting.

3.2 Lagrangian Description of Body Motion

The initial configuration of a body in the Lagrangian description of motion is the reference configuration and is usually used when boundary conditions are referred to the initial configuration. This motion is illustrated in **Fig. 3.1**.

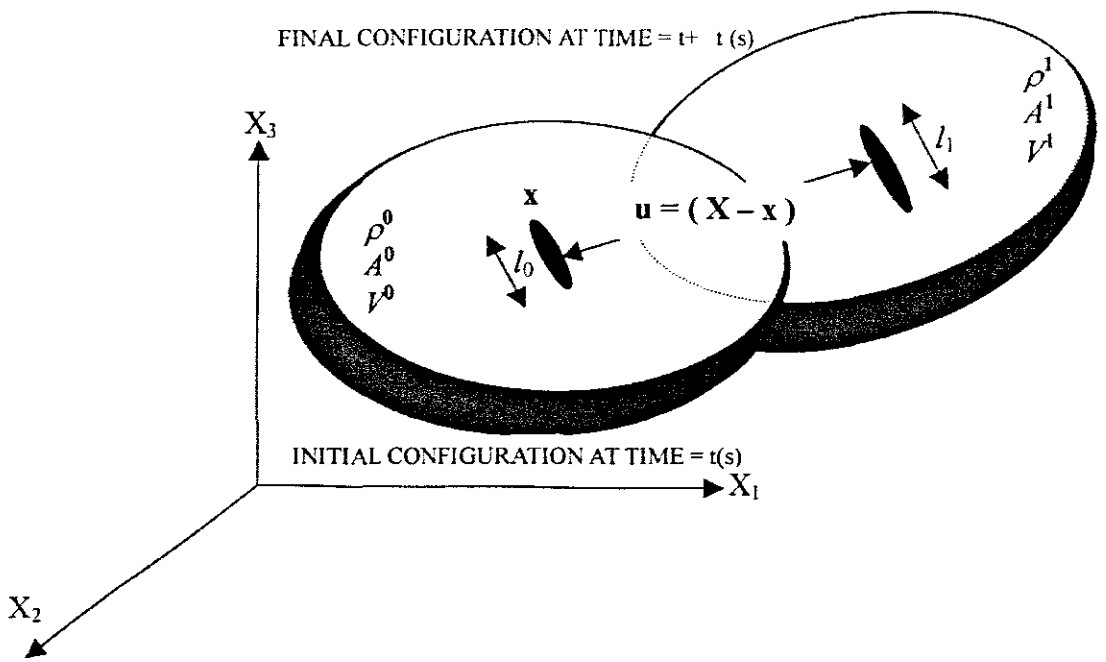

Figure 3.1 Lagrangian Description of Body Motion: Motion from initial time to final time configuration

The displacement $u(X,t)$ and temperature $\theta(X,t)$ of a particle in a proposed cut are unknown and the initial position of the particle $X=(X_1^0,X_2^0,X_3^0)$ and the time t are taken as independent variables. The vector joining the point X and its actual position in the space $x=(X_1^1,X_2^1,X_3^1)$ is the displacement vector given by $u=X-x$.

3.3 Constitutive Variables

The constitutive variables being the stress and strain measures used in the Lagrangian formulation are the second Piola-Kirchoff stress tensor and the Green-Lagrange strain tensors [2]. The second Piola-Kirchoff stress tensor $\hat{S}$, is given in terms of the Cauchy stress tensor T by

$$\hat{S} = \frac{\rho^0}{\rho^1} F^{-1} T \left\{F^{-1}\right\}^T, \tag{3.3.1}$$

where, ρ^0 and ρ^1 represents the initial and current densities.

The deformation gradient is given by

$$F = \frac{\partial x}{\partial X}; \qquad F_{iK} = x_{i,K} = \frac{\partial x_i}{\partial X_K}; \tag{3.3.2}$$

where x and $X = \chi(x,t)$ are the initial and current co-ordinates, respectively.

The Green-Lagrange strain conjugate with the second Piola-Kirchoff stress is defined by:

$$L = \frac{1}{2}\left(u_{I,J} + u_{J,I} + u_{K,I} u_{K,J}\right), \tag{3.3.3}$$

where the displacement gradient is defined as:

$$u_{I,J} = \frac{\partial u_I}{\partial X_J}. \tag{3.3.4}$$

The indices I, J, K refer to the reference configuration. The notation for the derivative with respect to the co-ordinates is given as ',' .

3.4 Balance Laws for the Thermo-Mechanical Process

The mathematical model of cutting consists of two principles expressing thermal and mechanical equilibrium being the balance of internal energy and the balance of momentum. According to [23], [31], these principles have been derived to account for the coupling of thermal and mechanical effects in thermo-inelastic body. The equilibrium equation for a particle $X \subset \Omega$ is given by the following equation:

$$\left(\hat{S}_{KL} x_{i,L}\right)_K - \left(b_i + r_i\right)\rho_0 = 0, \tag{3.4.1}$$

where x represents the current position of X and b_i is the body force, r_i is the surface force, and Ω is the body interior.
The equilibrium equation for a particle $X \subset \partial\Omega$ of a body is

$$\hat{S}_{KL} x_{i,L} N_K = T_i, \tag{3.4.2}$$

where N_K is the normal outward vector to the body surface $\partial\Gamma$and T_i is the nominal stress vector, and $\partial\Omega$ is the body surface.

If we assume that the actual co-ordinate system $\{X_i\}$, is collinear with the reference co-ordinate system $\{x_i\}$, these equations can be rewritten in the following form:

$$\begin{aligned} &\left(\hat{S}_{KL} + \hat{S}_{KL} u_{I,L}\right)_{,K} - (b_i + r_i)\rho_0 = 0, \\ &\left(\hat{S}_{KL} + \hat{S}_{KL} u_{I,L}\right) N_K = T_I. \end{aligned} \tag{3.4.3}$$

From the balance of internal energy, the 'heat equation' [23], [31] for an inelastic conductor is given by

$$\rho C_v \dot{\theta} + k_{IJ}\theta_{,JI} = f_\theta^B + f_\theta^S + \sum_J F_\theta^J, \tag{3.4.4}$$

Where

$$f^B_\theta = S_{IJ}\dot{L}_{IJ} \tag{3.4.5}$$

$$f^S_\theta = {}_{ext}q_J N_J + R \tag{3.4.6}$$

Eqs. 3.4.5 and 3.4.6 represents the rate of heat generated due to the dissipation of mechanical energy and the heat flux of the arc and outfluxes due to convection and radiation respectively. The last term on the RHS represents the concentrated heat fluxes, ρC_v is the specific heat and θ the temperature. It is important to note that the term determining the rate of heat generated due to mechanical dissipation Eq. 3.4.5 is not included in the SYSWELD program.

Thermal conductivity k, assumed to be the diagonal tensor, is defined by

$$k_{IJ} = \begin{bmatrix} k_{11} & 0 & 0 \\ 0 & k_{22} & 0 \\ 0 & 0 & k_{33} \end{bmatrix}.$$

The conductivity coefficients are assumed to be isotropic. Due to material istropy the conductivity terms are constant in the analysis.

Balance laws for momentum and internal energy can be expressed in the integral form and then approximated by Galerkin's type Finite Element Method. A derivation of the functional forms of the balance laws consists of several steps described in [23], which lead to the following expressions:

$$\int_{V_0} \hat{S}_{KL} u_{I,L} \upsilon_{I,K} dV + \int_{V_0} \left(\hat{S}_{KI,K} + \hat{S}_{KL,K} u_{I,L}\right) \upsilon_I dV + \int_{V_0} b_I \upsilon_I dV + \int_{\partial V_0} r_I \upsilon_I dP = 0 \tag{3.4.7}$$

$$\int_V k_{IJ}\theta_{,I}\,\vartheta_{,J}\,dV - \int_V c\dot{\theta}\,\vartheta dV + \int_V f_\theta^B \vartheta dV + \int_{\partial V} \hat{f}_\theta^S \vartheta dP + \sum_J F_\theta^J \vartheta\big|_J = 0, \tag{3.4.8}$$

with

$$\int_{\partial V} \hat{f}_\theta^S \vartheta dP = \int_{\partial V} f_\theta^S \vartheta dP + \int_V k_{IJ}\theta_{,I}\,\vartheta dP, \tag{3.4.9}$$

where $V = \{\upsilon_I, \vartheta | \upsilon_I, \vartheta \in H^1\}$ is a space of weighting functions (or variations) which corresponds to the class of trial solutions $S = \{u_I, \theta | u_I, \theta \in H^1\}$, and H^1 is the Hillbert space: once-differentiable and square integrable.

Stationary conditions for the functionals defined by Eqs. (3.4.7) and (3.4.8) are expressed by the following variational equations:

$$\int_{V_0} \hat{S}_{KL} u_{I,L} \delta\upsilon_{I,K} dV + \int_{V_0} (\hat{S}_{KI,K} + \hat{S}_{KL,K} u_{I,L}) \delta\upsilon_I dV + \int_{V_0} b_I \delta\upsilon_I dV + \int_{\partial V_0} r_I \delta\upsilon_I dP = 0 \tag{3.4.10}$$

and

$$\int_V k_{IJ}\theta_{,I}\,\delta\,\vartheta_{,J}\,dV - \int_V c\dot{\theta}\,\delta\,\vartheta dV + \int_V f_\theta^B \delta\,\vartheta dV + \int_{\partial V} \hat{f}_\theta^S \delta\,\vartheta dP + \sum_J F_\theta^J \upsilon\big|_J = 0. \tag{3.4.11}$$

The generalised Gateaux derivative was applied in Equ. (3.4.11) because of discontinuity of thermal field on the surface of phase transformation, e.g. melting/solidification surface.
The generalised (weak) solution can be evaluated for ϑ and υ.

3.5 Finite Element Approximation of a Cutting Process as a Coupled Thermo-Mechanical Problem.

The finite element method for the fully coupled thermo-mechanical problem is based on the Galerkin approximation of the two variational equations, i.e. the principle of virtual work Eq. (3.4.10) and the balance of internal energy Eq. (3.4.11). The discretization of the problem follows [23]. The equation of virtual work is solved by the Finite Element Method combined with linearization techniques for Finite Element Equations. Linearization is applied after the incremental decomposition of stress and strain tensors:

$$L^{n+1} = L^n + L^0 \tag{3.5.1}$$

$$\hat{S}^{n+1} = \hat{S}^n + \hat{S}^0, \tag{3.5.2}$$

where $\{L, \hat{S}\}^{n+1}$ and $\{L, \hat{S}\}^0$ correspond to the current and initial strain-stress states, and L^0 and $\hat{S}^0$ are increments of stress and strain. Following [23] and [31], increment of the Green-Lagrange strain L^0, can further be decomposed into linear and non-linear parts defined by:

$$L^0 = L + L_v , \tag{3.5.3}$$

$$L = \frac{1}{2}\left(\Delta u_{I,J} + \Delta u_{J,I}\right) \tag{3.5.4}$$

and

$$L_v = \Delta u_{K,I}\Delta u_{K,J} . \tag{3.5.5}$$

The Finite Element equation for virtual work, shown in [2], for the total Lagrangian formulation is obtained from Equ. (3.4.11) and expressed for the time instant (n + 1) by:

$$\left(K_L^n + K_{NL}^n\right)\Delta u\Big|_{(i)} = R_u^{n+1} - F^{n+1}\Big|_{(i-1)} , \tag{3.5.6}$$

K_L^n and K_{NL}^n represents the linear strain stiffness matrix and non-linear strain (geometric or initial stress) stiffness matrix respectively. $\Delta u\big|_{(i)}$ is the vector of increments of the nodal point displacements in iteration i. R_u^{n+1} is the vector of externally applied nodal point loads at time n + 1. $F^{n+1}\big|_{(i-1)}$ is the vector of nodal point forces equivalent to the element stresses at time (n + 1) and iteration (i - 1).

This equation is linear in respect of $\Delta u\big|_{(i)}$. Matrices in Eq. (3.5.6) are taken at four levels of solutions. These matrices are evaluated at two time steps, t and (t + Δt), and for two iterations i and (i - 1). The linear stiffness matrix is defined by:

$$K_L^n = \int_{V_0}\left[B_L^n\right]^T D B_L^n dV , \tag{3.5.7}$$

The matrix D, is the consistent or tangent modulus developed for the constitutive model, which has a decomposition of the total strain rate into elastic, thermal, plastic, transformation plastic and transformation induced plastic strain rates developed by Oliver [23]. B_L^n is the linear strain-displacement matrix.

Young's modulus and Poisson's ratio for the TM problem are temperature dependent. The non-linear stiffness matrix is defined by:

$$K_{NL}^n = \int_{V_0}\left[B_{NL}^n\right]^T \hat{S} B_{NL}^n dV , \tag{3.5.8}$$

The sense of the non-linear strain-displacement matrix B_{NL}^n comes from the expression

$$\left(\left[B_{NL}^n\right]^T \Delta u^T\right)\hat{S}\left(B_{NL}^n \Delta u\right) = \hat{S} : L_v , \tag{3.5.9}$$

where $\hat{s}$ is the matrix representation of the second Piola-Kirchoff stress. The linear and non-linear stiffness matrices are not modified in the iteration process at the step $(n + 1)$. They are updated, when the iteration process is completed. The vector of externally applied loads at nodal points is given by

$$R_u^{n+1} = \int_{\partial V_0} [H_s]^T r^{n+1} dP + \int_{\partial V} [H]^T b^{n+1} dV, \tag{3.5.10}$$

where,

H_s is the surface interpolation matrix, H is the volume interpolation matrix, $r^{n+1} = \{r_l\}$ is the nominal stress vector, and $b^{n+1} = \{b_i\}$ is vector of body forces. The vector of nodal point forces equivalent to the stresses at time $(n + 1)$ and defined by the previous iteration $(i - 1)$ is expressed in the form:

$$F^{n+1}\big|_{(i-1)} = \int_{V_0} B_L^n \hat{S}^{n+1}\big|_{(i-1)} dV. \tag{3.5.11}$$

The Galerkin type Finite Element Method also approximates the variational equation for the balance of internal energy (Eq. 3.4.9). The appropriate Finite Element Equation for the fully coupled thermo-mechanical problem is given by:

$$C^n \dot{\theta}^{n+1}\big|_{(i-1)} + \left(K_k^n + K_c^n + K_r^n\right)\Delta\theta\big|_{(i)} = F_{c(\theta)}^{n+1}\big|_{(i-1)} + F_{r(\theta)}^{n+1}\big|_{(i-1)} + F_{k(\theta)}^{n+1}\big|_{(i-1)} - F_{\Theta(\theta)}^{n+1}\big|_{(i-1)} \tag{3.5.12}$$

where K_k^n is the stiffness matrix corresponding to conduction, K_c^n is the stiffness matrix related to convection, and K_r^n is the stiffness matrix associated with radiation effects. The right hand side vectors are the thermal loads, $F_{c(\theta)}^{n+1}\big|_{(i-1)}$, $F_{r(\theta)}^{n+1}\big|_{(i-1)}$, and $F_{k(\theta)}^{n+1}\big|_{(i-1)}$ corresponding to thermal boundary conditions while, $F_{\Theta(\theta)}^{n+1}\big|_{(i-1)}$ is the internal heat flux through the body surface. The terms of Eq. (3.5.12), are defined by:

$$C^n = \int_{V_0} H^T (\rho C_v)^n H dV \tag{3.5.13}$$

Eq. 3.5.13 represents the heat capacity matrix

$$K_k^n = \int_{V_0} B^T k^n B dV \tag{3.5.14}$$

Eq. 3.5.14 represents the conductivity matrix

$$K_c^n = \int_{\partial V_0} H^T h_c^n H dP \tag{3.5.15}$$

Eq. 3.5.15 represents the convection matrix

$$K_r^n = \int_{\partial V_0} H^T \kappa H dP \tag{3.5.16}$$

Eq. 3.5.16 represents the Radiation matrix

The terms of the RHS of Eq. (3.5.12) represent the thermal boundary conditions and internal heat fluxes. They are defined as the following vectors related to:

The convection boundary condition

$$F_{c(\theta)}^{n+1}\Big|_{(i-1)} = \int_{\partial V_0} h_{c(\theta)}^{n+1} H_{s_c}^T \left[H_{s_c}\left(\theta_e^{n+1}\Big|_{(i-1)} - \theta^{n+1}\Big|_{(i-1)}\right)\right] dV \tag{3.5.17}$$

The radiation boundary conditions

$$F_{r(\theta)}^{n+1}\Big|_{(i-1)} = \int_{\partial V_0} \kappa^{n+1} H_{s_r}^T \left[H_{s_r}\left(\theta_r^{n+1}\Big|_{(i-1)} - \theta^{n+1}\Big|_{(i-1)}\right)\right] dP \tag{3.5.18}$$

The conductivity constitutive matrix

$$F_{k(\theta)}^{n+1} = \int_V B^T \left[k^{n+1} B\theta^{n+1}\Big|_{(i-1)}\right] dV \tag{3.5.19}$$

The heat fluxes in some nodal points

$$F_\Theta^{n+1}\Big|_{(i-1)} = F_{s_c}^{n+1}\Big|_{(i-1)} + F_{s_r}^{n+1}\Big|_{(i-1)} \tag{3.5.20}$$

which is defined by

$$F_{s_c}^{n+1}\Big|_{(i-1)} = \int_{\partial V_0} H_s q_{s_c}^{n+1} dP \tag{3.5.21}$$

for convection and,

$$F_{s_r}^{n+1}\Big|_{(i-1)} = \int_{\partial V_0} H_s q_{s_r}^{n+1} dP \tag{3.5.22}$$

for radiation.

3.6 Global Finite Element Equation for the fully coupled thermo-mechanical (TM) problem.

The combined Global Finite Element Equation for the fully coupled thermo-mechanical problem is expressed by

$$\begin{bmatrix} 0 & 0 \\ 0 & C^n \end{bmatrix} \begin{bmatrix} 0 \\ \dot{\theta}^{n+1} \end{bmatrix}^{(i)} + \begin{bmatrix} K_u^n & K_{u\theta}^n \\ K_{\theta u}^n & K_\theta^n \end{bmatrix} \begin{bmatrix} \Delta u \\ \Delta\theta \end{bmatrix}^{(i)} = \begin{bmatrix} R_u^{n+1} \\ R_\Theta^{n+1} \end{bmatrix} - \begin{bmatrix} F_u^{n+1} \\ F_\Theta^{n+1} \end{bmatrix}^{(i-1)}, \tag{3.6.1}$$

where K_u^n is the stiffness corresponding to mechanical effects, $K_{u\theta}^n$ is the matrix related to the transformation of mechanical energy into thermal one, and matrix $K_{\theta u}^n$ transforms thermal energy into mechanical one. The thermal stiffness K_θ^n is the sum of K_k^n, K_c^n and K_r^n. The RHS vectors in Eq. (3.6.1) are defined by

$$F_u^{n+1}\Big|_{(i-1)} = F^{n+1}\Big|_{(i-1)}, \tag{3.6.2}$$

and

$$R_\Theta^{n+1} = [F_{\theta k} + F_{\theta c} + F_{\theta r}]^{n+1}. \tag{3.6.3}$$

3.7 Metallurgical Analysis

The material model used in plasma arc cutting simulations accounts for heat flow and metallurgical phase transformations. A steel plate is a multiphase poly-crystalline alloy and is an assemblage of grains called a mesodomain. The mesodomain contains large number of micro-regions or dispersed particles. The micro-region is composed of a manifold of particles such as, e.g. crystals. A phase is a portion of a manifold of particles of an alloy whose properties and composition are homogeneous and which is physically different from other properties of an alloy.

A transformation of a daughter phase to a parent phase is directly related to the temperature history in a dispersed particle. In this analysis the Equilibrium Diagrams is used to determine when solid phase transformation occurs during heating. It is assumed that the initial phase of the material is austenite.

3.8 Coupled Thermo-metallurgical Analysis

The modeling of the metallurgical transformations are dealt with in a purely phenomenological way [3]. The metallurgical model used in SYSWELD is used for this analysis. In metallurgical terms, a material is defined in terms of metallurgical phase fractions y_a of volume of the various phases (austenite, ferrite, pearlite, bainite, and martensite) in the volume of a mixture, where "a" represents the various phases and assumes values: a = 1, 2, 3, 4, 5. The metallurgical model used in this study follows the Johnson-Mehl-Avrami type of phase transformation kinetics and gives the current phase proportion y_a of phase a according to time t and temperature θ. Following Bergheau and Leblond [3], when multiple transformation occurs in a material, Eq. (3.4.4) can be rewritten as

$$\left(\sum_{\text{phases}} y_a (\rho C_v)_a\right)\dot{\theta} + \left(\sum_{\text{phases}} y_a (k_{IJ})_a\right)_{,JI} = f_\theta^B + f_\theta^S + \sum_J F_\theta^J - \sum_{\text{phases}} \dot{y}_a L_a , \qquad (3.8.1)$$

where the specific heat and conductivity are dependent on the metallurgical phase fractions. The specific heat, following [3], is given in terms of the phase enthalpies H_a. For a given phase, a, it is given by

$$(\rho C_v)_a = \frac{\partial H_a}{\partial \theta}, \qquad (3.8.2)$$

The last term on the RHS of Eq. (3.2.1) is related to the latent heat and in SYSWELD is included as the further volumetric heat source [3]. This is done because the temperature ranges of phase transformations are dependent on temperature rates and L_a is given by

$$L_a = H_1 - H_2 \qquad (3.8.3)$$

The evolution of phase fractions $\dot{y}_a$ in the Johnson-Mehl-Avrami model are defined by

$$\frac{dy_a}{dt} = n\frac{(y_{eq}(\theta) - y_a)}{Tau(\theta)}\left[\ln\left(\frac{(y_{eq}(\theta))}{(y_{eq}(\theta) - y_a)}\right)\right]^{(n-1)/n} . \qquad (3.8.4)$$

This model is used for transformations during heating and cooling. The austenite proportion is given by y_1, and the equilibrium austenite proportion is given by y_{eq}, and can be read from the iron-carbon diagram, *Tau* (θ) is a time constant which reproduces a retardation effect.

Sysweld uses Eq. 3.8.1 which is the coupled thermo-metallurgical equation to calculate the temperature distribution and metal phase. Again it should be noted that the term for the rate of heat generated due to the mechanical dissapation is not included in Systus. The formulation of the kerf will be modelled using the equation 3.8.4 where the continuous change in material properties accounts for the removed of material. The parameters being considered are temperature and thermal properties of the material (conductivity and density). At 1550 °C, it is assumed that 90% of the material is in molten state and the first 10% increment of this temperature, being 1750°C, the material has been removed. Systus can consider 5 phases as mentioned elsewhere but this analysis considers only 2 phases. Initial phase being austinite represented by the number 1 and the final phase representing completely removed material is given as number 2. The cut material (removed material) is represented as a phase with very weak material properties for e.g. air.

Chapter 4

The Quality of a Plasma Arc Cut

4.1 Introduction

Besides the HAZ, several other factors (Fig. 4.1) that also must be considered in determining the quality of a plasma arc cut are the:

- Cut angle
- Dross
- Surface finish
- Top-edge squareness
- Kerf width

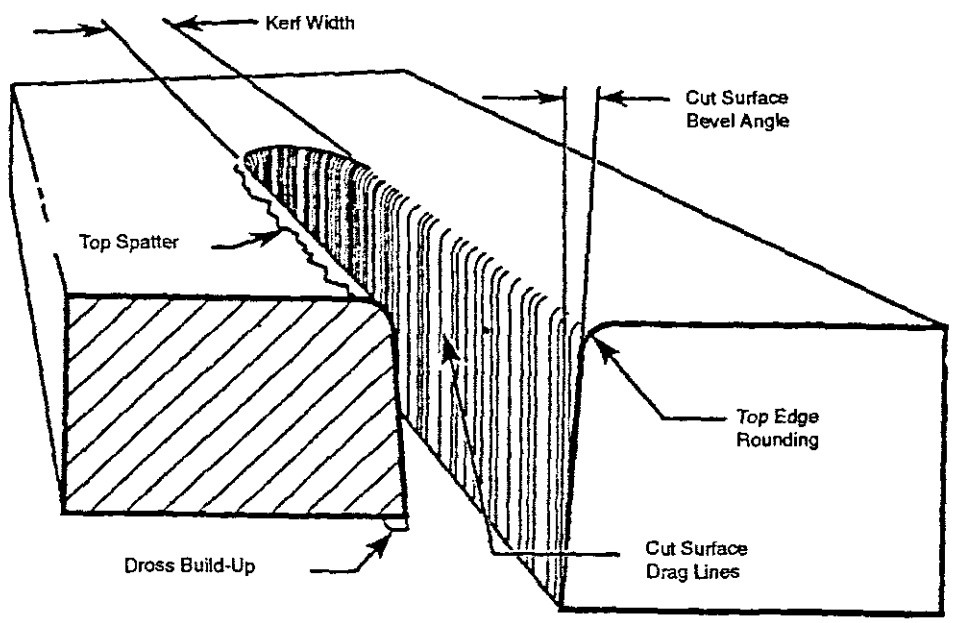

Figure 4.1 Diagram of Typical Plasma Arc Cut

4.2 The description of cut quality characteristics

4.2.1 Cut Angle

Plasma arc cutting will usually result in an angle on the cut surface of approximately 1 to 3° on the "good" side and 3 to 8° on the "bad" side, when using torches that swirl the plasma. With laminar-flow torches, the angle on both sides is usually about 4 to 8°. These angles are most noticeable in mechanized applications where the torch is square to the workpiece. The good and bad sides of the cut are determined by torch travel direction and plasma gas swirl. With a clock wise gas swirl, the good side of the cut will

be on the right with respect to torch motion. Therefore, in the cutting of a ring or flange in which the minimum angle is desired on both the inside and outside diameters, the outside would be cut in the clockwise direction, while the inside would be cut counterclockwise (Fig. 4.2).
This change in angle from good side to bad side of the cut is the result of the arc attachment point on the cut surface and the release of energy on the good side before contact with the bad side occurs. Changing an internal torch part, such as the electrode or gas distributor, can enable those plasma cutting torches that create a gas swirl to change from a clockwise to a counterclockwise swirl direction. This then enables mirror-image cutting when using two torches in a mechanized set-up, such as in strip-cutting applications.

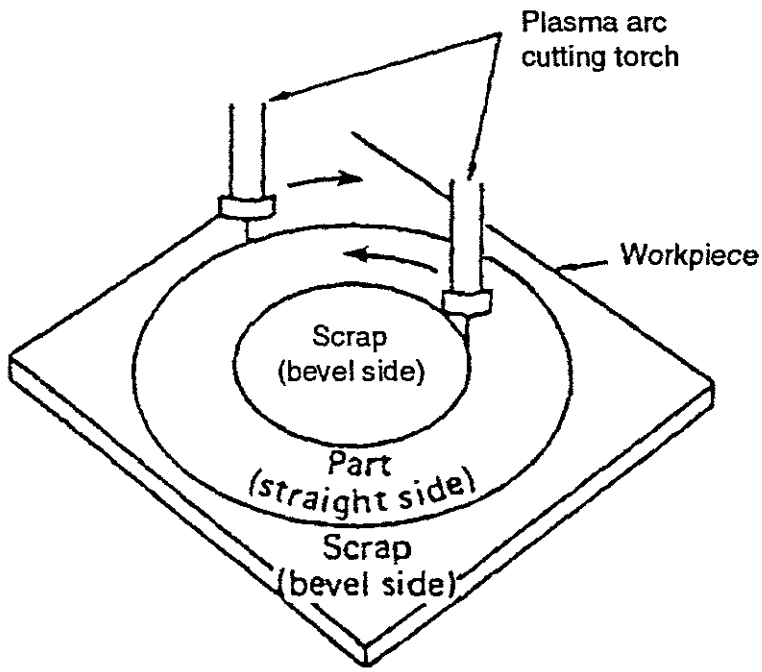

Figure 4.2 Indication of Directional Changes for Best Cut Quality

4.2.2 Dross (Resolidified metal)

This phenomenon refers to the resolidified metal that adheres to the bottom edge of the plasma cut. The concentration of dross will be heavier on the bad side of the cut. The amount of dross that forms is a result of the type of metal being cut, the cutting speed, and the arc current. Dross can be formed from either too high or too low a cutting speed, but there is a "window" between these two extremes in which dross-free cuts can usually be achieved. The dross-free range is greater on stainless steel and aluminium than it is on carbon steel and copper alloys. If dross-free cuts cannot be achieved, then a minimum amount of low speed dross is more desirable, because it is more easily removed than the high-speed variety.

4.2.3 Surface Finish

The cut surface from the plasma arc process is normally rougher than that achieved by oxyfuel cutting on carbon steels, and it is definitely more rough than most machining processes. In most metals, this roughness usually appears as a ripple along the cut

surface. This is partly due to the output waveform of the dc power supply (the smoother the output, the smoother the cut), but it is also determined to an extent by the gases used and the torch design. Water-shielded and water-injection plasma arc cutting provide much smoother cuts than gas-shielded or conventional plasma techniques. The use of argon-hydrogen as a plasma or a shielding gas will result in smoother cut surfaces on most metals than when using nitrogen plasma or any other gas shield.

4.2.4 Top-Edge Squareness.

Most metals experience some top-edge rounding when the PAC process is applied. Top-edge rounding is more pronounced on the thinner metals. This rounding is due to a higher heat concentration at the top of the cut, and can be minimized by using a gas shielded PAC process. It can be even better controlled when water-shielded or water-injection plasma arc cutting is used. The kerf width obtained by plasma arc cutting will be greater than that achieved by oxyfuel cutting on carbon steel, but not as great as that obtained by other processes, such as abrasive cutting or arc gouging. The rule of thumb for estimating the kerf in plasma cutting is that the width will be approximately 1.5 to 2.5 times the tip orifice diameter.

4.3 The Effects of Cutting Speeds on the Characteristics of the Cut

4.3.1 General

The characteristics of the cut depend greatly on the speed with which the torch moves with respect to the metal plate (the cutting speed V). There exists a cutting speed V_{max} above which it is not possible to make a through cut, and its value depends on the arc current, nozzle diameter and the metal thickness. However the cut quality may not be acceptable even when the cutting speed is less than V_{max} . An undesirable phenomenon occurs if the cutting speed is less than V_{max}. Some of the molten material does not leave the bottom of the plate, forming so-called high speed dross. The removal of which requires an additional operation, thus increasing the total cost of the cut. In most cases a reduction in the cutting speed alleviates the problem of high-speed dross formation. The cut quality is characterized not only by the absence of dross but also by the squareness and smoothness of the cut. Reduction in the cutting speed thus increases the quality of the cut. However, a further reduction in cutting speed below some limit V_{min}, once more leads to dross formation; this time the so-called low-speed dross. A high quality cut is therefore possible within a range of cutting speeds which typically can be represented by Fig 4.3

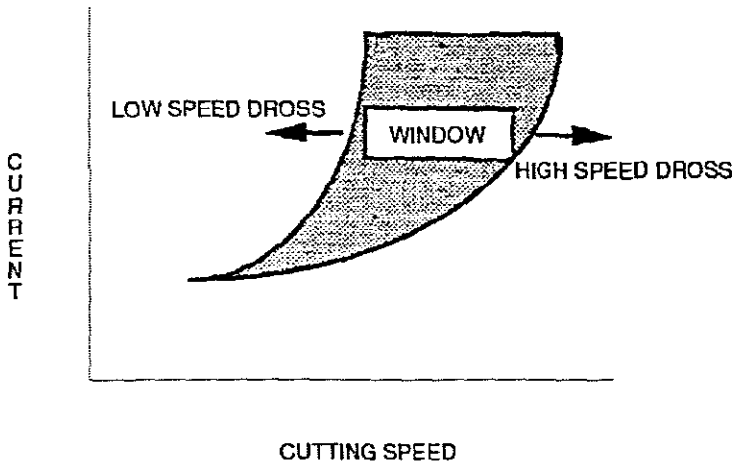

Figure 4.3 Dross Free Cutting Window

This range becomes narrower as the plate thickness increases. Increasing the arc current increases the range but at the expense of shortening the electrode and nozzle lifetimes. The dross-free cutting speed range also depends on the kind of plasma gas used. Formally, the most commonly used gas was nitrogen. This gas has a very narrow dross-free window. During the last decade oxygen and air plasma arc cutting has become more popular. These gases provide a wider dross-free window. However, the window still exists thus limiting the technological capability of plasma arc cutting, more so when cutting thick plates.

There is limited available data on V_{max} and V_{min} for air PAC. The data available are almost exclusively related to nitrogen and oxygen plasma arc cutting.

Following Nemchinski [20] Eq. 4.1 can be used to estimate the maximum cutting speed for dross free cuts.

4.3.2 The Estimation of the High Speed Dross (HSD) Limit

(4.1)

where refers to the total power consumed by the cutting process which consists of the power lost due to the thermal conduction and the power that leaves the plate with the hot molten metal. The latter can be calculated as

(4.2)

where is the density, is the heat capacity, is the diameter of the nozzle, is the thickness of the plate and is the heat of fusion. For liquid iron ,
and .

Also Eq. 5.1 defines . According to [20] the maximum speed is inversely proportional to , the radius of the heating cylinder. In calculating the maximum cutting speed , we use the radius of the nozzle orifice for . The width of the kerf reduces with an increase in the cutting speed.

4.3.3 The Estimation of the Low Speed Dross (LSD) Limit

The model presented by Nemchinsky [20] describes this phenomenon quantitatively. According to this hypothesis, Eq 4.3 defines the minimum velocity for dross free cutting.

(4.3)

where is the melt density, represents the plate thickness, is the surface tension, is the thermal diffusivity and is the critical Weber number.

The higher the surface tension the larger the amount of molten metal it can retain and thus the higher the LSD speed limit. The quantity opposing the surface tension is the impulse of the molten metal emerging from the cut. The Weber number, , describes the comparative role of these two factors. There exists a critical Weber number so that when > then the role of surface tension is not so important. Thus the melt separates from the plate freely and no dross is formed. However, when < the surface tension is high enough to retain a significant amount of the melt or dross formation occurs. It is important to note that the gas/plasma flow rate does not affect the formula [4.3], since it was found that the flow rate exerts no influence on .

Tables 4.1-3 represents the dross free window of cutting speeds for the three selected thickness of plates (5 mm, 10mm and 20mm) and for arc currents ranging from 30 – 120 Amps with a step of 30. These cutting speeds are calculated using Eq. 4.1 and 4.3, defining the high speed dross free and low speed dross free limits respectively. It can be seen that the dross free window decreases with increasing thickness (for constant current) and increases with increasing current (for constant thickness). These ranges of cutting speeds relative to the specified thickness and current will be used in the simulations. The reason for this is that the model will represent a dross free status and hence conforms to the requirement associated with 'a good quality cut".

Table 4.1 Range of Velocity for Dross Free Cutting for Varying Current for 5mm plate

Plate Thickness (mm)	Current (Amps)	(mm/sec)	(mm/sec)
5	30	16.2	17.6
5	60	25	35
5	90	29	52.7
5	120	31.5	70

Table 4.2 Range of Velocity for Dross Free Cutting for Varying Current for 10mm plate

Plate Thickness (mm)	Current (Amps)	(mm/sec)	(mm/sec)
10	30	8.4	8.8
10	60	14	17.5
10	90	17.1	26.3
10	120	18.8	35.1

Table 4.3 Range of Velocity for Dross Free Cutting for Varying Current for 20mm plate

Plate Thickness (mm)	Current (Amps)	(mm/sec)	(mm/sec)
20	30	4.3	4.3
20	60	7.7	8.8
20	90	9.8	13
20	120	11	17.5

The following effects are taken into account in the experimental phase (see Chapter 8) of this project since these could cause discrepancies when validating the results from the simulations.

4.4 Other Factors Influencing Cut Quality

4.4.1 Effect of Steel Composition and Cutting Gas

In the case of nitrogen-based PAC systems, data collected from fabricators indicate that the operating window within which satisfactory cuts can be obtained becomes narrower

and shifts toward slower speeds with the higher Si content in the steel. Compared with Si-free steel, the maximum permissible speed to produce good quality cuts at a given current begins to drop around 0.12-0.15% Si and around 0.3% Si the cut speed has to be reduced as much as 50% to obtain acceptable cuts.

On the other hand, the cut quality with air or oxygen PAC does not appear to be affected by the composition of the steel. So with the introduction of oxygen into the plasma the effective window of cutting speed can be obtained over a wider range of parameters and compositional variations. The cut quality is very good, no "nitride" layer is formed and welding can be carried out without any blowhole formation. However compared with nitrogen and argon-hydrogen plasmas, the consumables erode more rapidly with air and oxygen PAC. Considerable progress has been made by manufacturers to prolong consumable life by material development, improved torch/nozzle/tip design and changes in arc-initiation procedures. These developments are discussed by Fernicola [6]. There is also indication that when the Al content of steel is high (above 0.07-0.08%), the cutting window becomes narrower for air and oxygen PAC and dross problems can result. If the carbon content of steel is low (less than 0.1%) then dross free cut can be obtained at high speeds.

4.4.2 Effect of Surface Oxides

Since dross formation is related to the degree to which the molten metal can adhere to the bottom surface of the plate, it is possible that surface oxides can play a role.

4.4.3 Effect of Plate Magnetization

Even though the plasma arc is considered to be relatively stiff and less prone to arc blow than a gas tungsten arc, it is possible that small differences in the degree of plate magnetization could be enough to push the cutting conditions out of the safe operating window, especially so if the operating point is close to the high speed limit. According to Ghosh, *et al.* [8], external magnetic fields have a much greater effect on the width of the cut at the bottom of the plate than at the top. It is believed that under the influence of a magnetic field, the arc column could become so divergent that the arc pressure may not be enough to expel the molten metal at the plate bottom. Magnetism could be introduced in the plate after handling using magnetic lifts. Grounding and magnetic fields induced by power cables could also play a role.

4.4.4 Effect of Heat Deformation and Residual Stress

In many cases coils from the hot strip mill are straightened before fabrication, it is possible that the plate could still have some residual stress when cutting begins. These residual stresses could be locally relieved to a certain degree as cutting proceeds and this could cause a change in torch standoff, or the kerf opening (due to strains in the direction perpendicular to the cut), or both. This could result in dross formation and undercut.

The effects of the variations in the steel composition or process characteristics as discussed in section 4.4 could push the cutting process operating point out of the "safe cutting window" see Fig. 4.4 and Fig. 4.5.

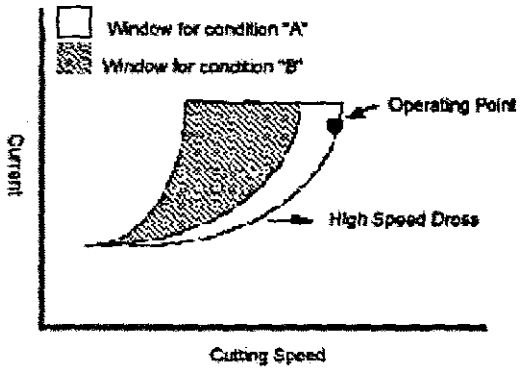

Figure 4.4 Operating point shifting out of dross free window

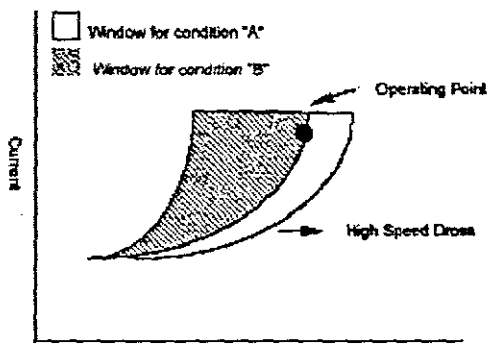

Figure 4.5 Operating point shifting back into dross free window

Chapter 5

Development of the Model and Benchmark Problem

5.1 The development of the model

Plasma arc cutting is modelled in the framework of a Thermo-mechano-metallurgical framework as proposed by Ronda and Oliver [30]. The model used here is limited to a Thermo-metallurgical analysis as implemented in SYSWELD makes this possible. The heat flow boundary conditions into and out of the body is taken into account in SYSWELD using simplified Fortran. The metallurgical equations are contained within the SYSWELD program and the details for the transformation temperatures are extracted from the equilibrium diagrams. The Continuous Cooling Transformation (CCT) and Time Temperature Transformation (TTT) diagrams will be used to determine the phase transformation during heating. This can be done for cooling as well however, the objective of this project is to develop a technique to determine the minimum energy input required to cut a plate based on certain inputs related to the plasma arc cutting process. The achievement of this objective will ensure the narrowest HAZ and consequently smallest machining depth if the HAZ needs to be removed. The Fortran code is also used to define the process variables that were selected to conduct the variable sensitivity analysis.

5.2 The Model of the Arc

5.2.1 Heat flux input

The arc for the plasma arc cutting process is modelled as a travelling heat flux. The heat flux input for the cutting process is given as

$$Q = \zeta VI \tag{5.1}$$

where

ζ = Efficiency
V = Voltage input
I = Current input

The arc is assumed to have a ring like shape and the maximum power is concentrated at the circle with some mean radius. Thus considering that the arc is modelled as a travelling heat flux the equation is used as

$$q\ (x,y,z,t) = Pe^{-r} \tag{5.2}$$

where P (W/mm^3) is the volumetric heat source that determines the magnitude and shape of the arc and is given as

$$P = \frac{6\sqrt{3}Q}{\pi\sqrt{\pi}abc} \tag{5.3}$$

and $$r = 3\left(\frac{x^2}{a^2} + \frac{z^2}{c^2} + \frac{(y+VT)^2}{b^2}\right) \quad (5.4)$$

where a, b and c represents the arc distribution parameters, VT is the position of the arc in the y plane and is a function of the cutting velocity and time. The exponential equation has a negative power and thus as r increases the function follows the law of decay. For a specific voltage V, Current I, distribution parameters a, b and c and cutting speed the arc shape and heat affected (HAZ) can be defined. The arc and plasma jet generated for plasma cutting needs to be narrow to obtain a narrow kerf, have sufficient energy to melt the metal at the required cutting speeds and have the required momentum to eject the molten metal from the plate without forming dross. An appropriate arc model is necessary to accurately represent the application of the heat source to the workpiece. The selection of the arc shape variables a, b and c as described in Eq. 5.4 which defines the shape of the transfered arc is based on work done by Ramakrishnan and Rogozinski [28]. The measurements from the study indicates that the arc diameter at a height of ± 9mm from the workpiece using a nozzle with bore of 1.5mm at a nominal current of 100A is 1.0mm.

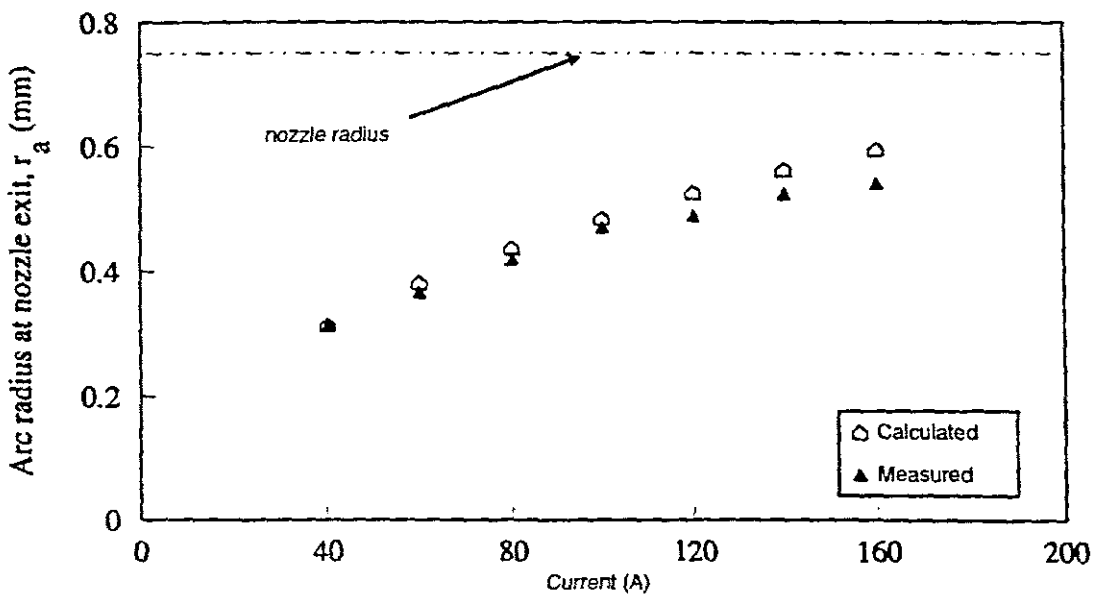

Figure 5.1 Variation of arc radius at nozzle exit with arc current

Several (729) simulations were conducted to determine the combination of constants necessary to produce an ellipsoidal arc with the required diameter as specified. The graphs indicating the relationship between current and arc radius at exit and at a height of ± 9mm from the workpiece is shown in fig. 5.1. Fig. 5.2 represents the shape of the arc used in the simulations.

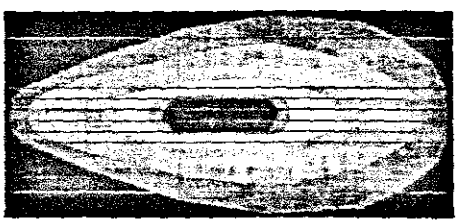

Figure 5.2 - Shape arc

A more accurate representation of the shape of the arc can be achieved if the mesh is further refined towards the line of cut. This was not feasible due to the limitation on the total number of elements allowed for the calculation. The calculation time increases substantially and computer memory utilization also presents a constraint with increased elements.

5.2.2 Convection from the workpiece

The thermal convection from the workpiece is given as empirical relations in terms of dimensionless constants [14]. The flux due to of thermal convection is given by

$$q_c = -h_c(\theta_s - \theta_e) \tag{5.5}$$

where the flow of heat out of the body is indicated by the negative sign, θ_e represents the known environment temperature, θ_s is the unknown surface temperature and h_c is the convection heat transfer coefficient that is a function of the dimensionless constants being the Grashof (Gr_f), Nusselt (Nu_f), Prandtl (Pr_f) and Rayliegh (Ra_f) numbers.

5.2.3 Radiation from the workpiece

The heat flux due to radiation heat transfer is given by

$$q_r = -h_r(\theta_s - \theta_{\sin k}) \tag{5.6}$$

where h_r is the radiation coefficient [14] given by

$$h_r = \sigma_s \varepsilon(\theta_s^4 - \theta_{\sin k}^4) \tag{5.7}$$

where σ_s is the Stefan Boltzmann constant, ε is the emmisivity of the particular material, θ_s is the temperature of the surface of the body and $\theta_{\sin k}$ is the temperature of the environment.

5.3 Benchmark Problem

The air plasma arc cutting of steel plates of varying thickness is the benchmark problem for this study. The dimensions of the plates considered for the simulations were 100mm by 100mm by 5mm, 10mm and 20mm. To facilitate arc stability during the experiments it was decided to select a dimension of 100mm by 150mm for the 5mm plate for the simulation as well. SYSWORLD+2, an interactive design-computation graphic system was used to conduct the simulations. The pre-processing stage is divided into two phases. Phase one being geometry/meshing, this system generates the input data for phase two (analysis). In the analysis, loads are applied to the model defined in phase one. The finite element mesh configurations are shown in fig. 5.3.

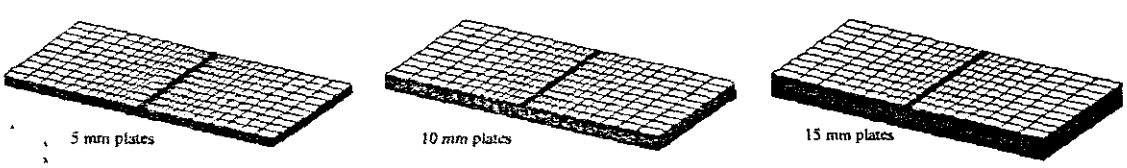

Figure 5.3 – Finite element mesh configurations

In all the cases 8 node brick elements were used to discretize the plates. The mesh was regular and increasing in density towards the line of cut to ensure accurate calculation of the temperatures and consequently the kerf. The chemical composition and the material properties i.e. Young's Modulus, Poisson's Ratio, density, thermal conductivity, etc., is given in APPENDIX C.

The following assumptions are made regarding the workpiece:

- The initial phase of the material is assumed to be austenite.
- The carbon content of the steel is low (less than 0.1%).
- Very little or no surface oxides exist in the material.
- No magnetic fields exist in the plate.
- Torch standoff distance remains constant throughout the cutting process.
- The plate is free of residual stress.

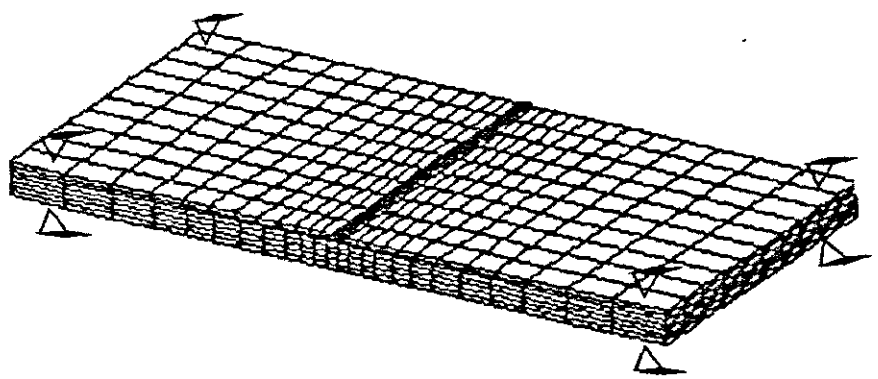

Figure 5.4 Clamping configuration

It is assumed that the plasma jet is operated in the transferred mode where the current flows between the plasma torch (cathode) and the workpiece (anode). This method is invariably used in plasma cutting because the usable heat input to the workpiece is more efficiently applied when the arc is in electrical contact with the workpiece. The nozzle is assumed to have a diameter of 1.5mm and is constantly positioned at a height (arc standoff height) of ± 9mm from the workpiece. The plate is assumed to be located on very small area supports thus no heat sink effect is established, see fig. 5.4

For this reason thermal contact conductance has been omitted from the boundary conditions. Thermal convection and radiation occurs from the top of the plate.

5.4 Computational Assumptions

The simulation was approached by following two successive steps, with the main objective of predicting the HAZ and the details of the resulting kerf (width and depth). These steps can be listed as follows:

- Non-linear thermal computational analysis

- Non-linear thermo-metallurgical computational analysis

The thermal boundary conditions relating to the plate were inputted into SYSWORLD+2 using simplified FORTRAN as illustrated in APPENDIX C. User defined heat fluxes can also be entered to further define the metallurgical phase transformations.

The thermo-metallurgical analysis of thermal cutting exhibits a highly transient and non-linear characteristic. To this end one of two quasi-Newton (matrix update) methods can be used to solve the finite element equations. The Newton-Rhaphson and the Broyden-Fletcher-Goldfarb-Shanno (BFGS) solving methods were used. It was found that the BFGS solving method was more appropriate to solve the finite element equations. An iterative solving scheme was used to further solve the linear equations obtained after applying the BFGS method.

5.5 Optimization of the Simulation Procedure

A typical input file used in SYSWORLD+2 can be seen in APPENDIX C. Formally these input files needed to be created and the run command executed manually. This is a very time consuming procedure in that the efficiency is operator dependent. An automated procedure has been developed during this study to increase the computational efficiency with regard to the simulations. This was particularly helpful in the determination of the applicable arc shape variables as discussed in Chapter 5.1 as well as the execution of the variable sensitivity analysis. A brief description of the process is given below, the detailed flow charts for the two functions below are illustrated in Figs. 5.5 – 5.7.

The command is generated in shell script to fulfill the following functions:

1. Arc optimization

- Automatic generation of the input data files considering the selected range of arc shape variables a, b and c.
- Repetitive execution of the run command.
- Automatic generation of the output files with the input file name relation.

2. Process variable sensitivity analysis

- Automatic generation of the input data files for the selected variables thickness (Z), current (I) and velocity (V)
- Repetitive execution of the run command.
- Automatic generation of the output files with the input file name relation.

The specification of the capacity of the Risk machine (SGI) determines the number of simultaneous runs possible. In both cases a sleep command was added to facilitate consistent reliability of the operation. This basically allows the program to run to completion and then restart the next program without causing depletion in computer swap space memory.
For the creation and run execution of the input files for current setting of 100Amps, voltage of 110V and standoff of 0.9mm the following flow chart represents the arc

shape parameter optimization process. The selection of the appropriate combination was based on the shape and diameter of the arc on the workpiece as given in Table 5.1. The variables a, b and c range of values were 1-10. Thus 729 files were run.

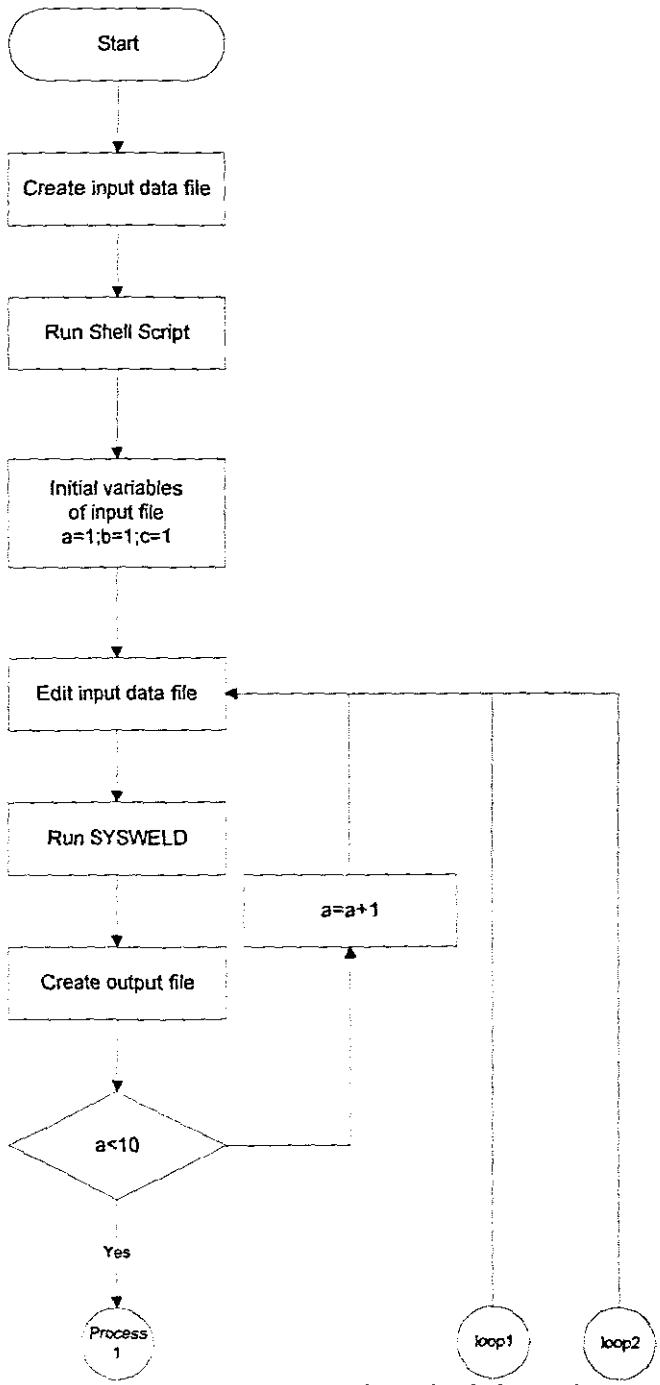

Figure 5.5 – Flow chart describing arc shape simulation optimisation

The following process diagrams indicates the procedure for the variable sensitivity analysis.

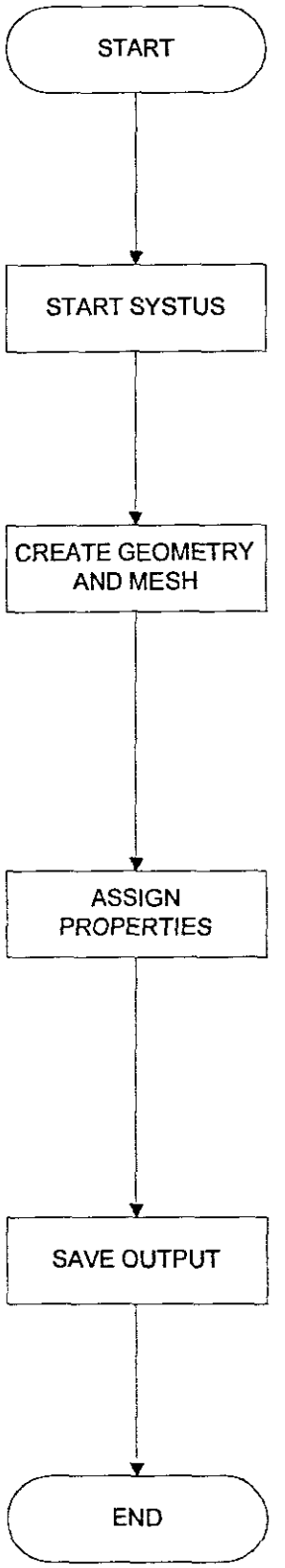

Figure 5.6 Process for input data into SYSWELD

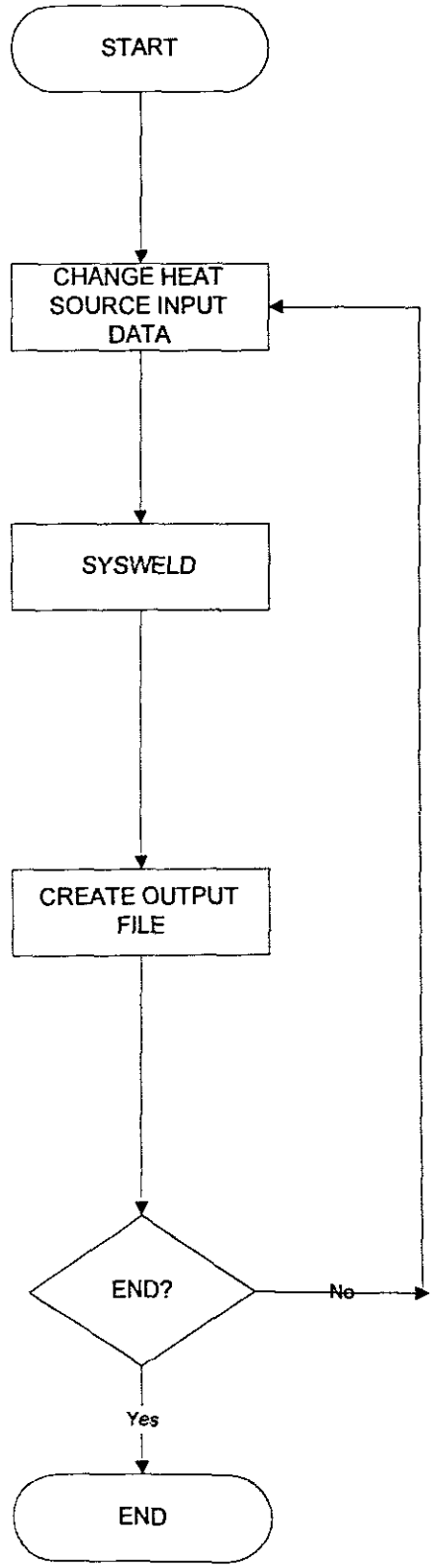

Figure 5.7 Flow chart describing operation of shell script

Chapter 6

Numerical Results

6.1 Introduction

It is generally understood that a high quality cut is characterized by sharp corners, a smooth cut surface, parallel sides, non-adherent dross and a narrow kerf. The inability of the plasma arc process to produce cuts with all these desirable characteristics has been recognized for years.

In PAC a suitable selection of several operating and equipment variables are necessary to achieve the best results. This involves the use of a properly shaped arc chamber and nozzles, selection of the correct gas flow rates and best cutting gas composition, determination of the cutting speed limitations, selection of the optimum arc current, and the optimum nozzle elevation above the workpiece. Frequently an improvement in one character is obtained at a sacrifice in another.

The variables that have been selected for the analysis are cutting speed, arc current and plate thickness. The Finite Element Method was implemented to study the effect of these cutting variables on the resulting heat affected zones and kerf details.

Using these results we can establish the optimum combination of arc current and cutting speed to produce a dross free cut for the said range of plate thickness. When referring to "optimum" there are two considerations, cost implications or production rates. To keep operation costs to a minimum we need to identify the minimum energy input required to cut the plate. To maximize the production rate we need to cut the plate as fast as possible maintaining the ability to reduce the input of excess energy. In both cases the quality of the cut needs to be acceptable in that it exhibits the characteristics of a good quality cut.

The data used to statistically evaluate the process outcome based on process parameters variation is extracted from the simulations of the plasma arc cutting process. Figure 6.4 illustrates a typical virtual cutting process with random parameter settings. The figure shows the process at initiation to various intervals of the cut. The detailed description of the physical influence of the variables selected for the sensitivity analysis is presented in the ensuing text.

The heat affected zone (HAZ) will have an effect on the overall strength, corrosion resistance and susceptibility to surface cracking of the cut part. If the application is such that the cut part must undergo machining to remove the HAZ then the depth of the machining depends on the size of the HAZ. Thus it is obvious that the narrower the HAZ the better the part integrity and the lower the production cost for machining, if required.

6.2 The Effect of the Selected Cutting Variables on the HAZ and Kerf Width

The effects of arc current and cutting speed on the HAZ are discussed below and outputs from the simulations are presented. Graphical representations formulated from data extracted from the simulation results are also presented to clearly illustrate the following:

- The effects of varying cutting speeds on the resulting HAZ and kerf width at constant current for various plate thicknesses.
- The effects of varying current on the resulting HAZ and kerf width at constant cutting speed for various plate thicknesses.

6.2.1 Cutting Current

The arc radius increases monotonically with arc current. The proportion of arc power also increases as the arc current increases. The current density can be determined if the arc radius and the arc current is known. The plasma jet generated needs to have sufficient energy to melt the metal at the required cutting speeds. For a specific plate thickness and a given cutting speed there exists an optimum arc current that will produce the desired cut.

The power density within an arc plasma is a function of the current density and the axial electrical field at the nozzle exit. The current density varies with varying current. The axial electrical field is constant since the voltage, nozzle diameter and standoff height is constant. The current density is thus the governing factor when determining the energy density required to cut a plate. Figure 6.3 represents the typical relationship between energy density and cutting speed. Figs. 6.4 and 6.5 further illustrates this relationship.

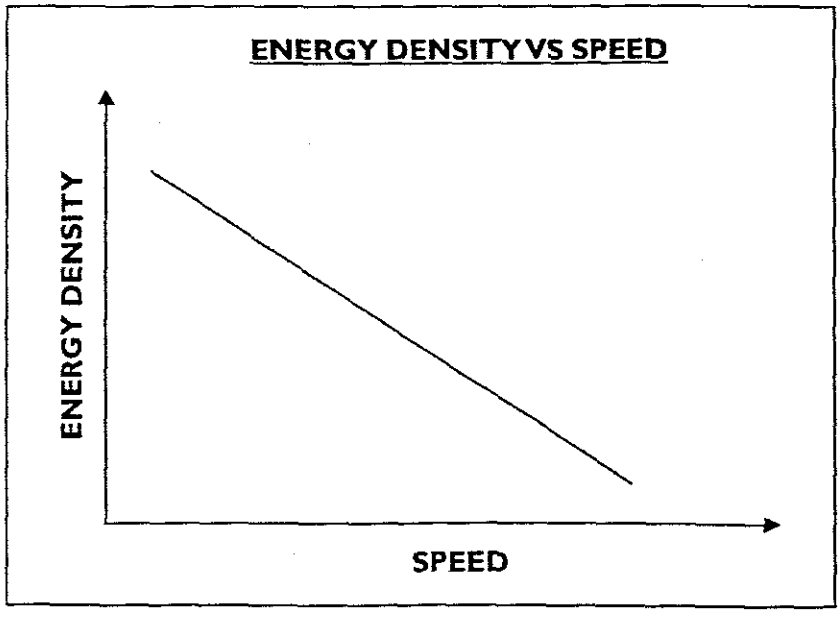

Figure 6.3 Relationship of energy density and cutting speed

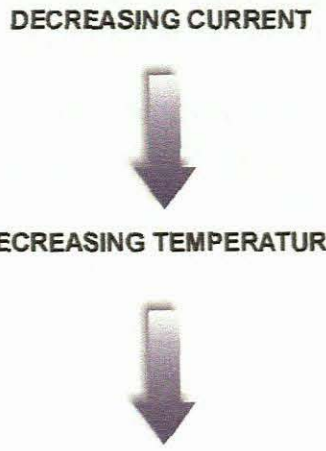

Figure 6.2 Diagram for decreasing current

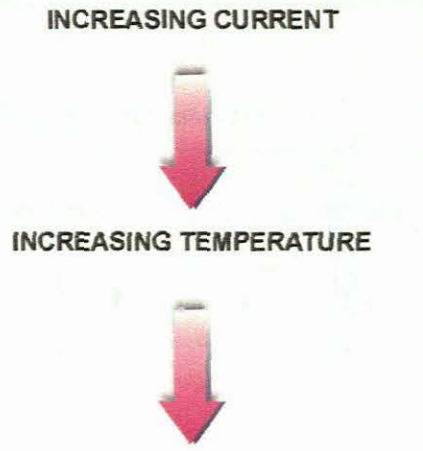

Figure 6.3 Diagram for increasing current

The first study that was conducted was to assess the effects of changing cutting current for constant velocity on shape and size of the heat affected zone from the simulations. The simulations were of plasma arc cuts of 5mm, 10mm and 20mm thick plates.

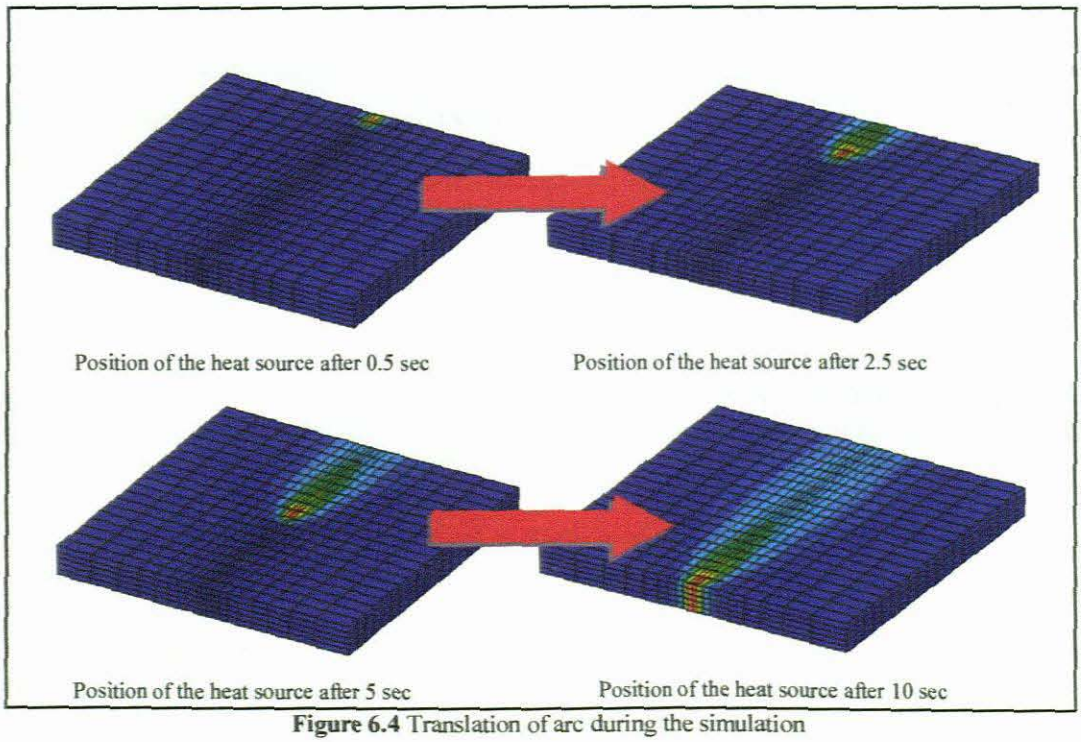

Figure 6.4 Translation of arc during the simulation

As mentioned earlier the formation of kerf width is dependent on the magnitude of the HAZ. Figure 6.2 gives an indication of the translation of a typical plasma arc across a plate at certain time intervals. The results from the simulations are given in detail in Appendix A.

Table 6.1 - 6.3 gives the range of the variables selected for the simulations. This should be read in conjunction with Tables 4.1-4.3.

Table 6.1 Range of Arc Current and Cutting Velocities for 5 mm plate

Plate Thickness (mm)	Cutting Current (Amps)	V_{min} (mm/sec)	V_{max} (mm/sec)
5	30	15	20
5	60	20	40
5	90	25	55
5	120	30	75

Table 6.2 Range of Arc Current and Cutting Velocities for 10 mm plate

Plate Thickness (mm)	Cutting Current (Amps)	V_{min} (mm/sec)	V_{max} (mm/sec)
10	30	5	10
10	60	10	20
10	90	15	30
10	120	15	40

Table 6.3 Range of Arc Current and Cutting Velocities for 20 mm plate

Plate Thickness (mm)	Cutting Current (Amps)	V_{min} (mm/sec)	V_{max} (mm/sec)
20	30	5	5
20	60	5	10
20	90	5	15
20	120	10	20

The results presented in Appendix A represent the HAZ from the thermal analysis and the corresponding kerf details i.e. width and depth of the kerf for the settings as specified in the title block adjacent to each figure.

It can be clearly seen in Fig A1.1-27 that there is an increase in size and magnitude of the HAZ with increasing current for the 5mm plate. The 5mm plate has been used in the experimental verification due to the current limitation of the PAC unit. Figure A2.1-12 and A3.1-12 represents the results for the 10mm and 20mm plates respectively. When studying the computational output it can be seen that the theory holds.

The Equilibrium diagram shows that the austenitic phase of the material reaches molten state at a temperature of approximately 1550 degrees Celsius. For the simulations we have allowed for an increase of 10%, thus the temperature indicating fully molten state is approximately 1750 degrees Celcius. The results of these simulations are graphically represented in the figures below. These figures show the maximum temperature and kerf width (in millimetres) versus the cutting current (in Amperes) at various constant velocities. For increased energy density the width of the kerf increases as expected. It should be noted that for increasing concentration of current density, as mentioned

earlier, the heat affected zone and consequently the kerf width increases. There exists, in reality, a maximum kerf width for any particular thickness of plate, which cannot be exceeded since the metal is removed once it has reached molten state. The simulations however, have been conducted and unrealistic kerf widths have been obtained but this data is used to obtain functions governing the specific process variable discussed. This can be further justified by the fact that the objective is to determine the minimum energy required to cut the plate and to determine the resulting kerf size.

Curve 4+ has been used to extract functions for the relationships. The best fit to 25 functions is selected and the values are forecasted to the desired range. The forecasted data has been plotted and an error of ± 5% can realistically be taken into account.

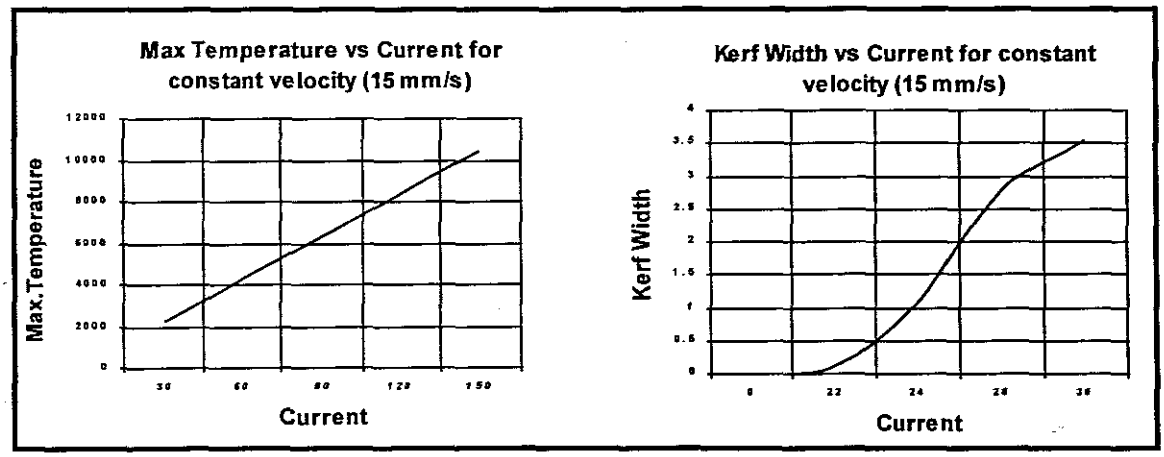

Figure 6.5 Max. temp. and kerf width Vs current for constant velocity of 15m/sec

The left graph of Fig. 6.5 indicates the maximum temperature which will be located at the center of the arc. Considering the previous discussion regarding the minimum temperature required for total molten status under the said operating conditions (voltage, nozzle diameter and standoff) and for constant velocity of 15mm/s, the minimum current required to cut the 5mm plate shall be 23 amps. Considering the graph on the right of Fig 6.5 the corresponding kerf width for the same operating conditions would be 1.1mm. This also is the minimum kerf width obtainable for this voltage and speed setting.

The graphs represented by Figs 6.5-6.8 have been used to extract mathematical functions which can now be used to predict the maximum temperatures and the corresponding kerf widths for any given cutting current at the specified constant cutting voltage and speed.

For the relationship of maximum temperature and varying current for the constant velocity of 15mm/s for the plasma arc cutting of 5mm thick plates with the material specification as given in Appendix C and the said operating variable settings the following Eq. 6.1 has been determined. θ and I represents the maximum temperature and the cutting current respectively.

$$\theta = a + bI \tag{6.1}$$

where $a = 181.23$ and $b = 68.3$.

For the kerf width and current relationship depicted in Fig. 6.5

$$K_w = a + b \ln I \tag{6.2}$$

where $a = -33.9118$ and $b = 11.007$, K_w and I represents the kerf width and current respectively.

The following Table 6.4 gives the required cutting current and corresponding kerf width for the specified cutting speed for the 5mm model. The figure number indicates the relevant graphs. The Equation numbers refers to the relevant Equations for the temperature vs. current and kerf vs. current relationships.

Table 6.4 Predicted current and kerf width for specified velocity for 5mm plate

Figure	Cutting Speed (mm/s)	Cutting Current (Amps)	Temp ($^{\circ}C$)	Kerf Width (mm)	Equ. No. for Temp vs Current	Equ. No. for Kerf vs Current
6.6	15	23	1750	1.10	6.1	6.2
6.7	25	36	1750	1.44	6.3	6.4
6.8	35	48	1750	1.40	6.5	6.6
6.9	75	93.5	1750	1.70	6.5	6.6

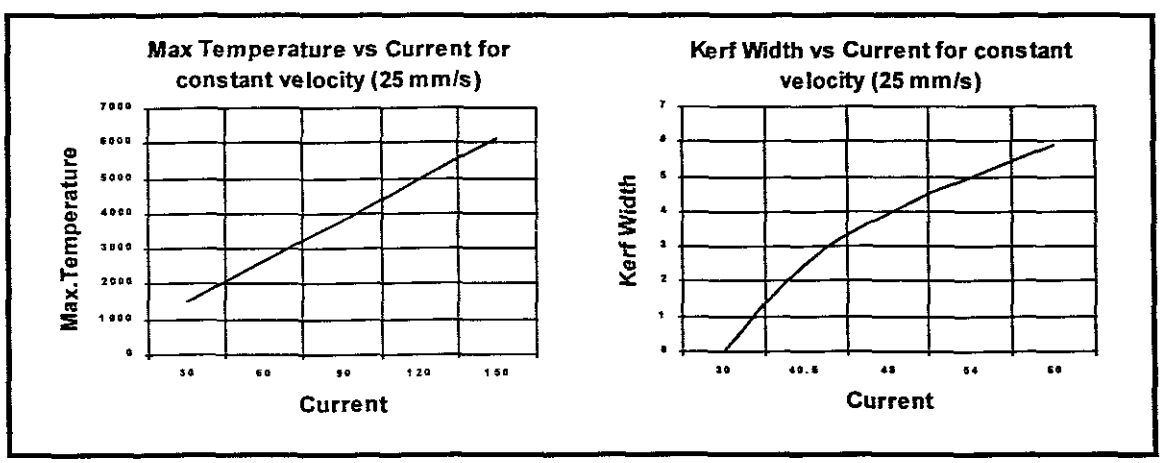

Figure 6.6 Max. temp. and kerf width Vs current for constant velocity of 25m/sec

From Fig. 6.6 Eq. 6.3 defines the relationship between the maximum temperature and cutting current for constant cutting velocity of 25mm/s.

$$\theta = a + bI \tag{6.3}$$

where $a = 374.83$ and $b = 38.39$.

For the kerf width and current relationship depicted in Fig. 6.6

$$K_w = a + b \ln I \tag{6.4}$$

where $a = -29.85$ and $b = 8.73$.

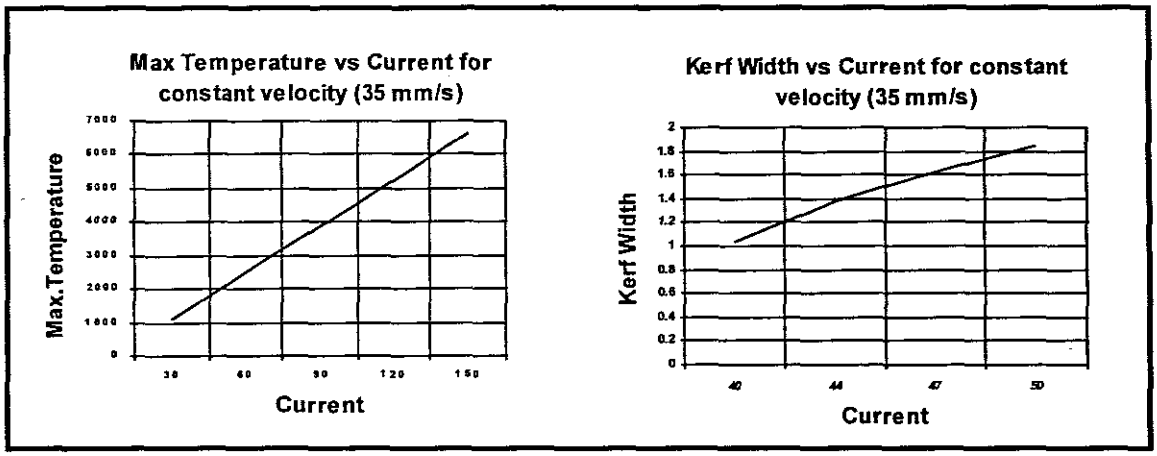

Figure 6.7 Max. temp. and kerf width Vs current for constant velocity of 35m/sec

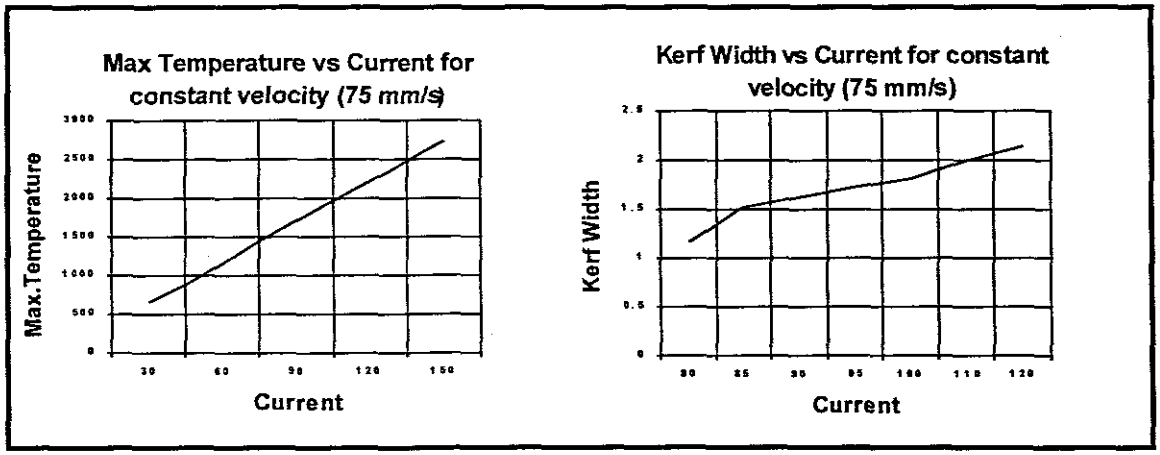

Figure 6.8 Max. temp. and kerf width Vs current for constant velocity of 75m/sec

From Fig. 6.7 and 6.8 Eq. 6.5 defines the relationship between the maximum temperature and cutting current for constant cutting velocity of 35mm/s and 75mm/s is also given by

$$\theta = a + bI \tag{6.5}$$

where $a = -251.81$ and $b = 45.82$ for Fig 6.7, and $a = 140.72$ and $b = 17.22$ for Fig. 6.8.

Similarly, for the kerf width and current relationship depicted in Fig. 6.7 and 6.8 for 35mm/s and 75mm/s respectively can be given by

$$K_w = a + b \ln I \tag{6.6}$$

where $a = -12.38$ and $b = 3.64$ for Fig 6.7, and $a = -6.55$ and $b = 1.82$ for Fig 6.8.

The graphical representations of the computational outputs for the 10mm plate are shown in Appendix B. Table 6.5 gives an indication of the effects of an increasing cutting current for constant cutting speed for the 10mm plate. The minimum required energy needed to cut the plate and the resulting kerf widths are presented. The graphs describing the relationships of the maximum temperature vs. current and kerf width vs. current are given in Appendix B.

Table 6.5 Predicted current and kerf width for specified velocity for 10mm plate

Figure No.	Cutting Speed (mm/s)	Cutting Current (Amps)	Maximum Temperature ($^{\circ}C$)	Kerf Width (mm)
B.1	5	10	1750	4.2
B.2	10	16.5	1750	2.2
B.3	15	26	1750	1.95

6.2.2 Cutting Speed

The cutting speed is defined as the rate of arc travel with respect to the work piece. This variable affects the rate of production as well as the quality of the cut (as discussed in Chapter 4). The HAZ also changes with changing cutting speeds. The lower the cutting speed (for constant current) the greater the HAZ and consequently the larger the molten metal bath volume (see Fig. 6.10). This results in a wider kerf. The higher the cutting speed (for constant current) the smaller the HAZ and molten metal bath volume. This results in a narrower kerf (see Fig. 6.9).

The range of cutting speeds have been determined for each thickness using Eq. 4.1 and 4.3. The calculated range of speeds falls within the range of values given by the manufacturer of the plasma arc cutting unit, PCA 30/60, which is the unit used for the experimental verification. Tables 4.1-4.3 represents the range of arc currents and the respective cutting speeds for each plate thickness. The cutting velocities used in the simulations, range from the said minimum to maximum value in increments of 5. The minimum and maximum values have been decreased and increased to the next integer being a factor of 5. This is done to evaluate the validity of Eq. 4.1 and 4.2 defining the dross free cutting speed window during the experiments.

The cutting speed is dependent on plate thickness and the range varies for a particular plate thickness with varying current. It can be clearly seen that there is a decrease in size and magnitude of the HAZ with increasing cutting speed at constant current. Due to the increase in travel speed the localized heating is reduced, this results in a much narrower HAZ. Consequently, the kerf width reduces as the cutting speed increases for constant current.

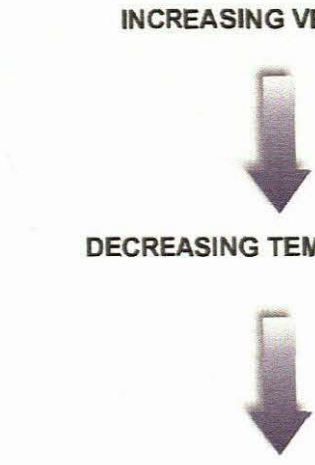

Figure 6.9 Diagram for increasing velocity

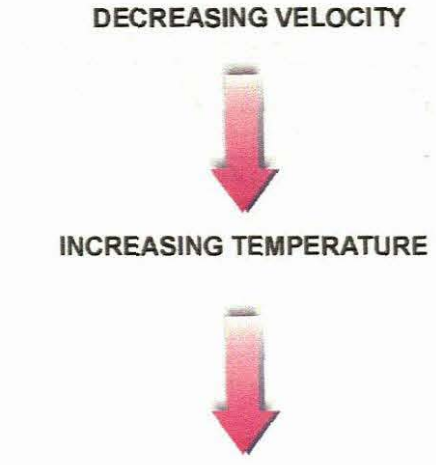

Figure 6.10 Diagram for decreasing velocity

The results presented in Appendix A represent the HAZ from the thermal analysis and the corresponding kerf details i.e. width and depth of the kerf for the settings as specified in the title block adjacent to each figure. It can be clearly seen in Fig A1-A27 that there is a decrease in size and magnitude of the HAZ with increasing cutting speed for the 5mm plate. Figure A2.1- 2.12 and A3.1-3.12 represents the results for the 10mm and 20mm plates respectively. The results of these simulations are graphically represented in figures below. These figures show the maximum temperature and kerf width (in mm) versus the cutting speed (in mm/s) at various constant current settings. The computational output compares well with the theoretical concept.

The graphs represented by Figs 6.11-6.14 have been used to extract mathematical functions which can now be used to predict the maximum temperatures and the corresponding kerf widths for any given cutting speed at the specified constant cutting voltage and current.

Figure 6.11 represents the graphs for constant current of 30Amps and varying velocity.

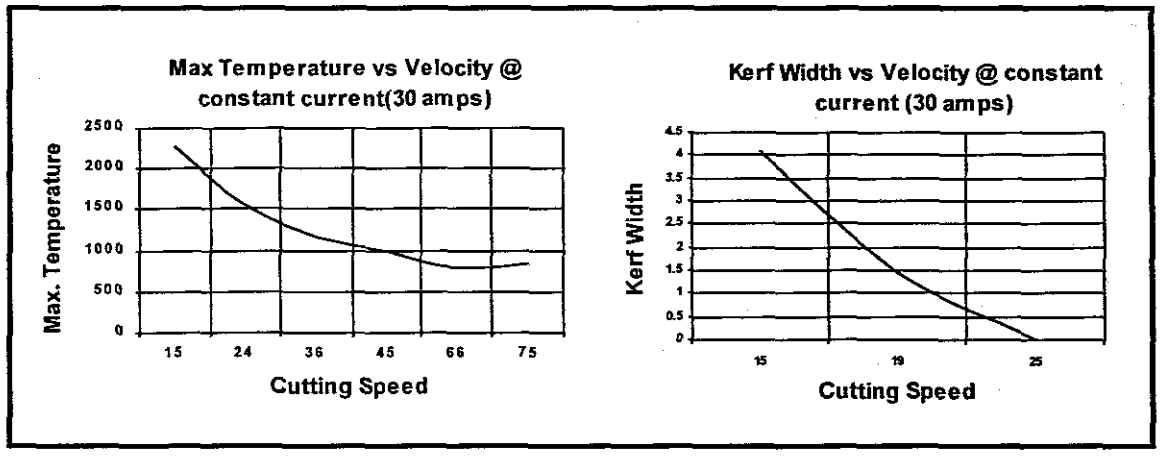

Figure 6.11 Max. temp. and kerf width Vs speed for constant current of 30Amps

Figure 6.11 (left) indicates the maximum temperature which will be located at the center of the arc. Considering the previous discussion regarding the minimum temperature required for total molten status under the said operating conditions (voltage, nozzle diameter and standoff) and for constant current of 30Amps, the minimum cutting velocity required to cut the 5mm plate shall be 21mm/s. Considering Fig. 6.11 (right) the corresponding kerf width for the same operating conditions would be 0.8mm. This also is the minimum kerf width obtainable for this voltage current and speed setting.

For the above relationship of maximum temperature and varying cutting velocity for the constant current of 30Amps for the plasma arc cutting of 5mm thick plates with the material specification as given in Table C.1 and the said operating variable settings the following Eq. 6.7 has been determined. θ and V represents the maximum temperature and the cutting velocity respectively.

$$\theta = a + \frac{b}{V} \tag{6.7}$$

where $a = 346.44$ and $b = 29048.45$

For the kerf width and velocity relationship depicted in Fig 6.11

$$K_w = a + \frac{b}{V} + \frac{b}{V^2} \tag{6.8}$$

where $a = 1.72$, $b = -157.07$ and $c = 2887.86$, K_w and I represents the kerf width and velocity respectively. The graph is defined for the domain $0 - 25$mm/s.

The following Table 6.7 gives the required cutting velocity and corresponding kerf width for the specified cutting current for the 5mm model. The figure number indicates

the relevant graphs. The equation numbers refers to the relevant Equations for the temperature vs. velocity and kerf vs. velocity relationships.

Table 6.6 Predicted speed and kerf width for specified current for 5mm plate

Figure	Cutting Current (Amps)	Cutting Speed (mm/s)	Temp (°C)	Kerf Width (mm)	Eq. No. for Temp vs Current	Eq. No. for Kerf vs Current
6.11	30	21	1750	0.8	6.7	6.8
6.12	60	44	1750	1.4	6.9	6.10
6.13	90	72	1750	0.31	6.11	6.12
6.14	120	120	1750	0.35	6.13	6.14

From Fig. 6.12 Eq. 6.9 defines the relationship between the maximum temperature and cutting velocity for constant cutting current of 60Amps.

$$\theta = a + \frac{b}{V} \tag{6.9}$$

where $a = 503.82$ and $b = 56034.37$.

For the kerf width and velocity relationship depicted in Fig . 6.12

$$K_w = ae^{bV} \tag{6.10}$$

where $a = 27.37$ and $b = -0.067$.

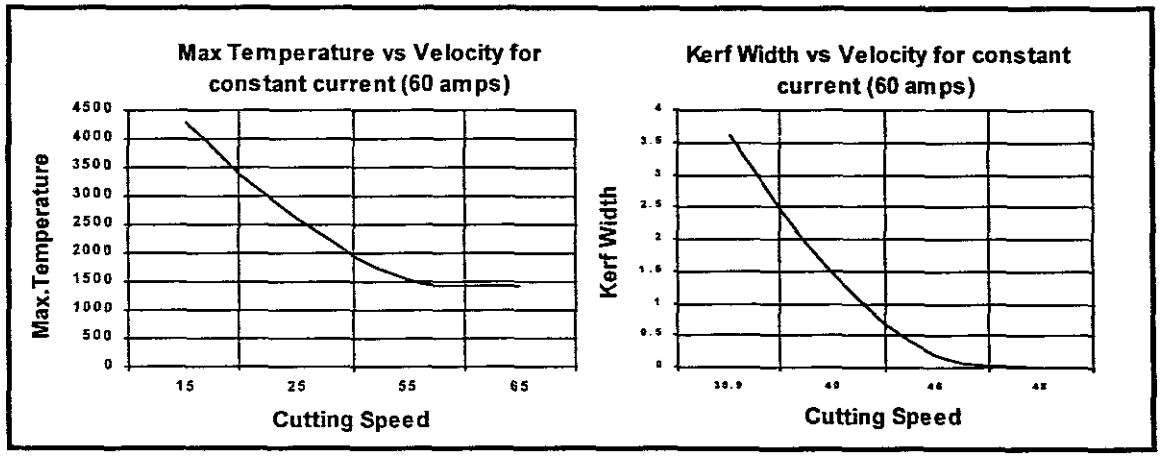

Figure 6.12 Max. temp. and kerf width Vs speed for constant current of 60Amps

From Fig. 6.13 Eq. 6.11 defines the relationship between the maximum temperature and cutting velocity for constant cutting current of 90Amps.

$$\theta = ab^{V} \tag{6.11}$$

where $a = 8026.55$ and $b = 0.98$.

For the kerf width and velocity relationship depicted in Fig. 6.13

$$K_w = ae^{bV} \tag{6.12}$$

where $a = 51.15$ and $b = -0.071$.

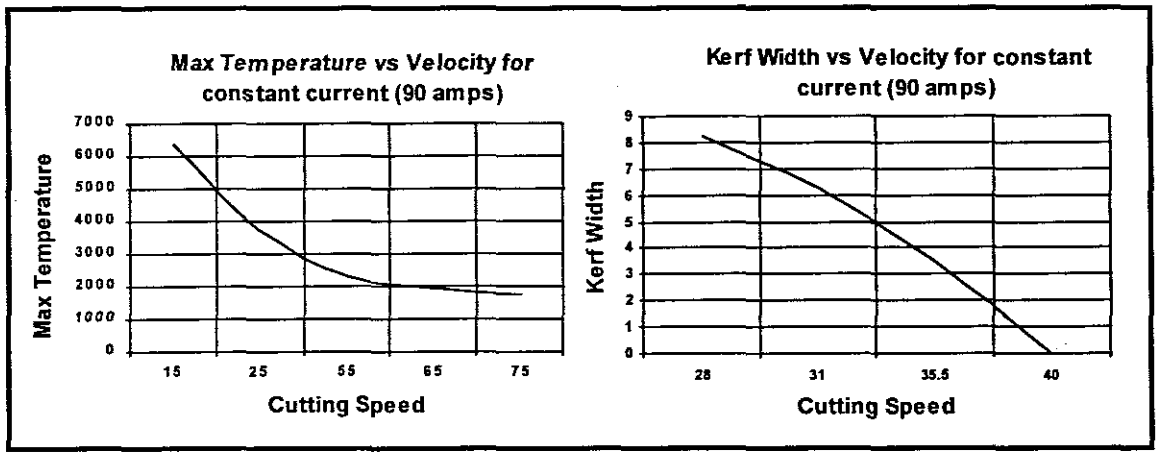

Figure 6.13 Max. temp. and kerf width Vs speed for constant current of 90Amps

From Fig 6.14 Eq. 6.13 defines the relationship between the maximum temperature and cutting velocity for constant cutting current of 120Amps.

$$\theta = a + \frac{b}{V} \tag{6.13}$$

where $a = 860.06$ and $b = 112072.15$.

For the kerf width and velocity relationship depicted in Fig. 6.14

$$K_w = ae^{bV} \tag{6.14}$$

where $a = 37.43$ and $b = -0.037$

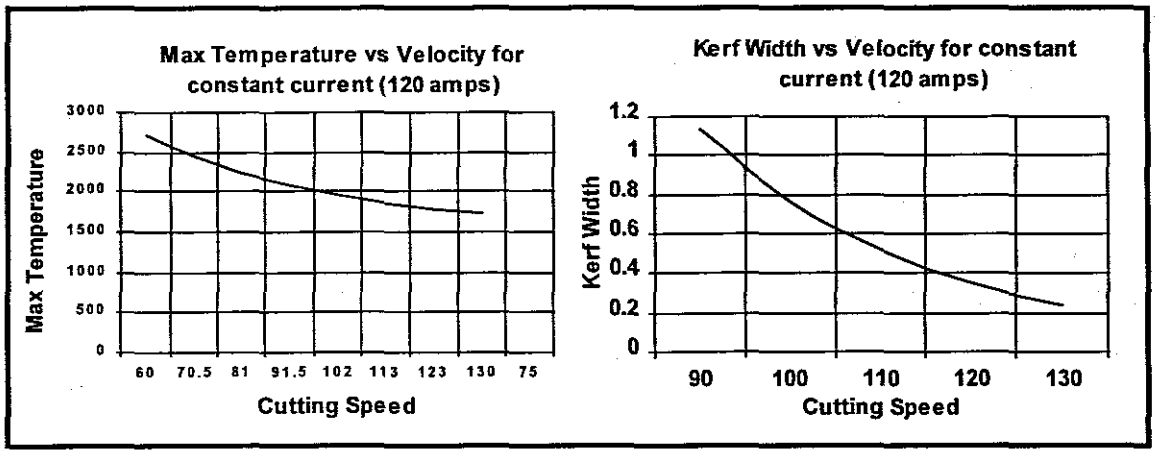

Figure 6.14 Max. temp. and kerf width Vs speed for constant current of 120Amps

The graphical representation of the computational outputs for the 10mm are shown in Appendix B. Table 6.8 gives an indication of the effects of an increasing cutting velocity for constant cutting current for the 10mm plate. The minimum required energy needed to cut the plate and the resulting kerf widths are presented. The graphical representations of the relationships of the maximum temperature vs. velocity and kerf width vs. velocity are given in Appendix B. The results for the simulations for the 20mm plate are presented in Appendix A3. The same exercise as described in this chapter can be followed to extract the results.

Table 6.7 Predicted speed and kerf width for specified current for 10mm plate

Figure No.	Cutting Current (Amps)	Cutting Speed (mm/s)	Maximum Temperature (°C)	Kerf Width (mm)
B.4	30	16.8	1750	2.96
B.5	60	30	1750	2.37
B.6	90	50	1750	3.55
B.7	120	80	1750	0.55

When studying Tables 6.6 and 6.7 it is clear that for constant current and increasing thickness, the cutting velocity decreases.

Chapter 7

Experimental Verification

7.1 Introduction

The plasma arc cutting experiments were performed at the Welding and Cutting Research Laboratory at the Peninsula Technikon.

The objective of the cutting experiments was to verify the numerical results obtained from the simulations for the 5mm plate. The verification of the model with respect to the minimum energy required, in particular, to cut a plate and the maximum allowable cutting rate is presented. The kerf widths produced from the induced HAZ have been measured to evaluate the accuracy of the results obtained from the numerical model The characteristics of the cut quality has also been assessed to validate the incorporation of Eqs. 4.1 and 4.3 into the model to guarantee dross free cuts.

7.2 Cutting Experiments

The results presented in this chapter were obtained using a PCA 30/60 plasma arc cutting system operating with a cutting torch having a nozzle of 1.5mm exit bore diameter. Air is used as the plasma gas that flows under pressure (6 bar) from the upstream chamber around the cathode and through the nozzle towards the workpiece. The test set-up is shown in Fig. (7.1).

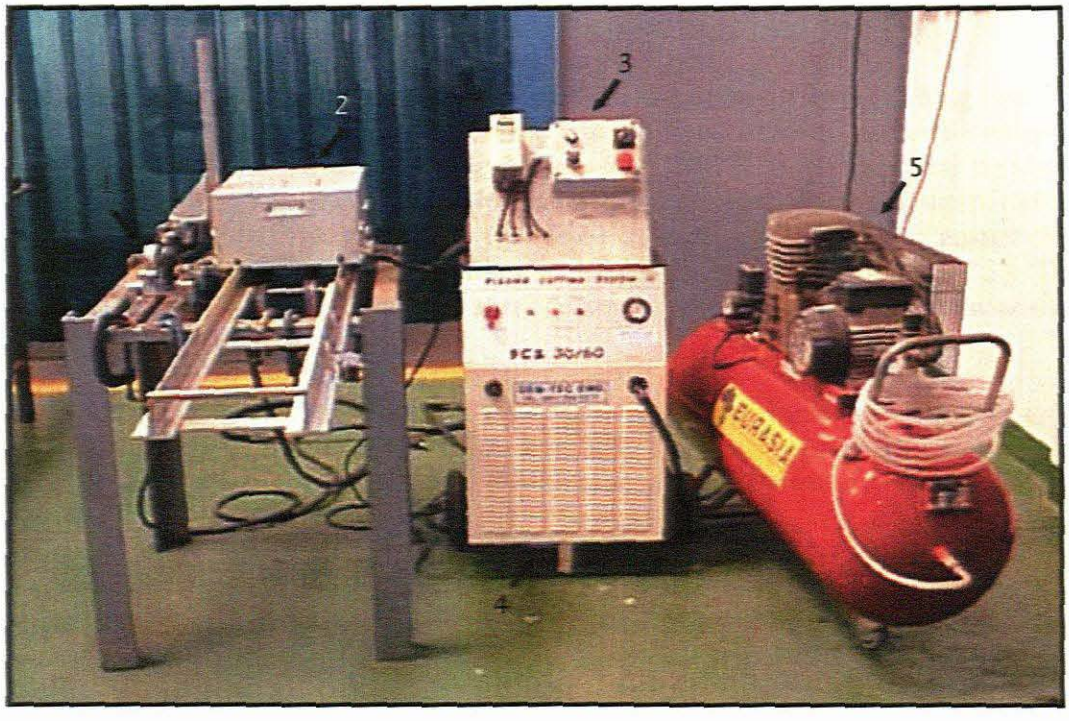

Figure 7.1 Experimental setup

The torch, workpiece and clamping configuration is indicated by "1" in Fig. 7.1 and is shown in more detail in Fig. 7.2. The linear transfer unit and the speed control unit is indicated by "2" and "3". The plasma arc cutting unit PCA 30/60 and the compressor is indicated by "4" and "5".

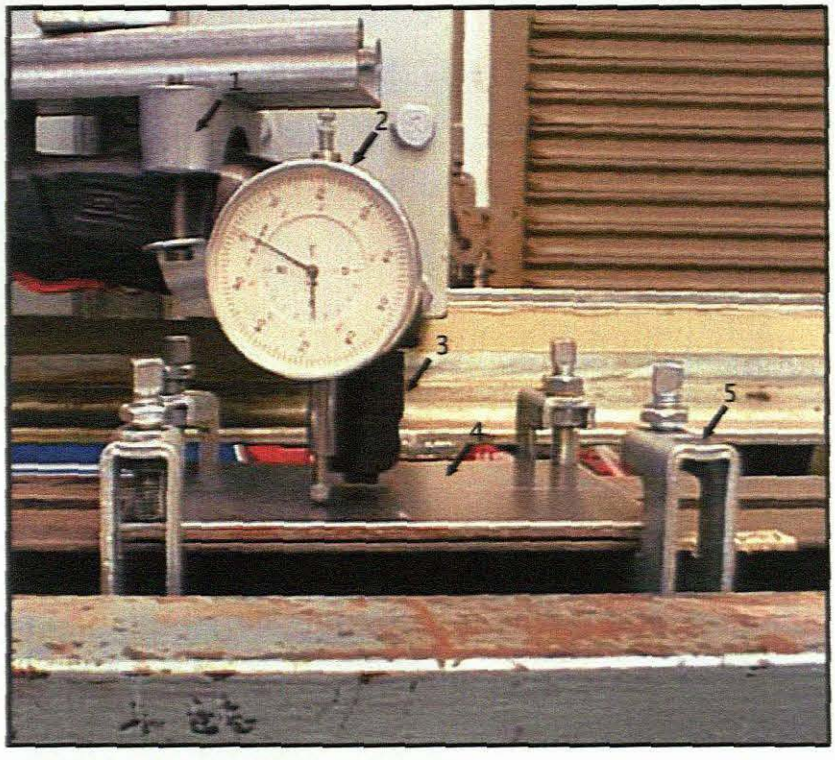

Figure 7.2 Nozzle and workpiece setup

The torch was securely fixed to prevent vibration and movement during cutting (see "1" Fig. 7.2). A dial gauge was fitted to ensure that the torch stand-off distance remained constant for the duration of the cutting process (see "2" Fig. 7.2). The torch stand-off distance was set at 0.9mm from the workpiece to correspond with the assumptions in the numerical model The workpiece was fixed in such a manner as to ensure that minimum heat was lost due to thermal contact conductance (see "5" Fig. 7.2). The workpieces (see "4" Fig. 7.2) were all stress relieved through a heat treatment process as specified by the supplier.

A digital photo/contact tachometer was attached to the linear cutting device to accurately measure the cutting speed (see Fig. 7.3). This device enables an accuracy of $\pm$ 0.05%. The surface speed test wheel was aligned to the linear cutting unit's track (see "1" Fig 7.3)

A photo showing the cutting process is shown in Fig. 7.4. A test run was conducted before each actual cut (without initiation of the arc) to ensure cutting speed setting and constant standoff distance was maintained

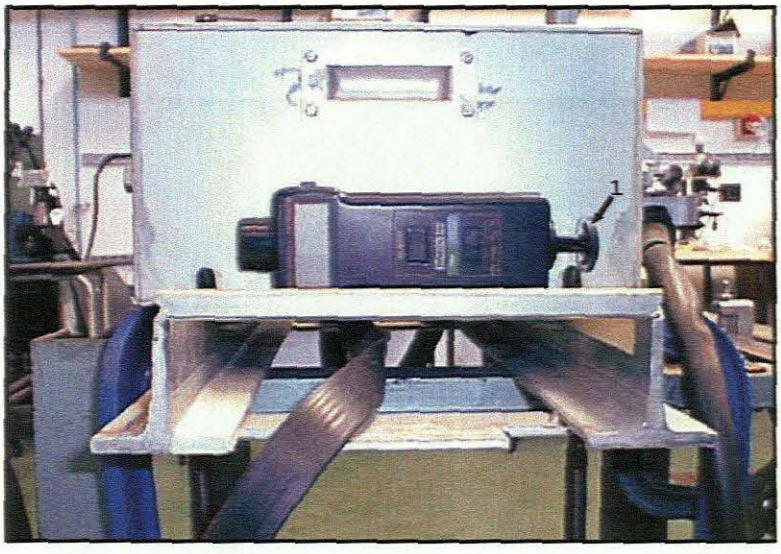

Figure 7.3 *Digital photo tachometer setup*

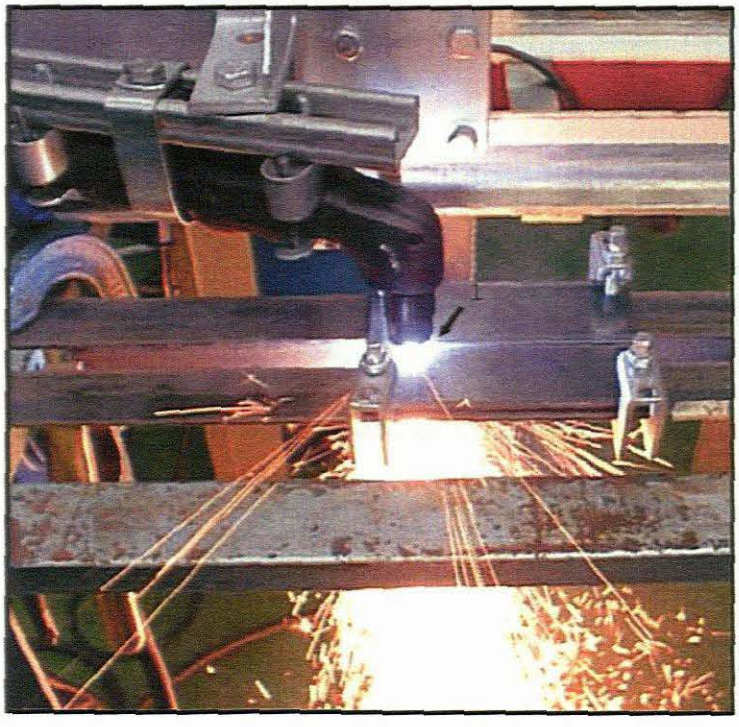

Figure 7.4 Image of actual cutting process

The test pieces selected for the experiment were of the following dimensions: group 1 – 100 x 150 x 5mm. The material that was used for these experiments is known as ROQ-TUF-690 and is the South African equivalent for the material specified in Table C.1. The surfaces of the plates were polished even though the plasma arc cutting process does not place any requirements on the condition of the plate surface.

The kerf widths were measured using a shadowgraph optical projector (see Fig. 7.5)

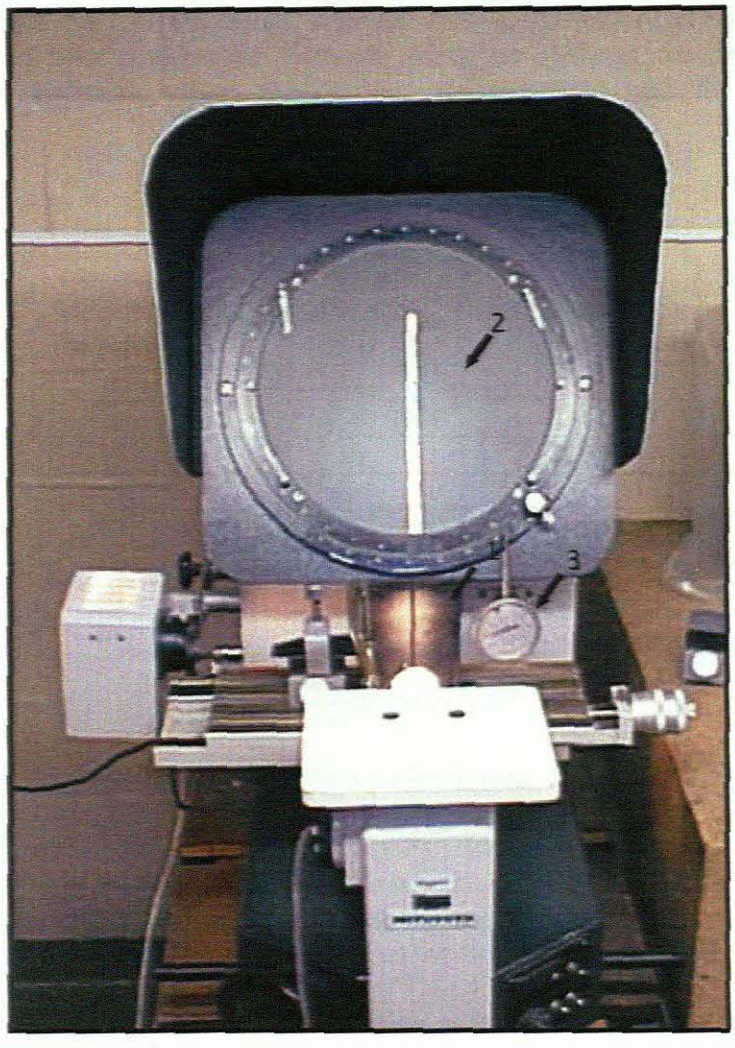

Figure 7.5 Shadowgraph with workpiece fixed in position

Operation of the Shadowgraph

The projector casts a shadow on the contour and surface details of the workpiece onto a screen with a magnified image of 5, 10, 20 or 50 times the full size (see "2" Fig 7.5). A micrometer stage is mounted on the base of the machine and is located between the projector lens and the condenser lens. The workpiece to be measured is placed on the stage (see "1" Fig 7.5) and the shadow focused on the screen. Cross lines on the screen provides reference points and measurements can be taken by moving the shadow across from one edge to another and noting the readings on the micrometer heads which are used to move the stage (see "3" Fig 7.5).

7.3 Verification of Numerical Results obtained for Kerf Widths

The data in Table 7.1 gives the details of the specimen's dimensions, number of repetitions for each experiment, the process variable parameter settings and the resulting kerf width. This data is compared with the simulated numerical result. Also the numerical kerf widths extracted from the functions obtained for process settings satisfying the minimum energy requirements are compared with the experimental results.

Table 7.1 Table of process settings and comparison of experimental and numerical results for 5mm plate

Cutting Current (Amps)	Cutting Velocity (mm/s)	Experiment 1 Kerf Width (mm)	Experiment 2 Kerf Width (mm)	Numerical Result Kerf Width (mm)
30	5	3.51	3.48	4.7
30	10	3.33	3.34	4.5
30	15	3.10	3.06	4.1
30	21	0	0	0.8
60	25	2.90	2.83	5.5
60	35	2.11	2.07	2.5
60	40	1.71	1.73	1.9
60	44	1.05	0.97	1.4

The results of the experiment compares relatively well with the numerical result for certain settings where the percentage error for the kerf widths ranging from 10 to 20%. These errors could be due to the efficiency (80%) selected in the model. The corrective action would be to input a range of efficiencies in the shell script and run these simulations. When assessing the output the simulation predicting a kerf width closest to the experimental result would be considered as the most accurate model.

In some cases the error percentage was as high as 40% but this is due to fact that for excess energy input into the model an unrealistic kerf width is obtained. However, the objective is to validate the accuracy of the numerical result indicating the minimum energy required to cut the plate.

Another issue to consider in the experimental setup that could influence the acquired result is the fact that the assumption is made that the input current is as specified. If, for example, the actual current input were 25Amps instead of 30Amps this would not give an accurate comparison with the simulated result since the energy input would obviously be lower than the simulated process.

It was not possible to execute experiments to assess the numerical results obtained for the required current settings for some constant velocity since the plasma arc cutting unit did not provide the option to vary the current between 30 and 60 Amps.

7.4 Quality Assessment of the Cut

An assessment of the quality of the cut was conducted with respect to dross formation, smoothness and top edge squareness. The following figures represents a plasma arc cut with the velocity and current setting of 44mm/s and 60Amps.

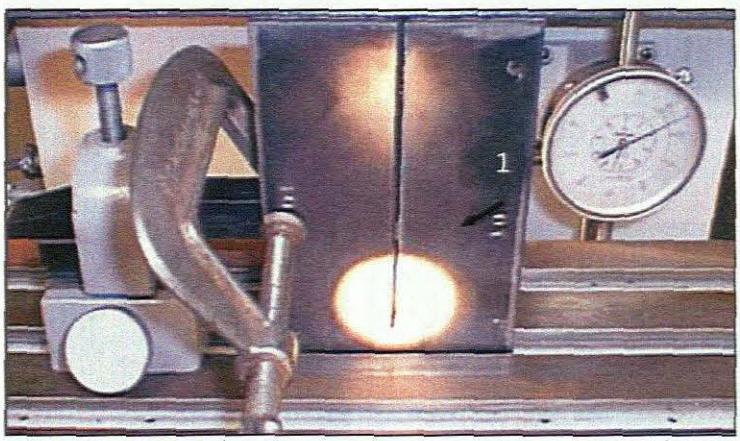

Figure 7.6 Workpiece (current: 60Amps and velocity: 44mm/sec)

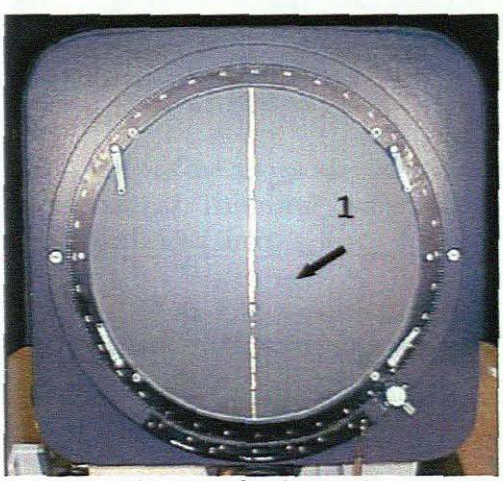

Figure 7.7 Shadowgraph

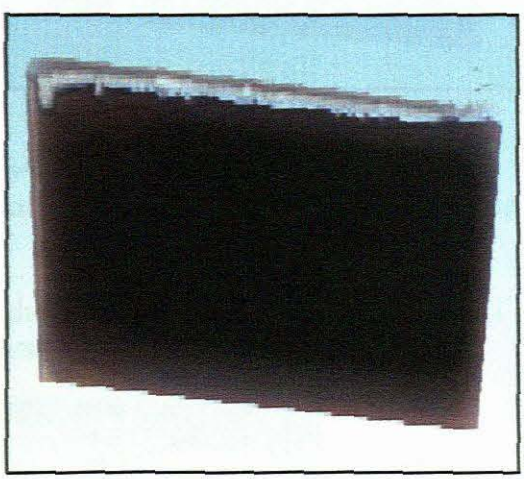

Figure 7.8 Image of dross formation

Figure 7.7 shows the image of the plate (Fig. 7.6)as projected by the shadowgraph. The plate was severed throughout it's thickness but with the formation of high-speed dross. Fig. 7.8 gives an indication of the dross formation. High speed dross is much harder and the removal would require an additional manufacturing process.

The results for the process settings for current and velocity being 60Amps and 35mm/s are given in the following page.

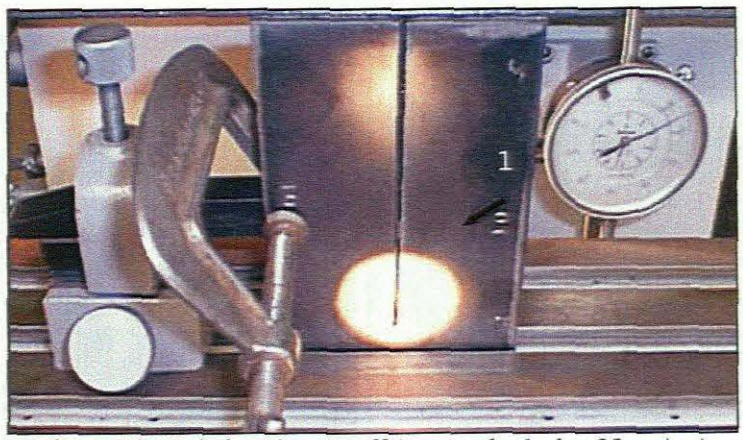

Figure 7.9 Workpiece (current: 60Amps and velocity: 35mm/sec)

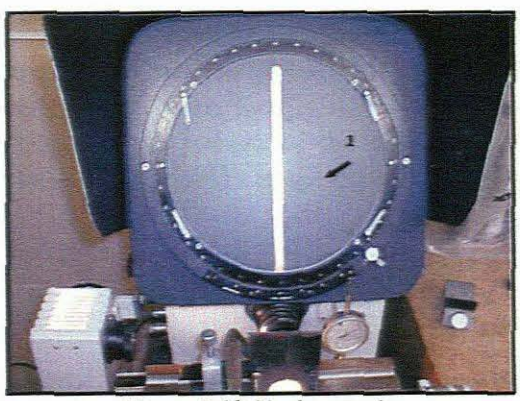

Figure 7.10 Shadowgraph

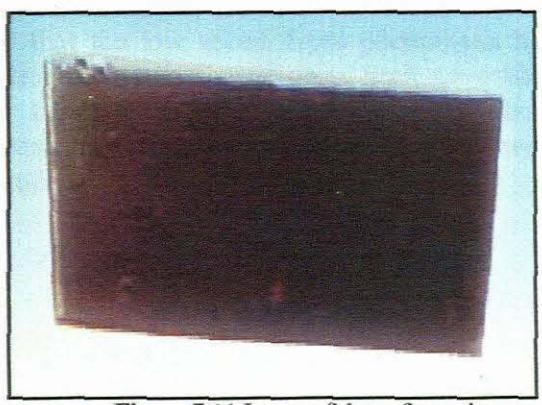

Figure 7.11 Image of dross formation

The quality of the above specimen conformed to the requirements of a high quality plasma arc cut. This results validates the incorporation of the equations governing the high speed dross limit.

Figures 7.12 to 7.14 represents results of the experiment for the process settings for current and velocity being 60Amps and 20mm/s respectively.

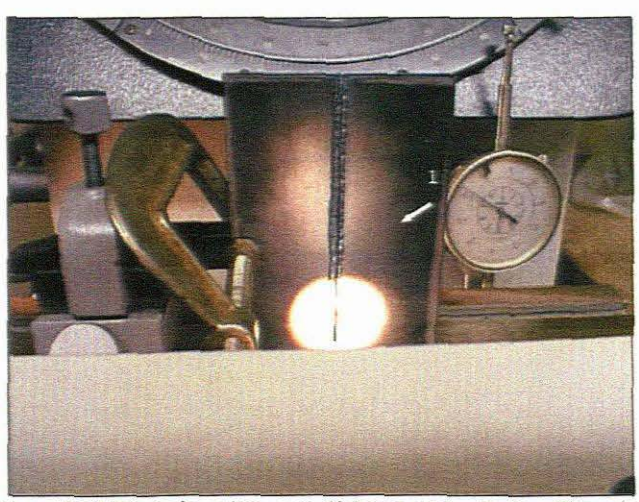

Figure 7.12 Workpiece (current: 60Amps and velocity: 20mm/sec)

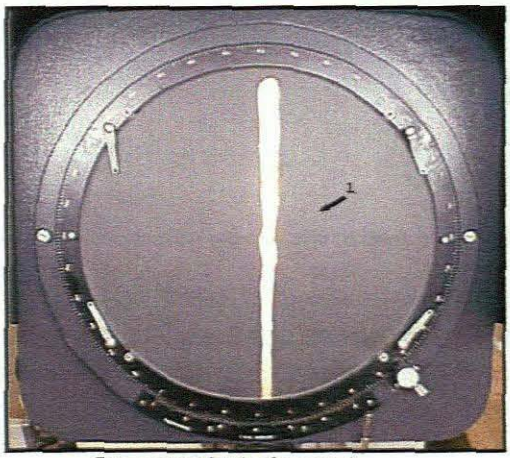

Figure 7.13 Shadowgraph

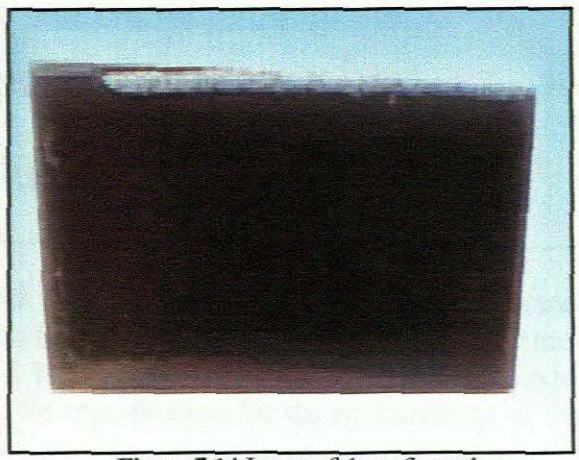

Figure 7.14 Image of dross formation

It is clearly evident in Figs.7.12 and 7.14 that the low speed dross phenomena has occurred. This also validates the incorporation of the low-speed dross limit governing equation as given by Eq. 4.3 in Chapter 4. Low speed dross usually does not adhere tightly to the bottom of the plate and is easily removed by scraping. This however, presents bottlenecks in the manufacturing process.

Chapter 8

Conclusion

The aim of this thesis is to establish a virtual model for the plasma arc cutting process. The modelling of the PAC process is done so in the framework of the proposed thermo-mechano-metallurgical theory as proposed by Ronda and Oliver [30]. The model provides a means of achieving process variable specification for the optimization of the energy input for the PAC process. This is achieved by conducting parametric sensitivity analysis. The objectives of this optimization are to determine the kerf width, and process parameters for optimal energy input. The PAC operating parameters included current, speeds of arc and plate thickness as variables in this analysis.

Plasma cutting is modeled in the framework of the thermo-mechano-matallurgical (TMM) problem. However, the analysis is restricted to a thermo-metallurgical analysis through the introduction of the artificial phase change. Boundary conditions included thermal interactions between plate and environment: conduction, convection and radiation. Heat in-fluxes and out-fluxes are incorporated into the software package using FORTRAN codes

The plasma cutting benchmark is formulated for plates of dimensions 100mm x 150mm x 5mm and 10mm and 20mm x 100mm x 100mm. The plasma arc is modeled by the moving heat source of the bell-shape surface.

The thermo-metallurgical problem has been solved by finite element method using SYSTUS/SYSWELD 2 program. The date-input deck is listed in Appendix D where one of data is the CCT diagram. Data for the steel that is utilized is found in Appendix C. The width of the kerf, shape and size of HAZ, temperature field, material removed determined by solid/liquid phase fractions, for the discussed range of current and speeds have been evaluated by SYSWELD 2.

The incorporation of the models for determining the dross free cutting speed window ensures that the characteristics of the cut conforms to the requirements of a "high quality cut".

The following functions are roughly identified on the basis of the results of the FEM simulations:

1. Current versus versus temperature
2. Current versus width of kerf
3. Cutting speed versus temperature
4. Cutting speed versus width of kerf

These functions can be used for evaluation of the kerf width, temperature, for other values of plasma cutting parameters i.e. variables of identified functions. These results are shown in Tables 6.4-6.7. For the 5mm plate it was found that for constant velocity

and increasing current, the HAZ widens and a larger kerf is produced. An optimum current can be obtained for any given velocity to provide just enough energy to sever the plate with the cut exhibiting "high quality" characteristics. Similarly, for any given current an optimum velocity can be determined to provide a solution to achieve the same objective as stated above. With increasing plate thickness the current, for constant velocity, increases. The velocity decreases for constant current as the plate increases in thickness.

The identified functions can be used in development of plasma on-line robotic systems that can control and maintain the minimum energy input into a plate of a given thickness and a prediction of the kerf width can be made given variations of plasma cutting operating parameters. By maintaining minimum energy input cost savings can be made through energy savings, limiting additional finishing processes and reducing expense of shortening the electrode and nozzle lifetimes.

Numerical results for have been verified by plasma cutting experiments performed at the Welding and Cutting Laboratory of the Peninsula Technikon in Belville with the use of a Plasma cutting unit. The results as shown in Table 7.1 compares relatively well with the experimental data. The efficiency variable needs to be decreased with all other process variables being constant for specified process settings, and the results compared with the experimental data, in order to adjust the model appropriately.

It is thus shown that the use of a virtual model for the PAC process can be useful in that contributions to the manufacturing industry with regard to process settings can be made. These results can be obtained very quickly given the development of simulation optimization as discussed in Chapter 5.

The model presented can be further extended in future works to incorporate plasma pressure and heating effect.

Bibliography

[1] Anderson, C.A., 1987, Comparison between laser, plasma, waterjet, oxygen cutting and other mechanical cutting processes for low thickness (0.5 up to 5mm), Welding in the World, Vol. 25, No. 5 / 6, pp.88-99.

[2] Bathe, K.J., 1982, Finite Element Procedures in Engineering Analysis, Prentice Hall, Englewood Cliffs.

[3] Bergheau, J.M. and Leblond, J.B., Coupling between heat flow, metallurgy and stress-strain computations in steels. The approach developed in the computer code SYSWELD for welding and quenching. Vth Engineering Foundation conference on Modeling of Casting, welding and Advanced Solidification Processes, 17-21 September 1990 – DAVOS (Suisse). FRAMASOFT+CSI, SYSWELD, User's Manual.

[4] Derse, J., 1992, Quality improvements in plasma cutting, Welding in the World, Vol. 30, No. 11/12, pp.305-306.

[5] Engblom, G. and Falck, K., 1992, Trends in materials, welding and cutting, Welding in the World, Vol. 30, No. 7/8, pp.201-209.

[6] Fernicola, R. C., 1994, New oxygen plasma process rivals laser cutting methods, Welding Journal, 73(6), pp.65-69.

[7] Freidman, E., 1978, Analysis of weld puddle distortion, Welding Journal Research Suppl., pp.161-166.

[8] Ghosh, S. K., Beitialarrangoitia, J. E. and Garcia de Vicuna, G. E., 1987, Some physical defects arising in laser, plasma and water jet cutting, Computational Methods for Predicting Material Processing Defects, Ed. M. Preddeleanu, Elsevier Science Publishers, Amsterdam, The Netherlands, pp.133 –159.

[9] Goldak, J.A., Chakravarati and Bibby, M.J., 1984, A few finite element model for welding heat sources, Trans. AIME, Vol. 15B, pp.299-305.

[10] Goldak, J., Oddy, A., McDill, M., Bibby, M.J., House, R. and Chakravarti, A.P., 1986, Progress in computing residual stress and strain in welds, in David, S.A. (ed.) Conf. Proc. Int. Trends in Welding Research, Gatlinburg, U.S.A. pp.1-6.

[11] Harris, I. D., 1989, Abrasive water jet cutting equipment and application, The Welding Institute, paper 48, Oct.-Nov.

[12] Hibbit, H. D., Marcal, P. V., Goldak, J. A. and Watt, D. F., 1988, Coupling transient heat transfer-microstructure weld computations, Acta Metal, Vol. 36, pp.3037-3047.

[13] Johnson, K., Murdock, S.G. and Davis, C.M., 1989, Cutting of ship plate, The Welding Institute, paper 29, Oct.-Nov.

[14] Leblond, J.B., Mottet, G. and Devaux, J.C., 1986, A theoretical and numerical approach to the plastic behaviour of steels during phase transformations of general relations - I derivation of general relations. Journal of the Mechanics and Physics of Solids Vol. 34, pp.395-409.

[15] Leblond J.B., Mottet, G. and Devaux J.C., 1986, A theoretical and numerical approach and numerical approach to the plastic behaviour of steels during phase transformations of general relations - II. Study of classical plasticity in steels foe ideal - plastic phases. Journal of the Mechanics and Physics of Solids Vol. 34. No. 4, pp.411-432.

[16] Leblond J.B., Devaux, J. and Devaux, J.C., 1989, Mathematical modeling of transformation plasticity in steels I : Case of ideal - plastic phases. International Journal of Plasticity, Vol. 5, pp.573-591.

[17] Leblond, J.B., Devaux, J. and Devaux, J.C. 1989, Mathematical modeling of transformation plasticity in steels II : Coupling with strain hardening phenomena. International Journal of Plasticity, Vol. 5, pp.573-591.

[18] Masubuchi, K., 1980, Analysis of welded structures, Pergamon Press, New York.

[19] Nemchinsky, V. A., 1996, Liquid metal movement during plasma arc cutting, Welding Journal, Vol. 75, pp.388–392.

[20] Nemchinsky, V. A., 1997, Dross formation and heat transfer during plasma arc cutting, J, Phys. D: Appl. Phys., Vol 30, pp.2566-2572.

[21] O' Brien, R.L., 1991, Welding Handbook, Eighth Edition, Vol. 2.

[22] Oliver, G. J., 1999, A mathematically consistent fully coupled thermo-mechano-metallurgical model of welding, PhD Thesis, IPPT, Warsaw.

[23] Oliver, G. J., 1994, Modeling of welding using various Constitutive Models of Steel, M.Sc. Thesis, University of Cape Town, Department of Mathematics and Applies Mathematics, Cape Town.

[24] Owen D.R.J. and Hinton, E., 1980, Finite Elements in Plasticity.

[25] Philander, O., Oliver, G.J. and Ronda, J., 1998, Mathematical Modeling of Welding: A study on the sensitivity of welding variables and their effects on residual stress, strain and deformation, 2nd South Africa Conference on Applied Mechanics, pp.781-790.

[26] Philander, O., Oliver, G.J. and Ronda, J., 1998, Mathematical Modeling of Welding: A study on the sensitivity of welding variables and their effects on residual stress, strain and deformation, 32th Solid Mechanics Conference, Zakopane, September 1-5.

[27] Philander, O. and Oliver, G.J., 1997, A study on the sensitivity of welding variables and their effects on the shape and size of heat affected zones, Research Probe, Peninsula Technikon, Vol. 3, No. 6, pp.7-10.

[28] Ramakrishnan, S. and Rogozinski, M W., 1997, Properties of electric arc plasma for metal cutting, J, Phys. D: Appl. Phys., Vol 30, pp.636-644.

[29] Ronda, J., Mahrenholtz, O. and Hamann, R., 1992, Thermomechanical simulation of underwater welding process, Arcive of Applied Mechanics, 62, pp.15-27.

[30] Ronda, J. and Oliver, G. J., 1996, Consistent thermo-mechano-metallurgical model of welding, 1'st South African Conference on Applied Mechanics, pp.61-68.

[31] Ronda, J. and Oliver, G.J., 1998, Comparison of applicability of Various thermo-viscoplastic constitutive models in modeling of welding, Computer Methods in Applied Mechanics and Engineering, 153, pp.195-221.

[32] Ronda, J. and Oliver, G.J., Work done in collaboration with Prof. O. Mahrenholtz.

[33] Ronda, J., Estrin, Y. and Oliver, G.J., 1996, Modeling of Welding – A comparison of a thermo-mechano-metallurgical constitutibe model with a thermo-viscoplastic material model, Journal of Materials Processing Technology 60, Elsevier, pp.629-636.

[34] Ronda, J., Oliver, G.J. and Meinert, N., 1993, Simulation of welding with phase transformation, Proc. Eighth Int. Conf. On Num. Meth. in Thermal Problems, in Lewis, R.W. (ed.), Pineridge Press, Swansea, pp.151-163.

[35] Rosenthal, D., 1946, The theory of moving sources of heat and its appliation to metal treatments, Trans. ASME, Vol. 68, pp.849-865.

[36] Systus\Sysweld User's Manuals. Framasoft + CSI : Framatome Information Systems.

[37] Ueda, Y. and Murakawa, H., 1984, Applications of computer and numerical analysis in welding research, Trans JWRI, Vol. 13, pp.337-346.

[38] Ueda, Y. and Yamakawa, T., 1985, Analysis of thermal elastic - plastic stress and strain during welding by finite element method, Trans. Japan Welding Soc. Vol. 1, pp.899-903.

Appendix A: Simulation Outputs

Simulation Outputs for 5mm Plate: A.1 – A.14

Simulation Outputs for 10mm Plate: A.15 – A.21

Simulation Outputs for 20mm Plate: A.22 – A.27

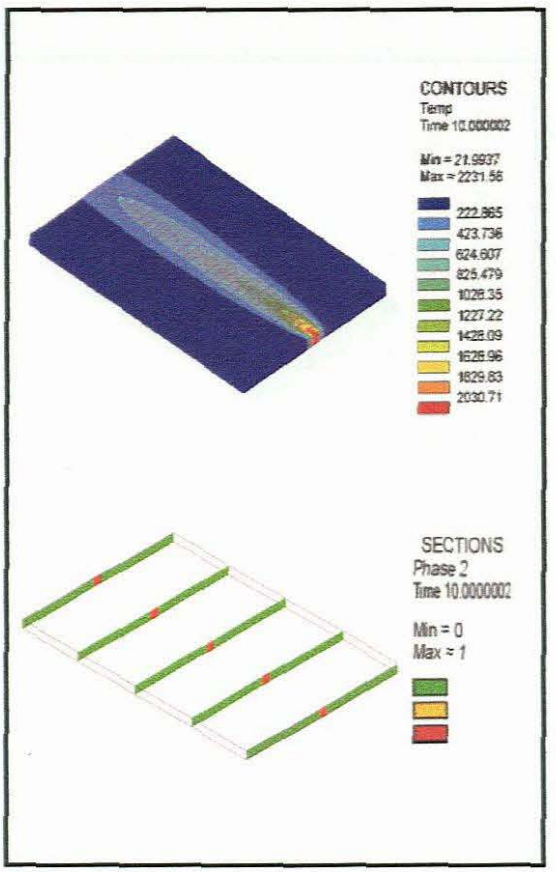

Figure A1.1 – HAZ and Kerf Width for the simulation of Plasma Arc Cuttting of a 5mm plate with the following cutting parameters

Efficiency = 80%
Voltage = 110V
Current = 30
Velocity = 15

Results
1) Thermal Analysis (Top Left)
Max Temperature = 2231.58

2) Thermo-Metallurgical Analysis (Bottom Left)
Kerf Width =4.1mm

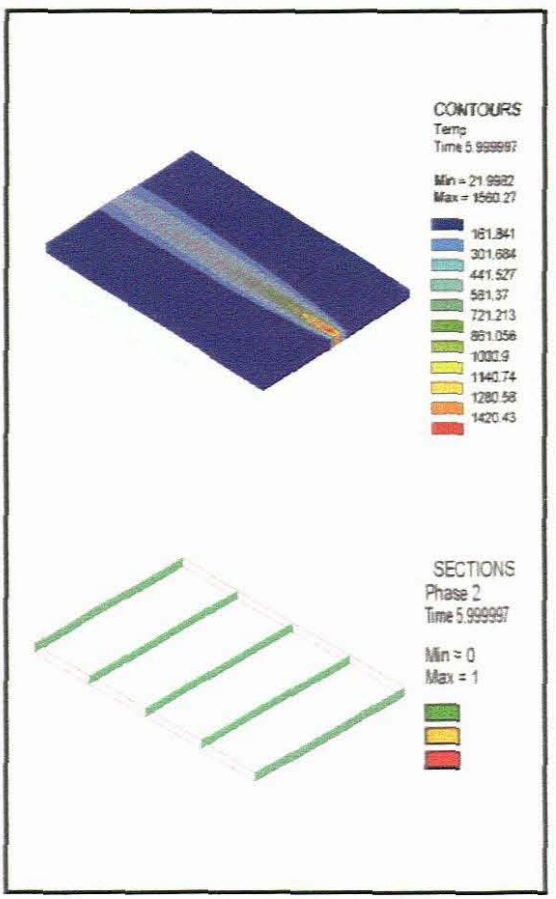

Figure A1.2 – HAZ and Kerf Width for the simulation of Plasma Arc Cuttting of a 5mm plate with the following cutting parameters

Efficiency = 80%
Voltage = 110V
Current = 30
Velocity = 25

Results
1) Thermal Analysis (Top Left)
Max Temperature = 1560.27

2) Thermo-Metallurgical Analysis (Bottom Left)
Kerf Width =0mm

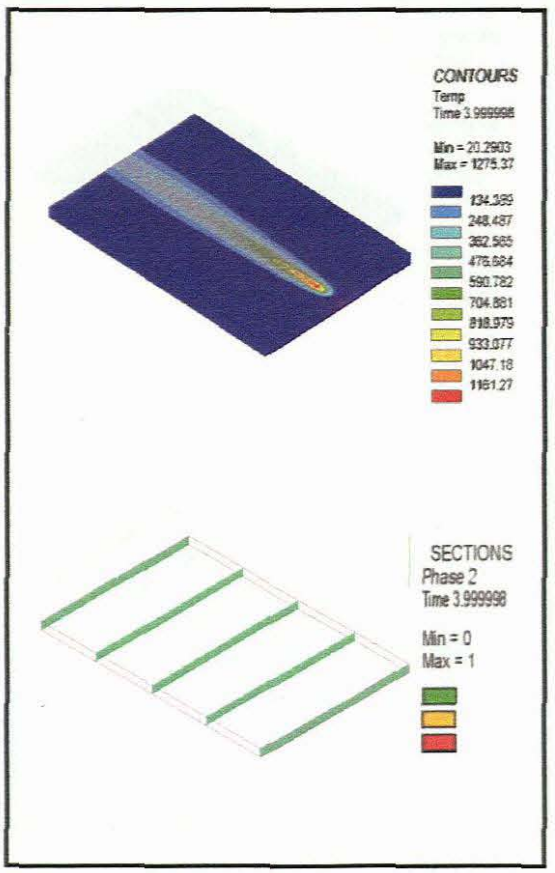

Figure A1.3 – HAZ and Kerf Width for the simulation of Plasma Arc Cuttting of a 5mm plate with the following cutting parameters

Efficiency = 80%
Voltage = 110V
Current = 30
Velocity = 35

Results
1) Thermal Analysis (Top Left)
Max Temperature = 1275.37

2) Thermo-Metallurgical Analysis (Bottom Left)
Kerf Width = 0mm

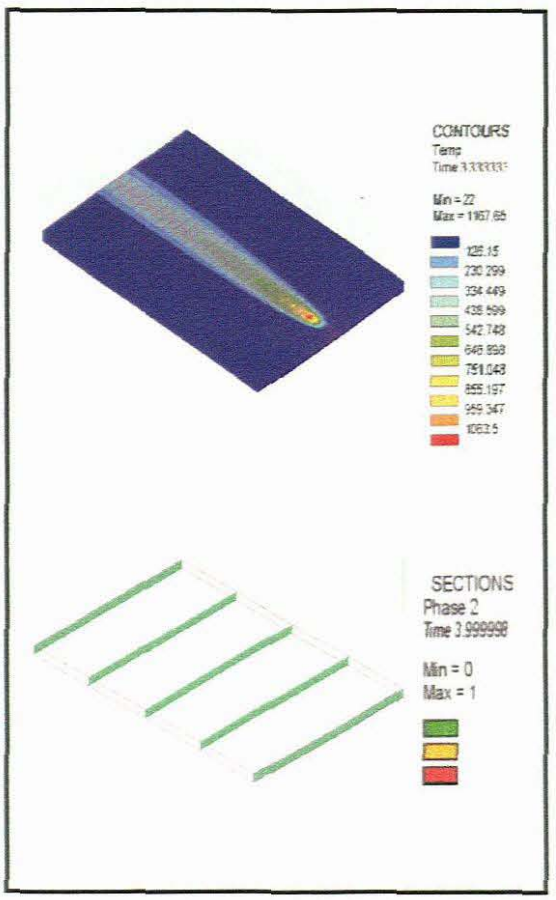

Figure A1.4 – HAZ and Kerf Width for the simulation of Plasma Arc Cuttting of a 5mm plate with the following cutting parameters

Efficiency = 80%
Voltage = 110V
Current = 30
Velocity = 45

Results
1) Thermal Analysis (Top Left)
Max Temperature = 1167.65

2) Thermo-Metallurgical Analysis (Bottom Left)
Kerf Width =0mm

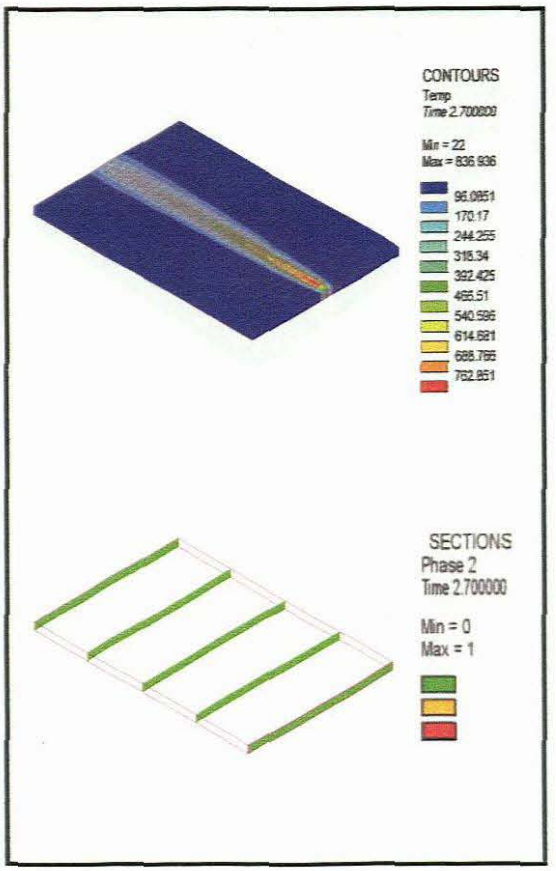

Figure A1.5 – HAZ and Kerf Width for the simulation of Plasma Arc Cuttting of a 5mm plate with the following cutting parameters

Efficiency = 80%
Voltage = 110V
Current = 30
Velocity = 55

Results
1) Thermal Analysis (Top Left)
Max Temperature = 836.936

2) Thermo-Metallurgical Analysis (Bottom Left)
Kerf Width =0mm

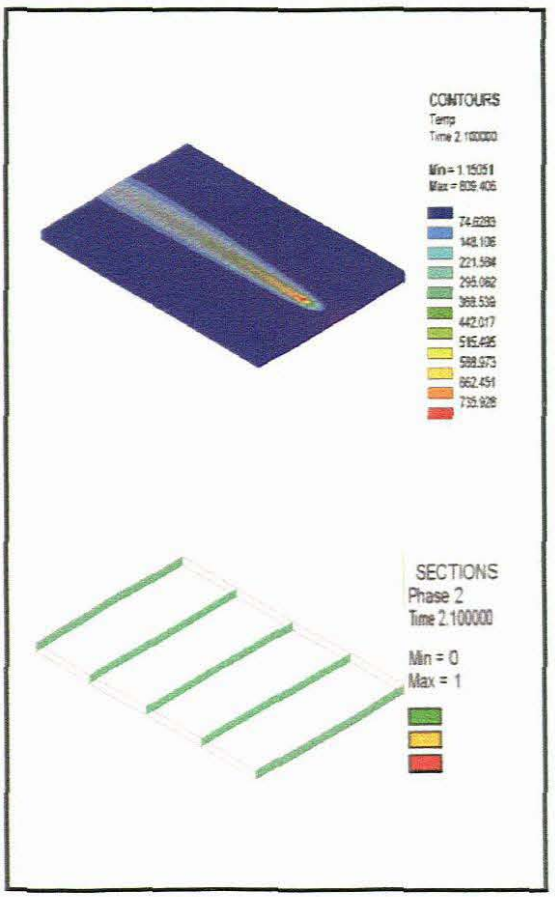

Figure A1.6 – HAZ and Kerf Width for the simulation of Plasma Arc Cuttting of a 5mm plate with the following cutting parameters

Efficiency = 80%
Voltage = 110V
Current = 30
Velocity = 65

Results
1) Thermal Analysis (Top Left)
Max Temperature = 809.406

2) Thermo-Metallurgical Analysis (Bottom Left)
Kerf Width = 0mm

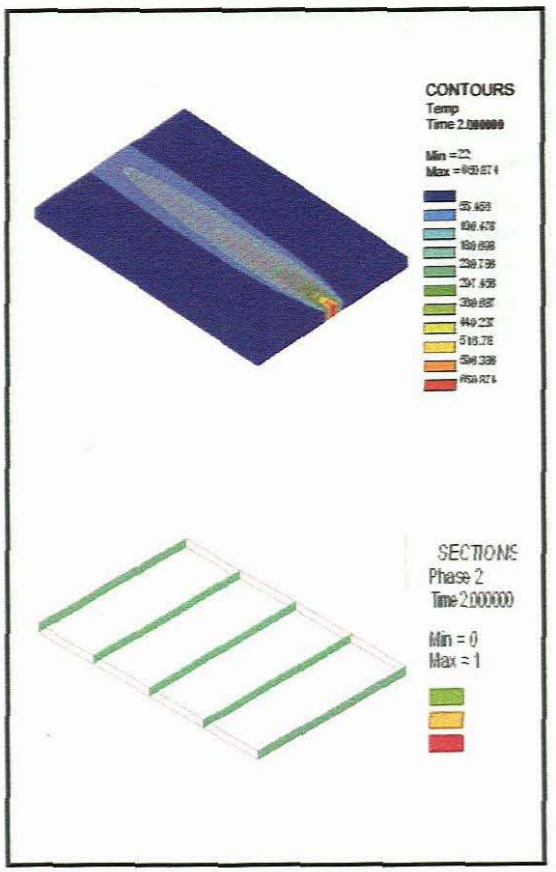

Figure A1.7 – HAZ and Kerf Width for the simulation of Plasma Arc Cuttting of a 5mm plate with the following cutting parameters

Efficiency = 80%
Voltage = 110V
Current = 30
Velocity = 75

Results
1) Thermal Analysis (Top Left)
Max Temperature =650.874

2) Thermo-Metallurgical Analysis (Bottom Left)
Kerf Width =0mm

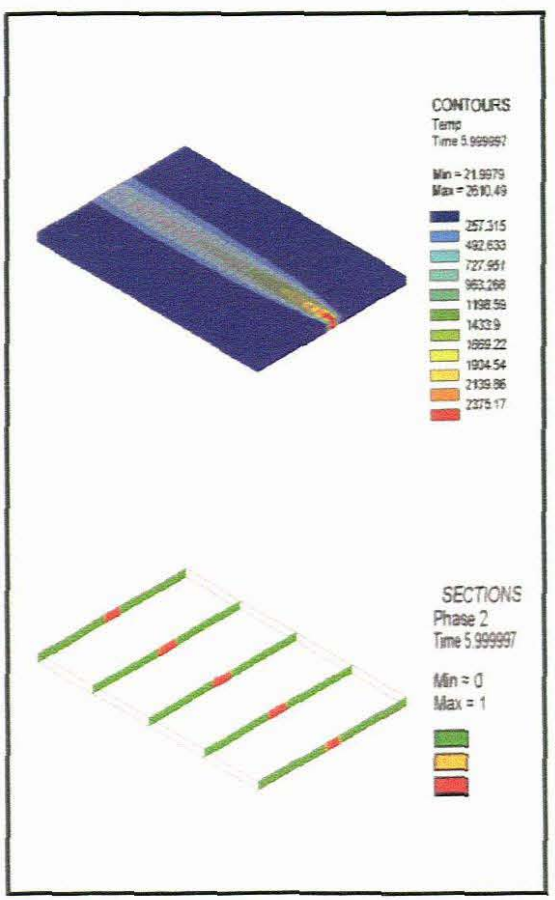

Figure A1.8 – HAZ and Kerf Width for the simulation of Plasma Arc Cuttting of a 5mm plate with the following cutting parameters

Efficiency = 80%
Voltage = 110V
Current = 60
Velocity = 15

Results
1) Thermal Analysis (Top Left)
Max Temperature =2610.49

2) Thermo-Metallurgical Analysis (Bottom Left)
Kerf Width =9.6

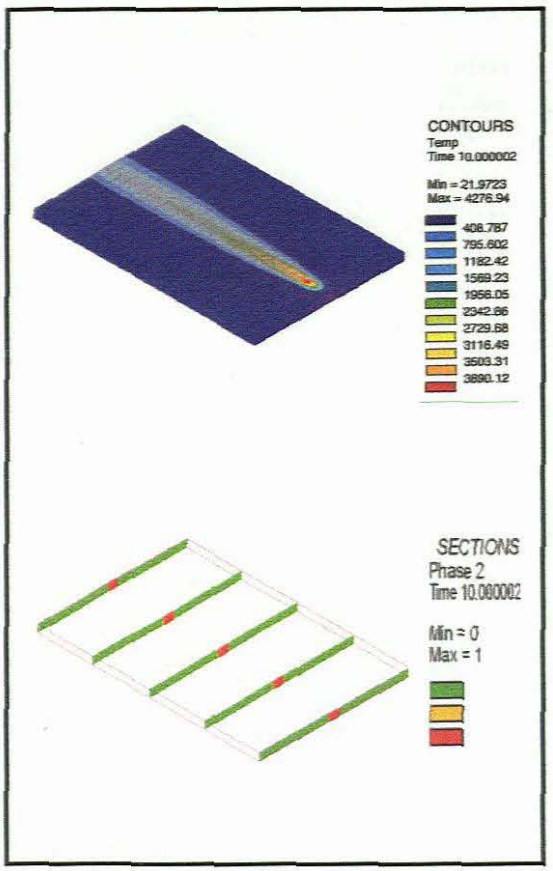

Figure A1.9 – HAZ and Kerf Width for the simulation of Plasma Arc Cuttting of a 5mm plate with the following cutting parameters

Efficiency = 80%
Voltage = 110V
Current = 60
Velocity = 25

Results
1) Thermal Analysis (Top Left)
Max Temperature = 4276.94

2) Thermo-Metallurgical Analysis (Bottom Left)
Kerf Width =5.5mm

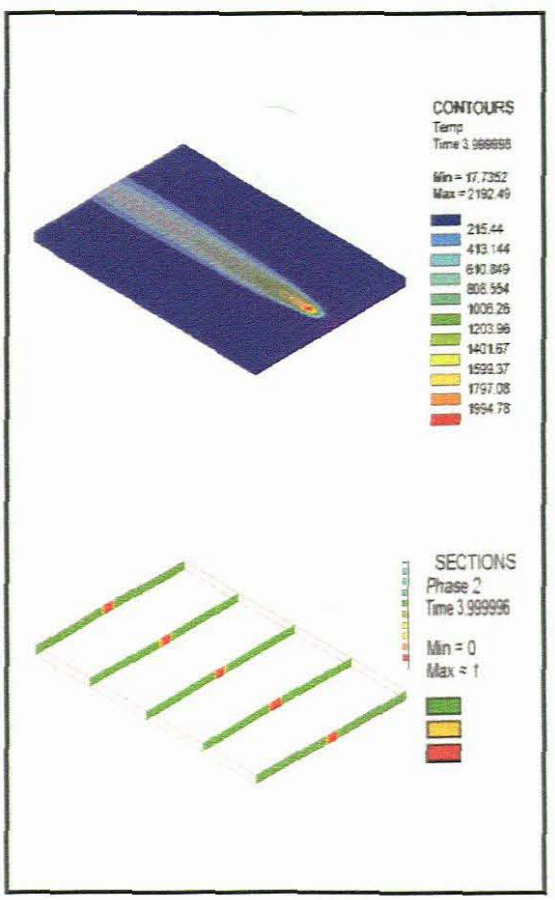

Figure A1.10 – HAZ and Kerf Width for the simulation of Plasma Arc Cuttting of a 5mm plate with the following cutting parameters

Efficiency = 80%
Voltage = 110V
Current = 60
Velocity = 35

Results
1) Thermal Analysis (Top Left)
Max Temperature = 2192.49

2) Thermo-Metallurgical Analysis (Bottom Left)
Kerf Width =2.5

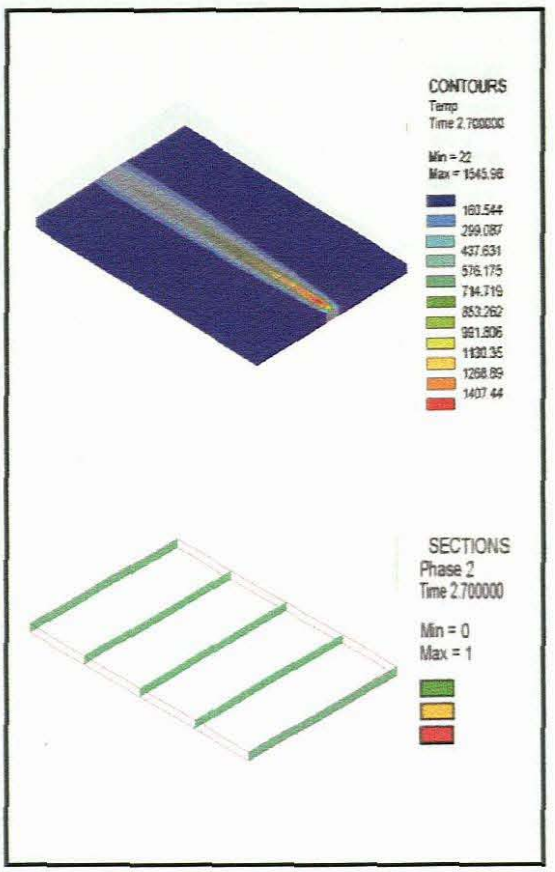

Figure A1.11 – HAZ and Kerf Width for the simulation of Plasma Arc Cuttting of a 5mm plate with the following cutting parameters

Efficiency = 80%
Voltage = 110V
Current = 60
Velocity = 45

Results
1) Thermal Analysis (Top Left)
Max Temperature = 1545.98

2) Thermo-Metallurgical Analysis (Bottom Left)
Kerf Width = 0mm

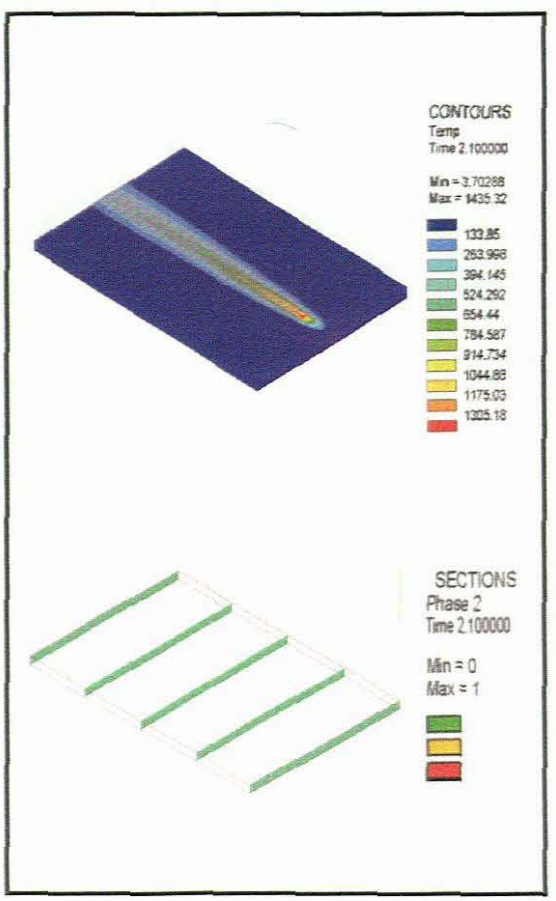

Figure A1.12 – HAZ and Kerf Width for the simulation of Plasma Arc Cuttting of a 5mm plate with the following cutting parameters

Efficiency = 80%
Voltage = 110V
Current = 60
Velocity = 55

Results
1) Thermal Analysis (Top Left)
Max Temperature = 1435.32

2) Thermo-Metallurgical Analysis (Bottom Left)
Kerf Width = 0mm

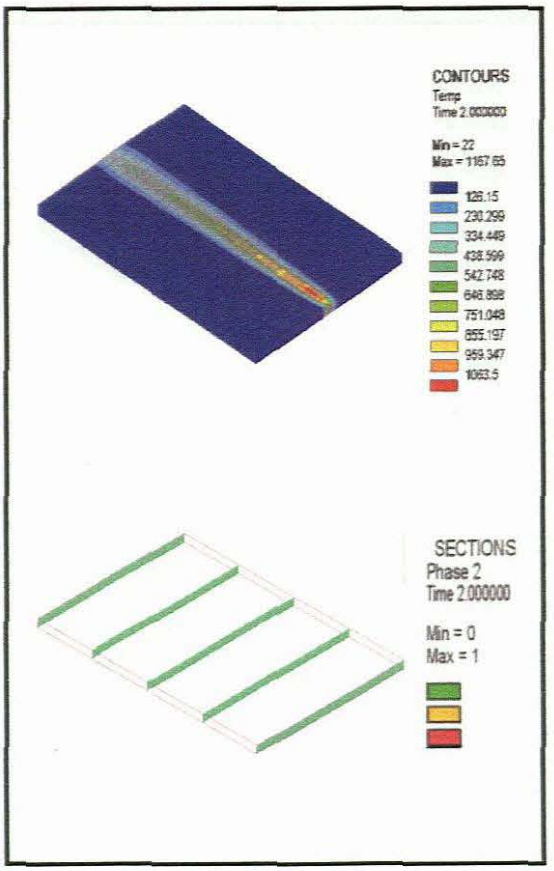

Figure A1.13 – HAZ and Kerf Width for the simulation of Plasma Arc Cuttting of a 5mm plate with the following cutting parameters

Efficiency = 80%
Voltage = 110V
Current = 60
Velocity = 65

Results
1) Thermal Analysis (Top Left)
Max Temperature = 1167.65

2) Thermo-Metallurgical Analysis (Bottom Left)
Kerf Width =0mm

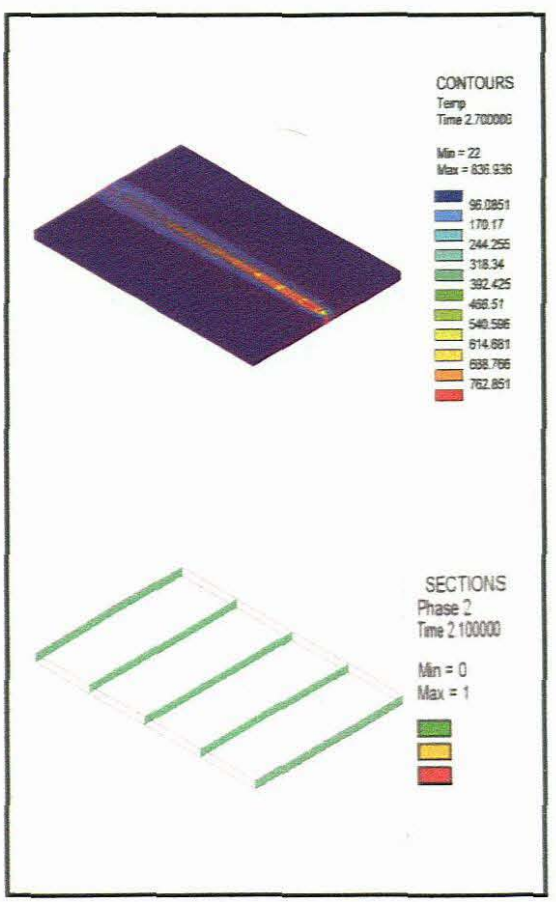

Figure A1.14 – HAZ and Kerf Width for the simulation of Plasma Arc Cutting of a 5mm plate with the following cutting parameters

Efficiency = 80%
Voltage = 110V
Current = 60
Velocity = 75

Results
1) Thermal Analysis (Top Left)
Max Temperature = 836.9

2) Thermo-Metallurgical Analysis (Bottom Left)
Kerf Width =0mm

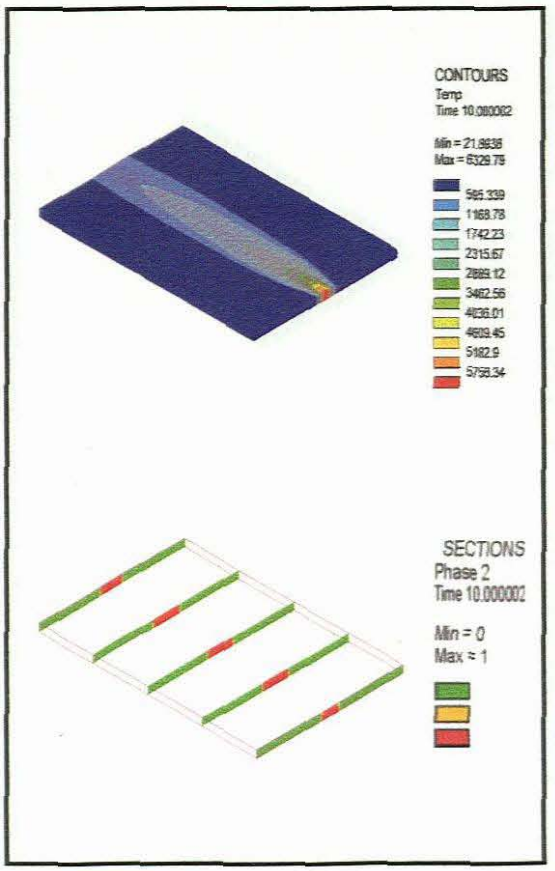

Figure A1.15 – HAZ and Kerf Width for the simulation of Plasma Arc Cuttting of a 5mm plate with the following cutting parameters

Efficiency = 80%
Voltage = 110V
Current = 90
Velocity = 15

Results
1) Thermal Analysis (Top Left)
Max Temperature = 6329.79

2) Thermo-Metallurgical Analysis (Bottom Left)
Kerf Width =16.6mm

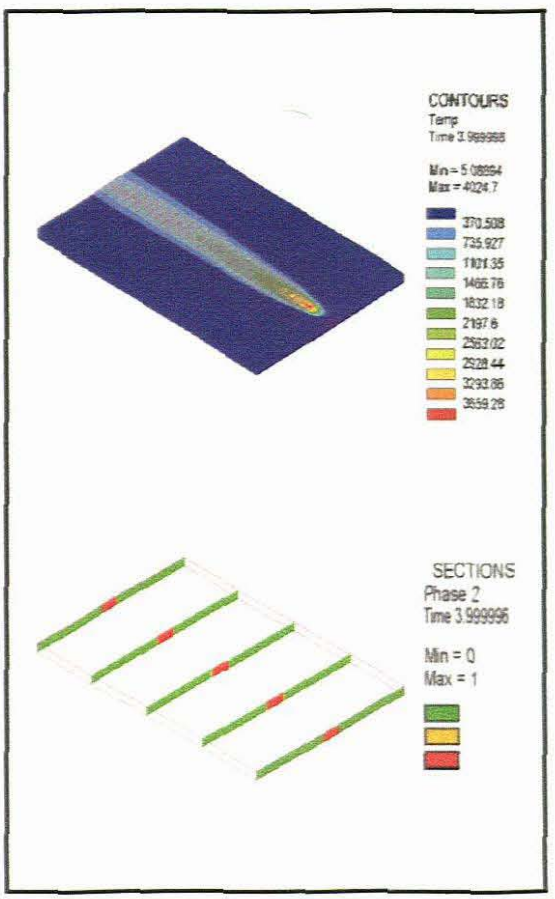

Figure A1.16 – HAZ and Kerf Width for the simulation of Plasma Arc Cuttting of a 5mm plate with the following cutting parameters

Efficiency = 80%
Voltage = 110V
Current = 90
Velocity = 25

Results
1) Thermal Analysis (Top Left)
Max Temperature = 4024.7

2) Thermo-Metallurgical Analysis (Bottom Left)
Kerf Width = 9.7mm

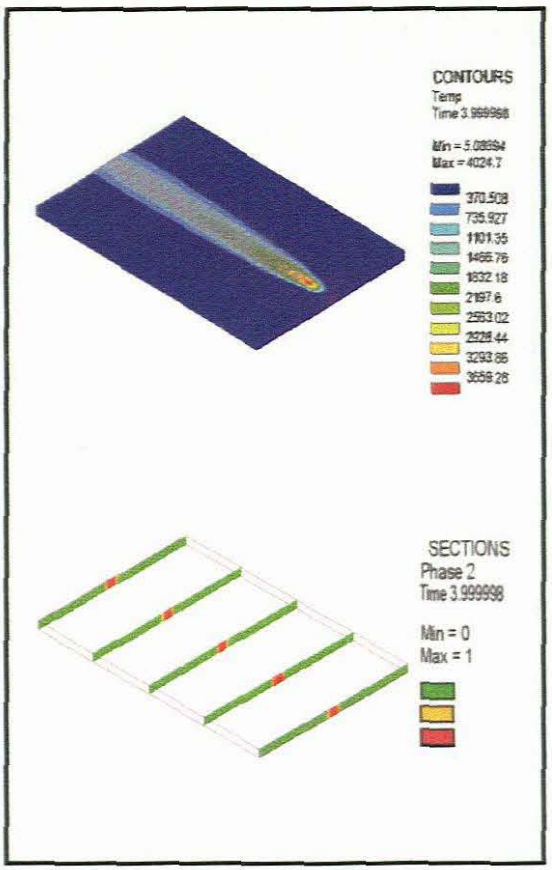

Figure A1.17 – HAZ and Kerf Width for the simulation of Plasma Arc Cuttting of a 5mm plate with the following cutting parameters

Efficiency = 80%
Voltage = 110V
Current = 90
Velocity = 35

Results
1) Thermal Analysis (Top Left)
Max Temperature = 4024.7

2) Thermo-Metallurgical Analysis (Bottom Left)
Kerf Width =4mm

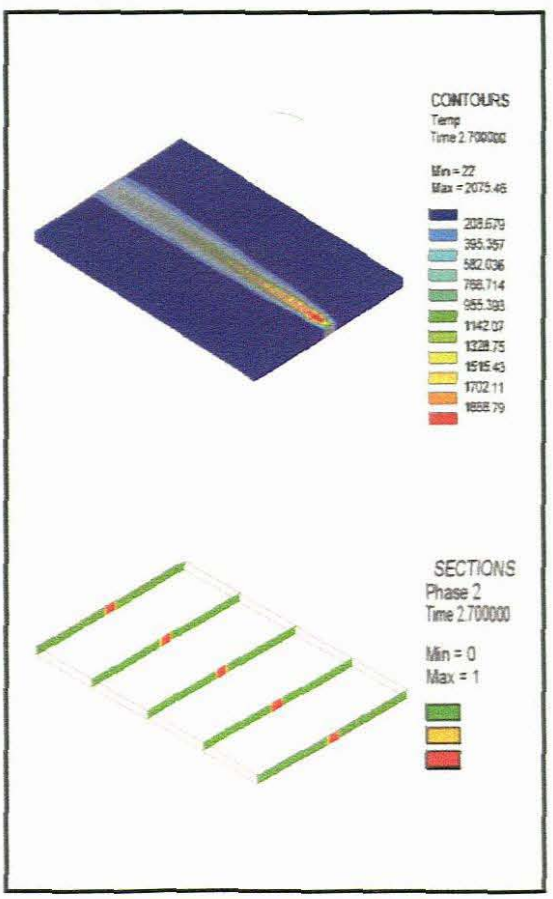

Figure A1.18 – HAZ and Kerf Width for the simulation of Plasma Arc Cuttting of a 5mm plate with the following cutting parameters

Efficiency = 80%
Voltage = 110V
Current = 90
Velocity = 45

Results
1) Thermal Analysis (Top Left)
Max Temperature = 2075.46

2) Thermo-Metallurgical Analysis (Bottom Left)
Kerf Width =2.57mm

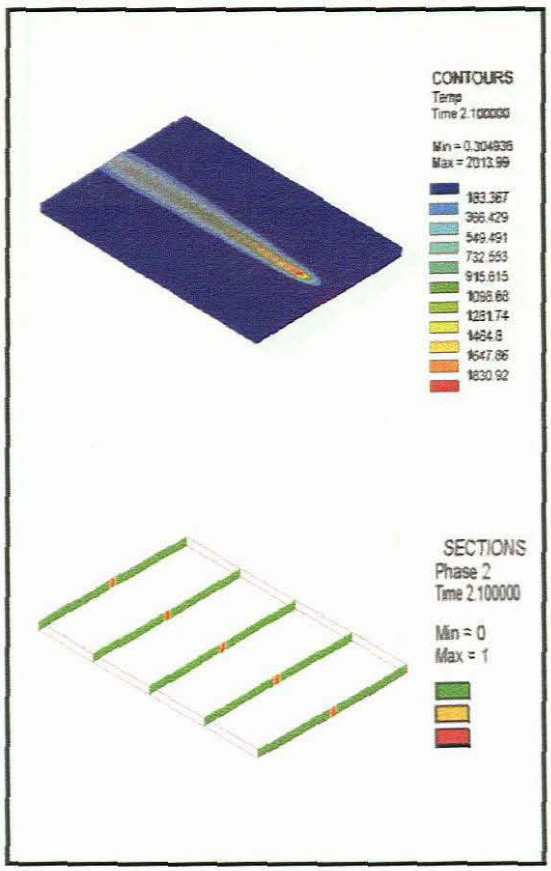

Figure A1.19 – HAZ and Kerf Width for the simulation of Plasma Arc Cuttting of a 5mm plate with the following cutting parameters

Efficiency = 80%
Voltage = 110V
Current = 90
Velocity = 55

Results
1) Thermal Analysis (Top Left)
Max Temperature = 2013.99

2) Thermo-Metallurgical Analysis (Bottom Left)
Kerf Width =1.4mm

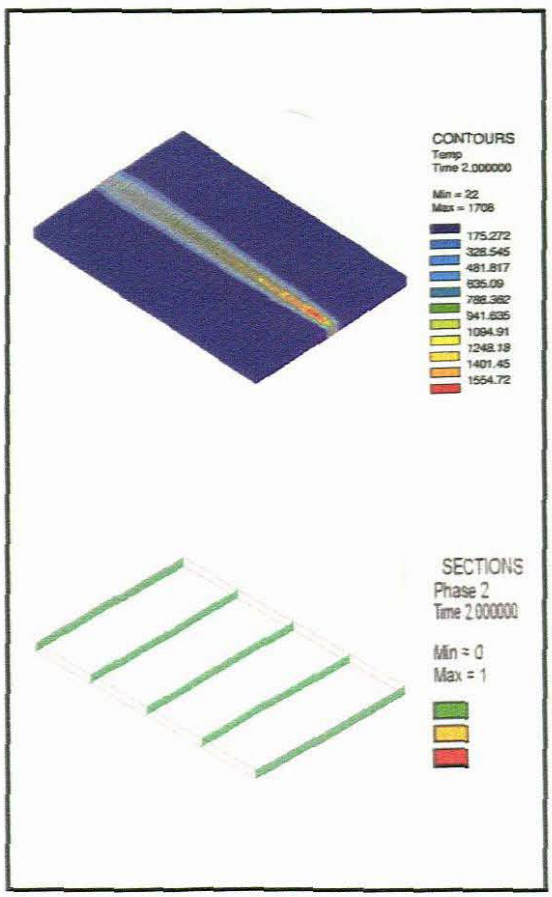

Figure A1.20 – HAZ and Kerf Width for the simulation of Plasma Arc Cuttting of a 5mm plate with the following cutting parameters

Efficiency = 80%
Voltage = 110V
Current = 90
Velocity = 65

Results
1) Thermal Analysis (Top Left)
Max Temperature = 1708

2) Thermo-Metallurgical Analysis (Bottom Left)
Kerf Width =0mm

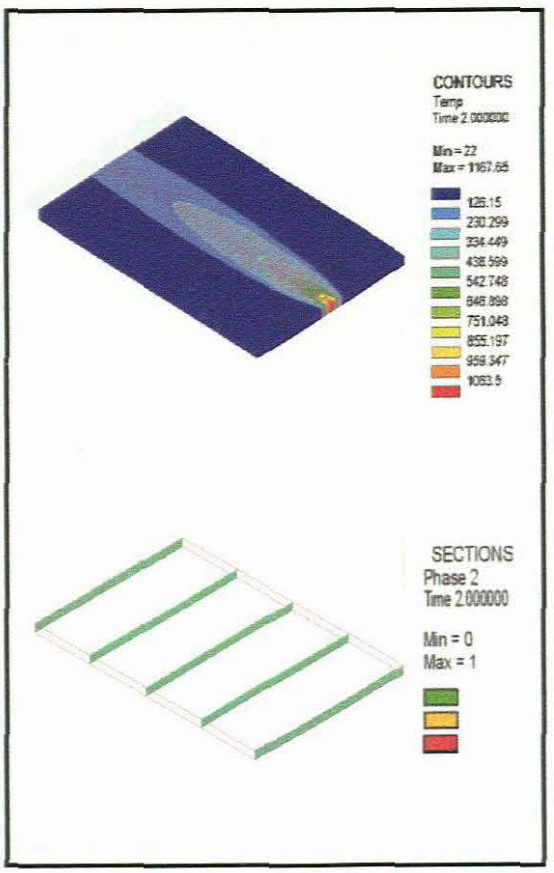

Figure A1.21 – HAZ and Kerf Width for the simulation of Plasma Arc Cuttting of a 5mm plate with the following cutting parameters

Efficiency = 80%
Voltage = 110V
Current = 90
Velocity = 75

Results
1) Thermal Analysis (Top Left)
Max Temperature = 1167.65

2) Thermo-Metallurgical Analysis (Bottom Left)
Kerf Width = 0mm

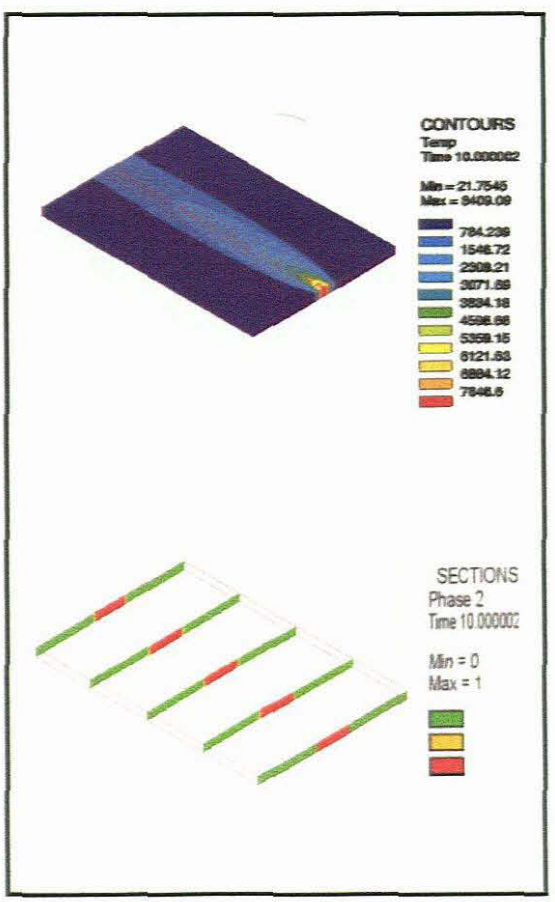

Figure A1.22 – HAZ and Kerf Width for the simulation of Plasma Arc Cuttting of a 5mm plate with the following cutting parameters

Efficiency = 80%
Voltage = 110V
Current = 120
Velocity = 15

Results
1) Thermal Analysis (Top Left)
Max Temperature = 8409.09

2) Thermo-Metallurgical Analysis (Bottom Left)
Kerf Width =21.1mm

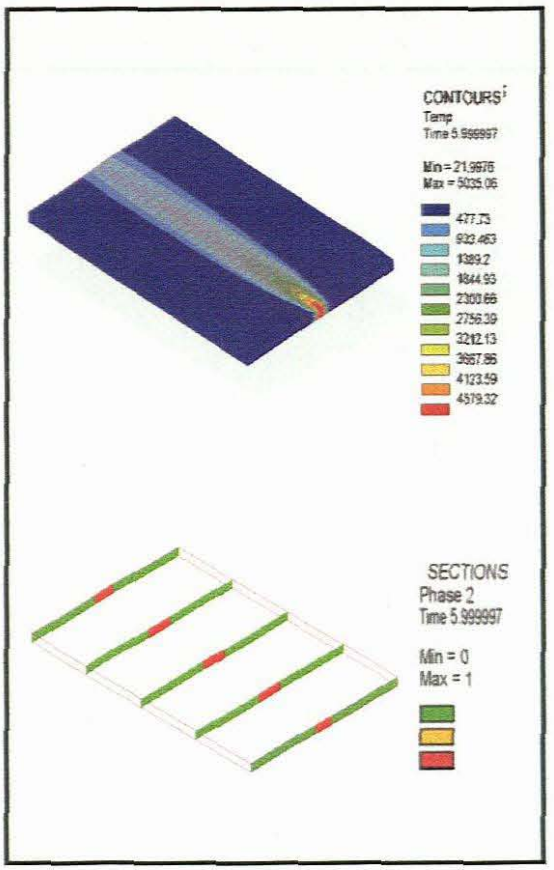

Figure A1.23 – HAZ and Kerf Width for the simulation of Plasma Arc Cuttting of a 5mm plate with the following cutting parameters

Efficiency = 80%
Voltage = 110V
Current = 120
Velocity = 25

Results
1) Thermal Analysis (Top Left)
Max Temperature = 5035.06

2) Thermo-Metallurgical Analysis (Bottom Left)
Kerf Width =13.9mm

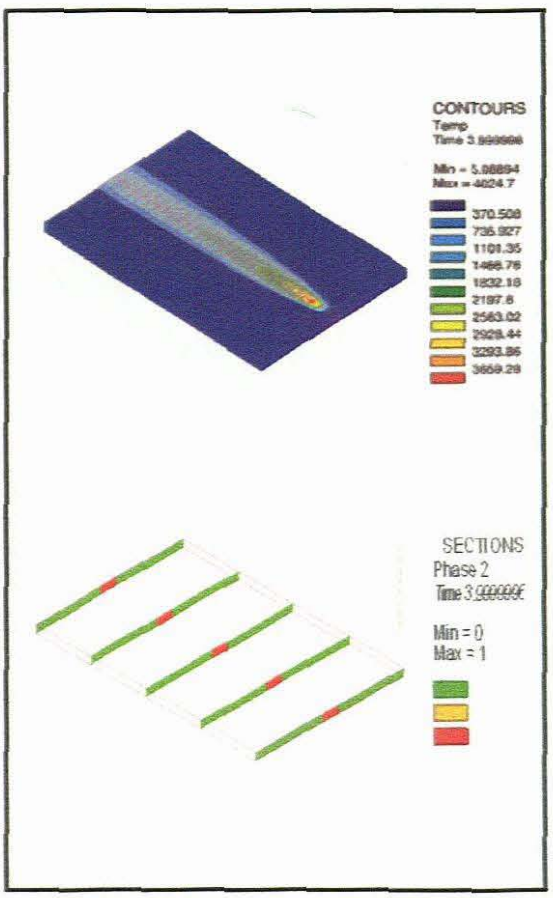

Figure A1.24 – HAZ and Kerf Width for the simulation of Plasma Arc Cuttting of a 5mm plate with the following cutting parameters

Efficiency = 80%
Voltage = 110V
Current = 120
Velocity = 35

Results
1) Thermal Analysis (Top Left)
Max Temperature = 4024.7

2) Thermo-Metallurgical Analysis (Bottom Left)
Kerf Width =9.7mm

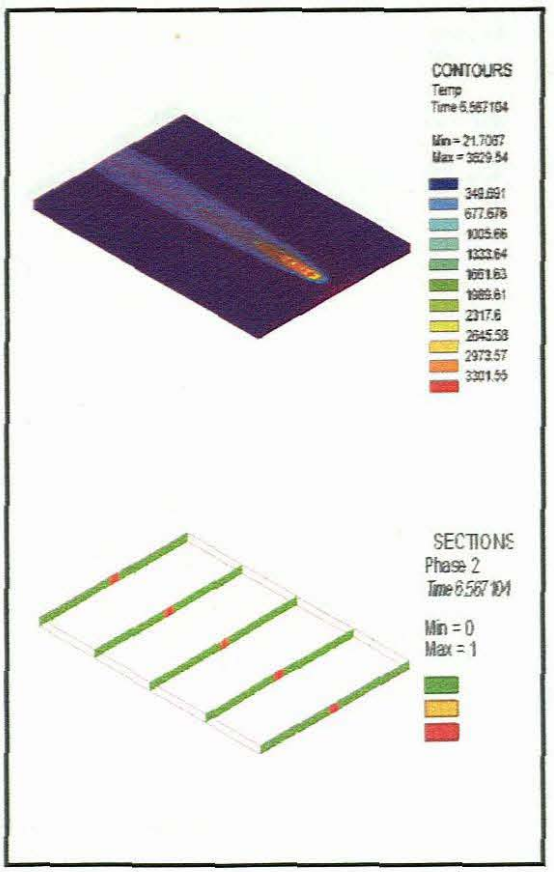

Figure A1.25 – HAZ and Kerf Width for the simulation of Plasma Arc Cuttting of a 5mm plate with the following cutting parameters

Efficiency = 80%
Voltage = 110V
Current = 120
Velocity = 45

Results
1) Thermal Analysis (Top Left)
Max Temperature = 3629.54

2) Thermo-Metallurgical Analysis (Bottom Left)
Kerf Width = 4.8mm

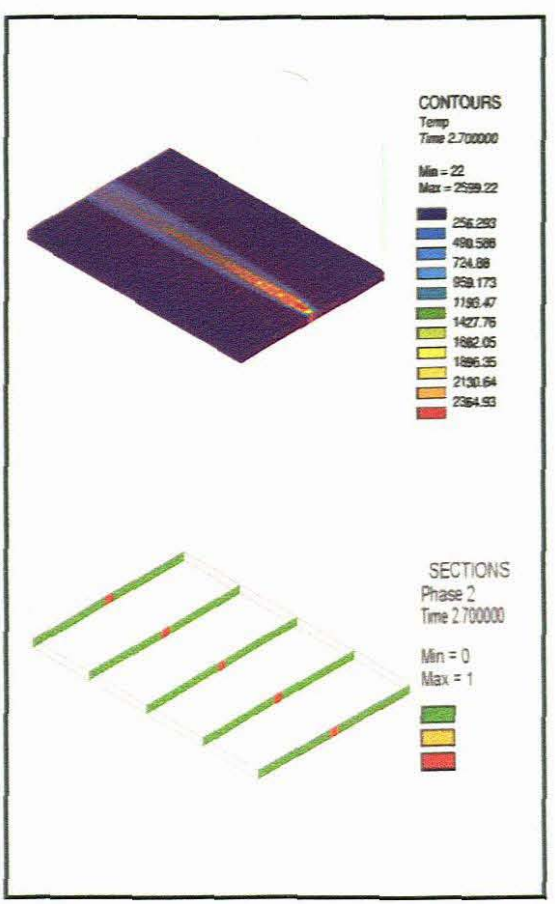

Figure A1.26 – HAZ and Kerf Width for the simulation of Plasma Arc Cuttting of a 5mm plate with the following cutting parameters

Efficiency = 80%
Voltage = 110V
Current = 120
Velocity = 55

Results
1) Thermal Analysis (Top Left)
Max Temperature = 2599.22

2) Thermo-Metallurgical Analysis (Bottom Left)
Kerf Width = 2.9mm

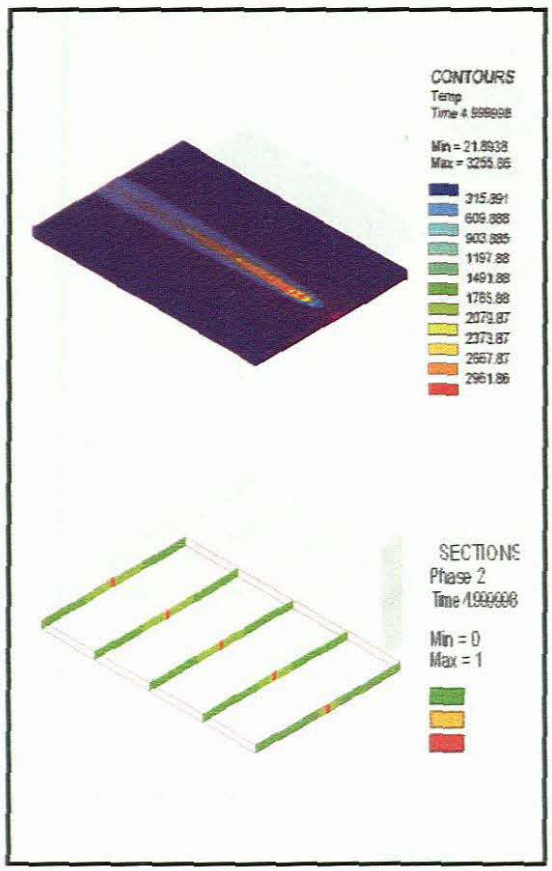

Figure A1.27 – HAZ and Kerf Width for the simulation of Plasma Arc Cuttting of a 5mm plate with the following cutting parameters

Efficiency = 80%
Voltage = 110V
Current = 120
Velocity = 65

Results

1) Thermal Analysis (Top Left)
Max Temperature = 3255.86

2) Thermo-Metallurgical Analysis (Bottom Left)
Kerf Width =2.1mm

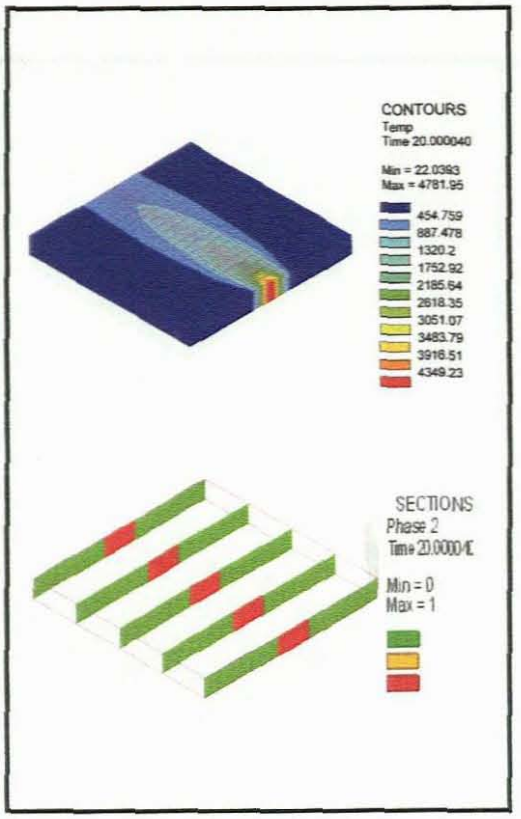

Figure A2.1 – HAZ and Kerf Width for the simulation of Plasma Arc Cuttting of a 10mm plate with the following cutting parameters

Efficiency = 80%
Voltage = 110V
Current = 30
Velocity = 5

Results
1) Thermal Analysis (Top Left)
Max Temperature = 4781.95

2) Thermo-Metallurgical Analysis (Bottom Left)
Kerf Width = 13.3mm

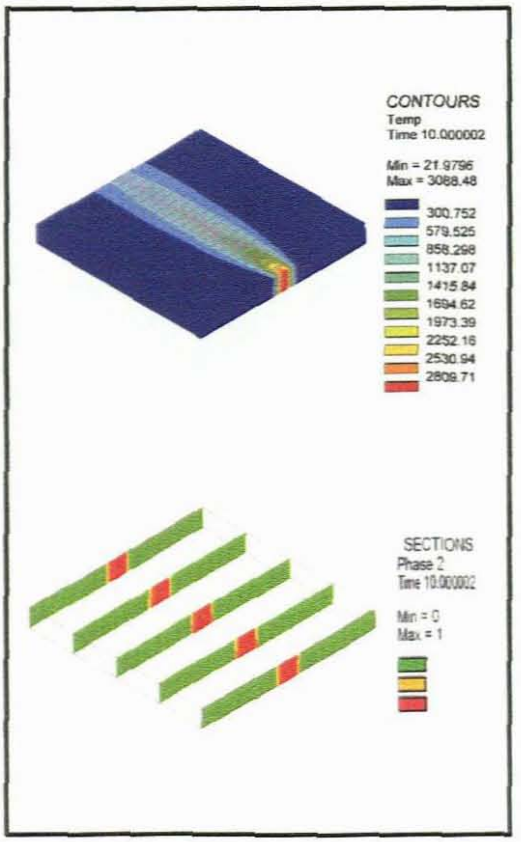

Figure A2.2 – HAZ and Kerf Width for the simulation of Plasma Arc Cuttting of a 10mm plate with the following cutting parameters

Efficiency = 80%
Voltage = 110V
Current = 30
Velocity = 10

Results
1) Thermal Analysis (Top Left)
Max Temperature = 3088.48

2) Thermo-Metallurgical Analysis (Bottom Left)
Kerf Width = 9mm

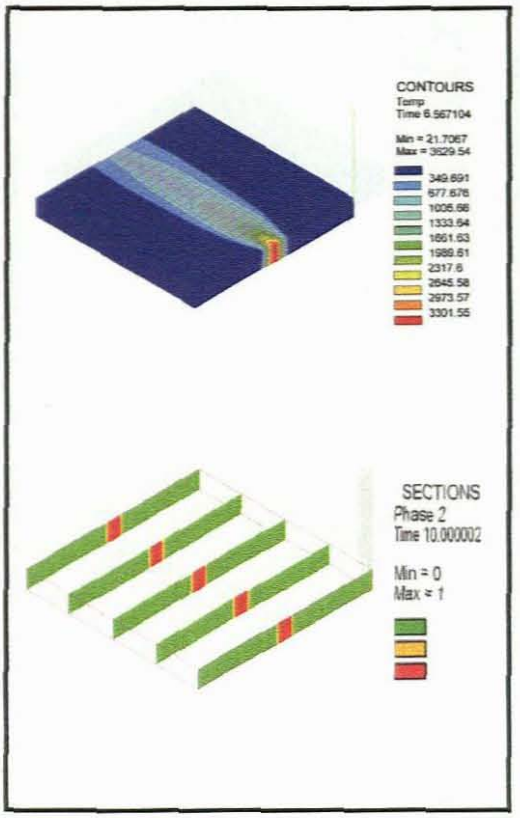

Figure A2.3 – HAZ and Kerf Width for the simulation of Plasma Arc Cuttting of a 10mm plate with the following cutting parameters

Efficiency = 80%
Voltage = 110V
Current = 30
Velocity = 15

Results
1) Thermal Analysis (Top Left)
Max Temperature = 3629.54

2) Thermo-Metallurgical Analysis (Bottom Left)
Kerf Width =6.5mm

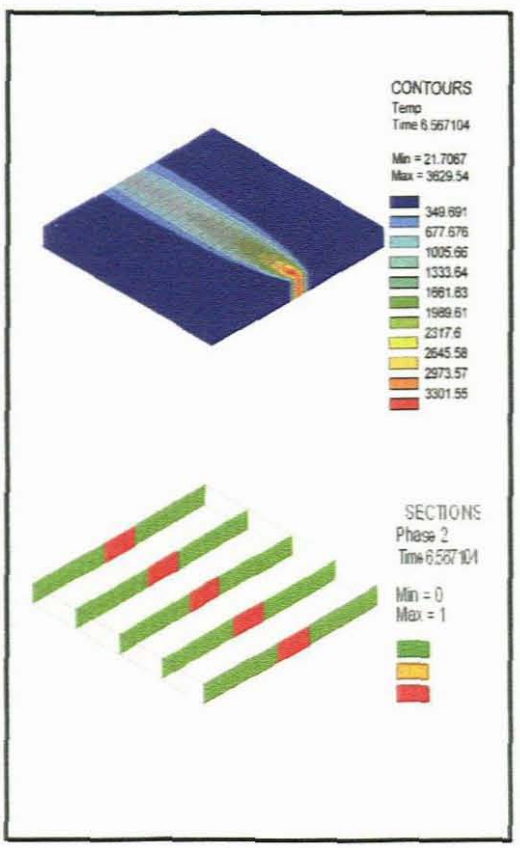

Figure A2.3 – HAZ and Kerf Width for the simulation of Plasma Arc Cuttting of a 10mm plate with the following cutting parameters

Efficiency = 80%
Voltage = 110V
Current = 60
Velocity =10

Results
1) Thermal Analysis (Top Left)
Max Temperature = 3629.54

2) Thermo-Metallurgical Analysis (Bottom Left)
Kerf Width = 12.6mm

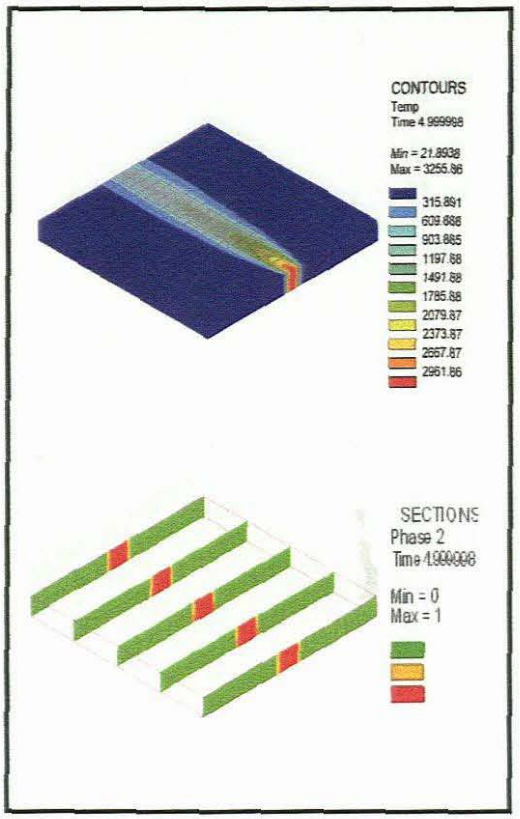

Figure A2.4 – HAZ and Kerf Width for the simulation of Plasma Arc Cuttting of a 10mm plate with the following cutting parameters

Efficiency = 80%
Voltage = 110V
Current = 60
Velocity = 20

Results
1) Thermal Analysis (Top Left)
Max Temperature = 3255.86

2) Thermo-Metallurgical Analysis (Bottom Left)
Kerf Width = 9.9mm

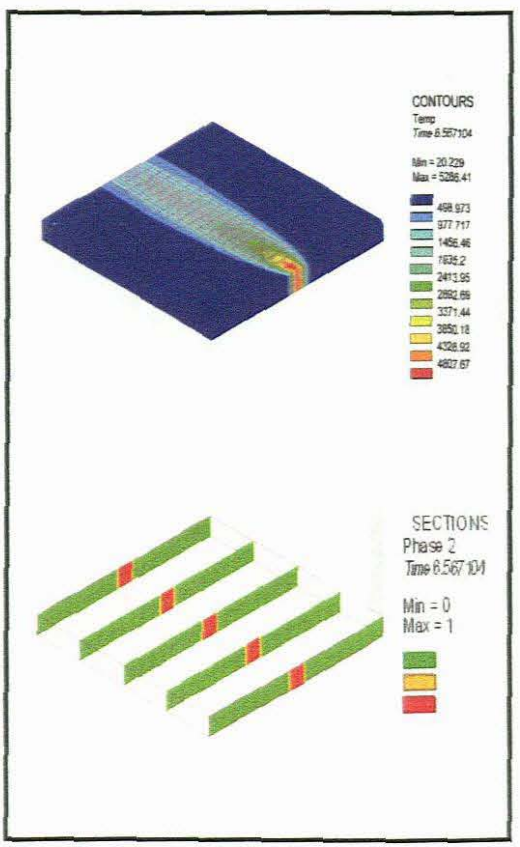

Figure A2.5 – HAZ and Kerf Width for the simulation of Plasma Arc Cuttting of a 10mm plate with the following cutting parameters

Efficiency = 80%
Voltage = 110V
Current = 90
Velocity = 15

Results
1) Thermal Analysis (Top Left)
Max Temperature = 5285.41

2) Thermo-Metallurgical Analysis (Bottom Left)
Kerf Width = 6.3mm

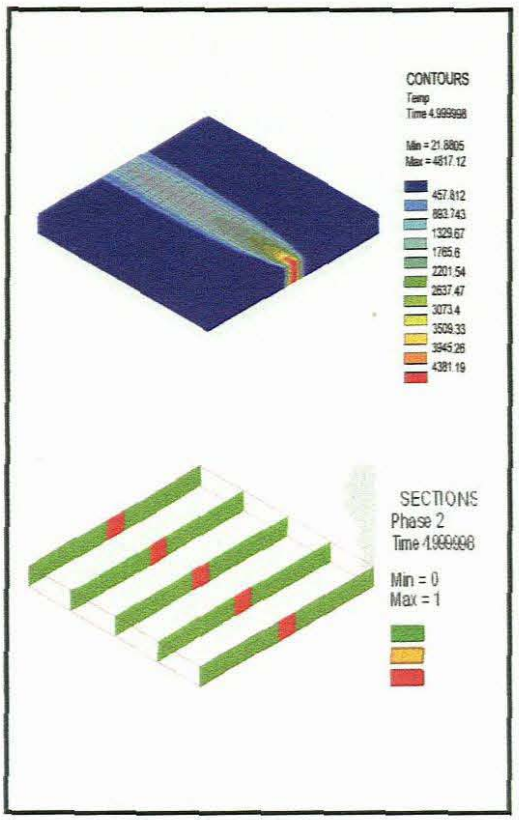

Figure A2.6 – HAZ and Kerf Width for the simulation of Plasma Arc Cuttting of a 10mm plate with the following cutting parameters

Efficiency = 80%
Voltage = 110V
Current = 90
Velocity = 20

Results
1) Thermal Analysis (Top Left)
Max Temperature = 4617.12

2) Thermo-Metallurgical Analysis (Bottom Left)
Kerf Width = 4.5mm

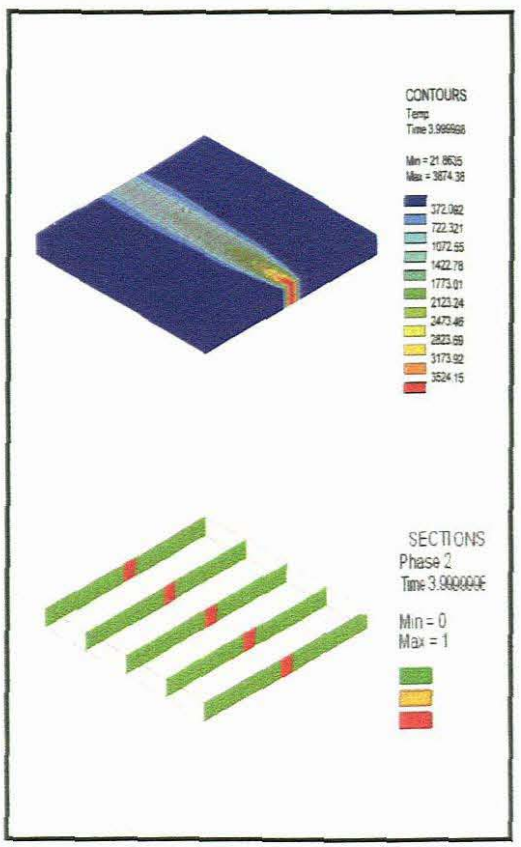

Figure A2.7 – HAZ and Kerf Width for the simulation of Plasma Arc Cuttting of a 10mm plate with the following cutting parameters

Efficiency = 80%
Voltage = 110V
Current = 90
Velocity = 25

Results
1) Thermal Analysis (Top Left)
Max Temperature = 3674.38

2) Thermo-Metallurgical Analysis (Bottom Left)
Kerf Width = 3.7mm

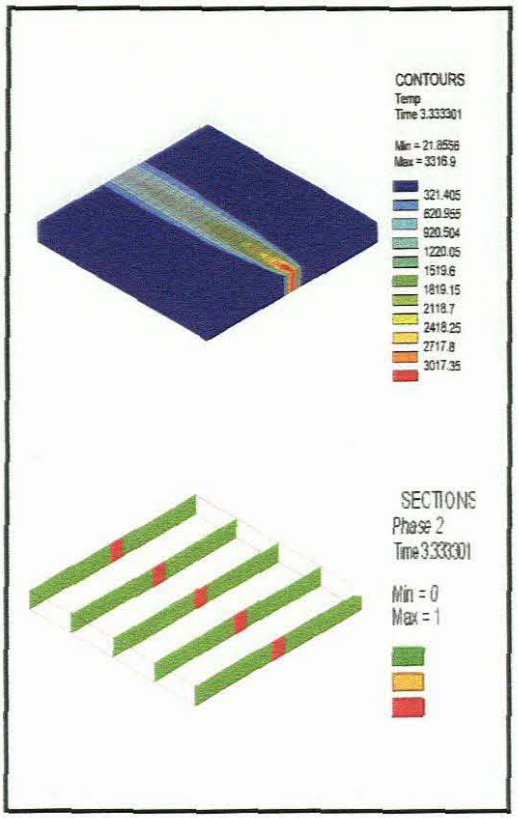

Figure A2.8 – HAZ and Kerf Width for the simulation of Plasma Arc Cuttting of a 10mm plate with the following cutting parameters

Efficiency = 80%
Voltage = 110V
Current = 90
Velocity = 30

Results
1) Thermal Analysis (Top Left)
Max Temperature = 3315.9

2) Thermo-Metallurgical Analysis (Bottom Left)
Kerf Width = 2.6mm

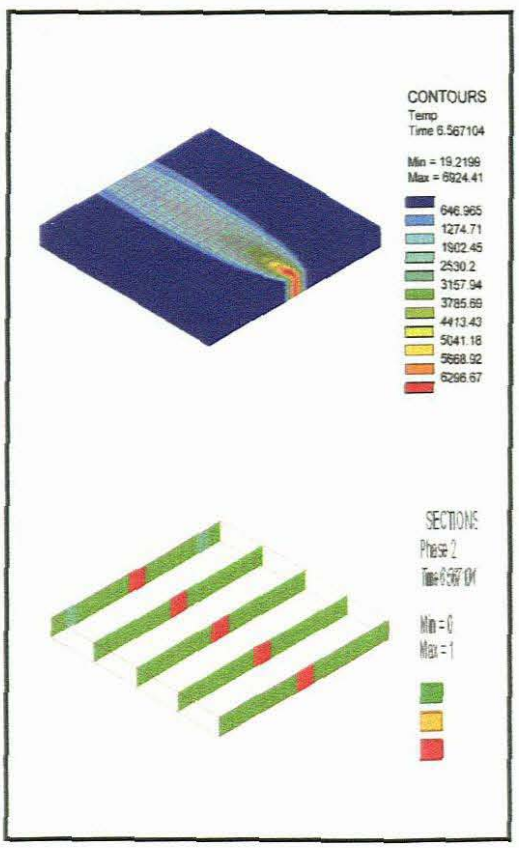

Figure A2.9 – HAZ and Kerf Width for the simulation of Plasma Arc Cuttting of a 10mm plate with the following cutting parameters

Efficiency = 80%
Voltage = 110V
Current = 120
Velocity = 15

Results
1) Thermal Analysis (Top Left)
Max Temperature = 6924.41

2) Thermo-Metallurgical Analysis (Bottom Left)
Kerf Width = 6.7mm

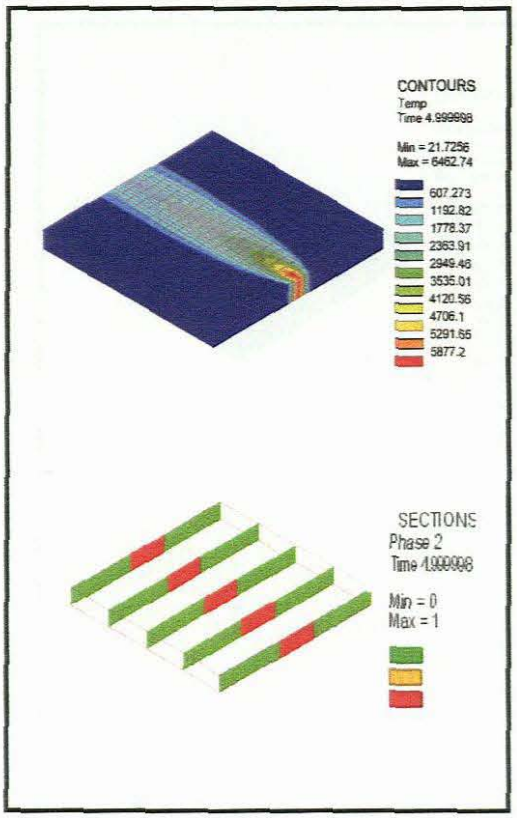

Figure A2.10 – HAZ and Kerf Width for the simulation of Plasma Arc Cuttting of a 10mm plate with the following cutting parameters

Efficiency = 80%
Voltage = 110V
Current = 120
Velocity = 20

Results
1) Thermal Analysis (Top Left)
Max Temperature = 6462.74

2) Thermo-Metallurgical Analysis (Bottom Left)
Kerf Width = 22.1mm

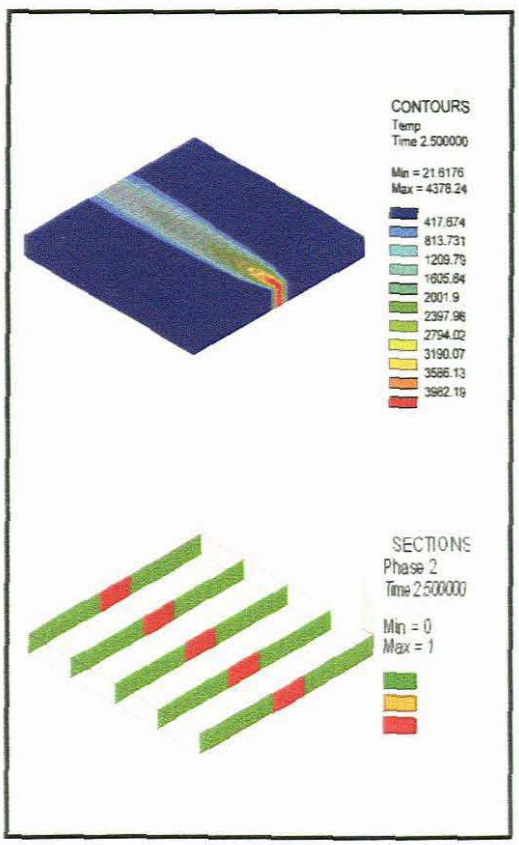

Figure A2.11 – HAZ and Kerf Width for the simulation of Plasma Arc Cuttting of a 10mm plate with the following cutting parameters

Efficiency = 80%
Voltage = 110V
Current = 120
Velocity = 30

Results
1) Thermal Analysis (Top Left)
Max Temperature = 4378.24

2) Thermo-Metallurgical Analysis (Bottom Left)
Kerf Width = 16.9mm

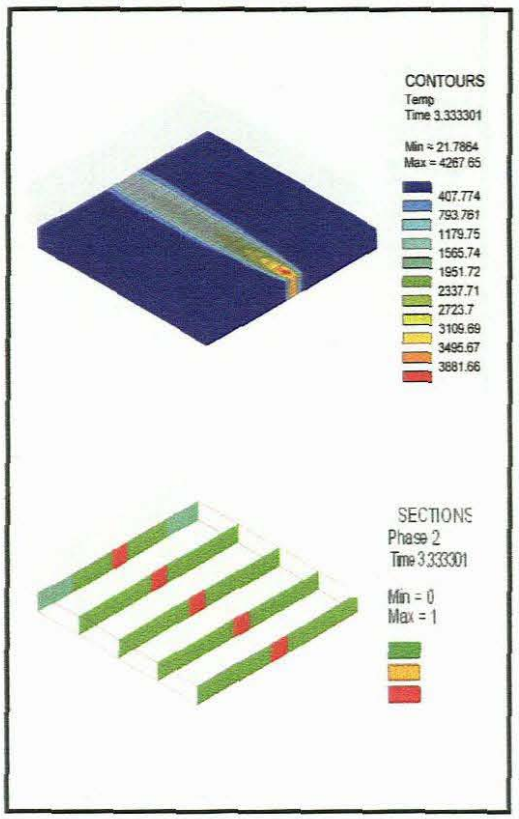

Figure A2.12 – HAZ and Kerf Width for the simulation of Plasma Arc Cuttting of a 10mm plate with the following cutting parameters

Efficiency = 80%
Voltage = 110V
Current = 120
Velocity = 40

Results

1) Thermal Analysis (Top Left)
Max Temperature = 4257.65

2) Thermo-Metallurgical Analysis (Bottom Left)
Kerf Width = 9.5mm

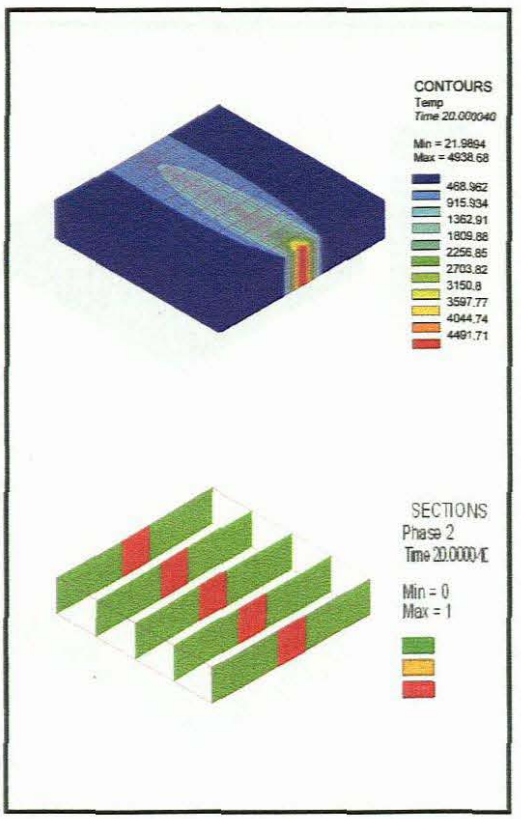

Figure A3.1 – HAZ and Kerf Width for the simulation of Plasma Arc Cuttting of a 10mm plate with the following cutting parameters

Efficiency = 80%
Voltage = 110V
Current = 30
Velocity = 5

Results
1) Thermal Analysis (Top Left)
Max Temperature = 4938.68

2) Thermo-Metallurgical Analysis (Bottom Left)
Kerf Width =17.3mm

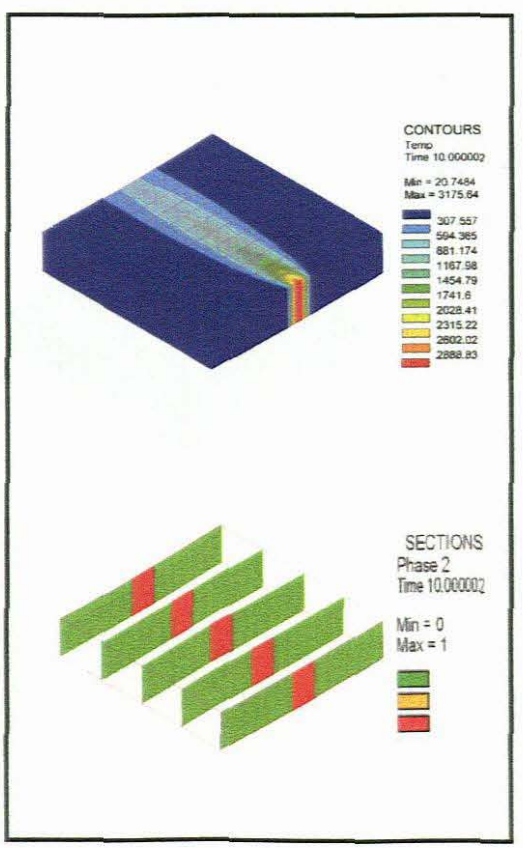

Figure A3.2 – HAZ and Kerf Width for the simulation of Plasma Arc Cuttting of a 10mm plate with the following cutting parameters

Efficiency = 80%
Voltage = 110V
Current = 30
Velocity = 10

Results
1) Thermal Analysis (Top Left)
Max Temperature = 3175.64

2) Thermo-Metallurgical Analysis (Bottom Left)
Kerf Width = 12.9mm

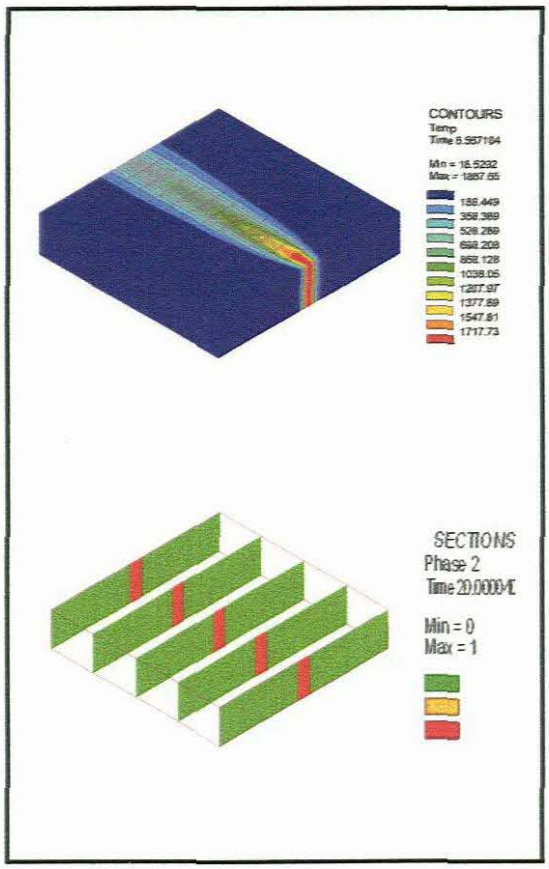

Figure A3.3 – HAZ and Kerf Width for the simulation of Plasma Arc Cuttting of a 10mm plate with the following cutting parameters

Efficiency = 80%
Voltage = 110V
Current = 30
Velocity = 15

Results
1) Thermal Analysis (Top Left)
Max Temperature = 1887.65

2) Thermo-Metallurgical Analysis (Bottom Left)
Kerf Width = 6.3mm

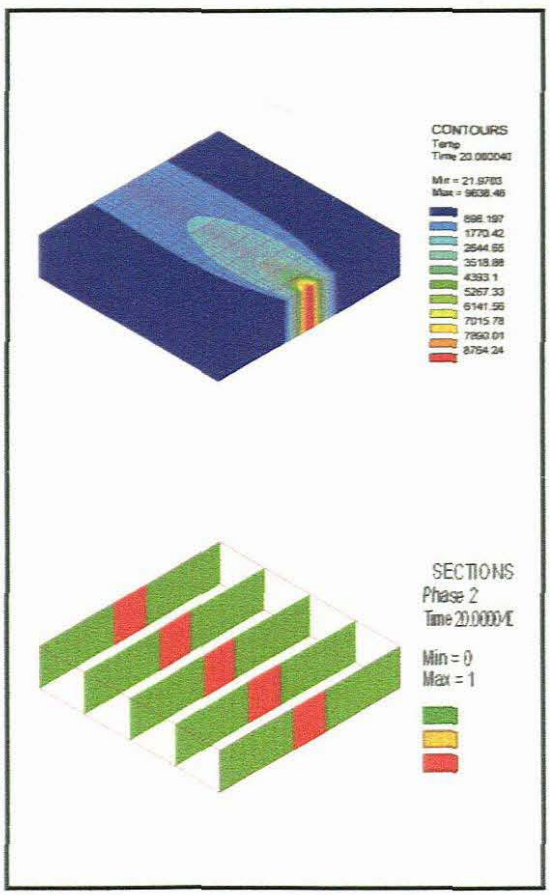

Figure A3.4 – HAZ and Kerf Width for the simulation of Plasma Arc Cuttting of a 10mm plate with the following cutting parameters

Efficiency = 80%
Voltage = 110V
Current = 60
Velocity = 5

Results
1) Thermal Analysis (Top Left)
Max Temperature = 9638.46

2) Thermo-Metallurgical Analysis (Bottom Left)
Kerf Width =16.8mm

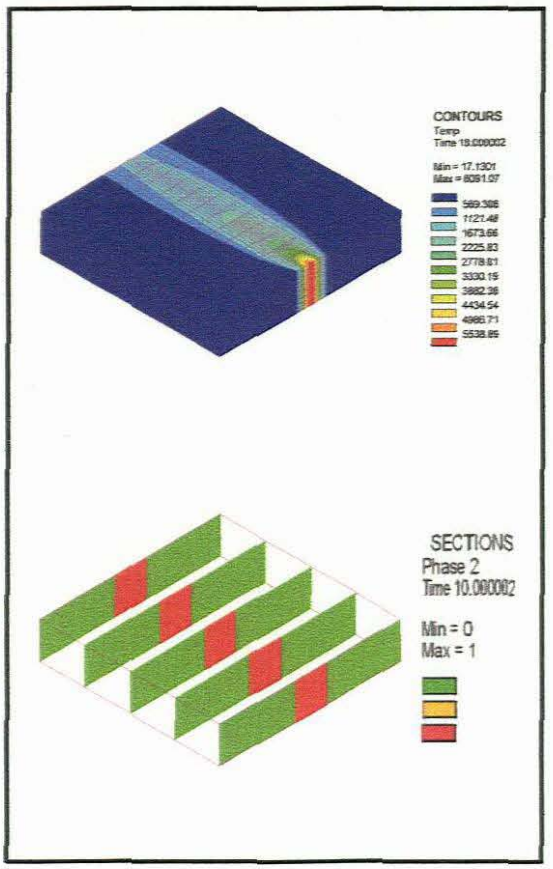

Figure A3.5 – HAZ and Kerf Width for the simulation of Plasma Arc Cuttting of a 10mm plate with the following cutting parameters

Efficiency = 80%
Voltage = 110V
Current = 60
Velocity = 10

Results
1) Thermal Analysis (Top Left)
Max Temperature = 6091.07

2) Thermo-Metallurgical Analysis (Bottom Left)
Kerf Width = 14.8mm

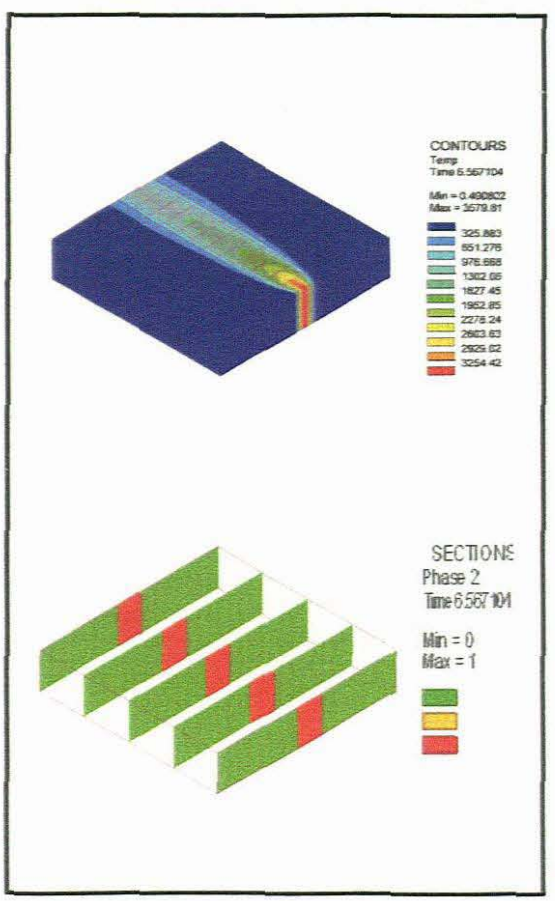

Figure A3.6 – HAZ and Kerf Width for the simulation of Plasma Arc Cuttting of a 10mm plate with the following cutting parameters

Efficiency = 80%
Voltage = 110V
Current = 60
Velocity = 15

Results
1) Thermal Analysis (Top Left)
Max Temperature = 3579.81

2) Thermo-Metallurgical Analysis (Bottom Left)
Kerf Width = 13 mm

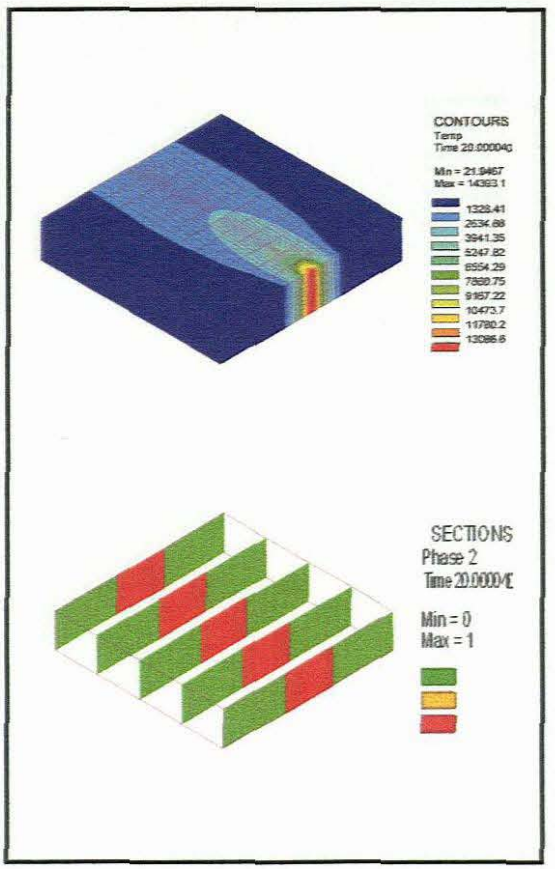

Figure A3.7 – HAZ and Kerf Width for the simulation of Plasma Arc Cuttting of a 10mm plate with the following cutting parameters

Efficiency = 80%
Voltage = 110V
Current = 90
Velocity = 5

Results
1) Thermal Analysis (Top Left)
Max Temperature = 14393.1

2) Thermo-Metallurgical Analysis (Bottom Left)
Kerf Width = 28mm

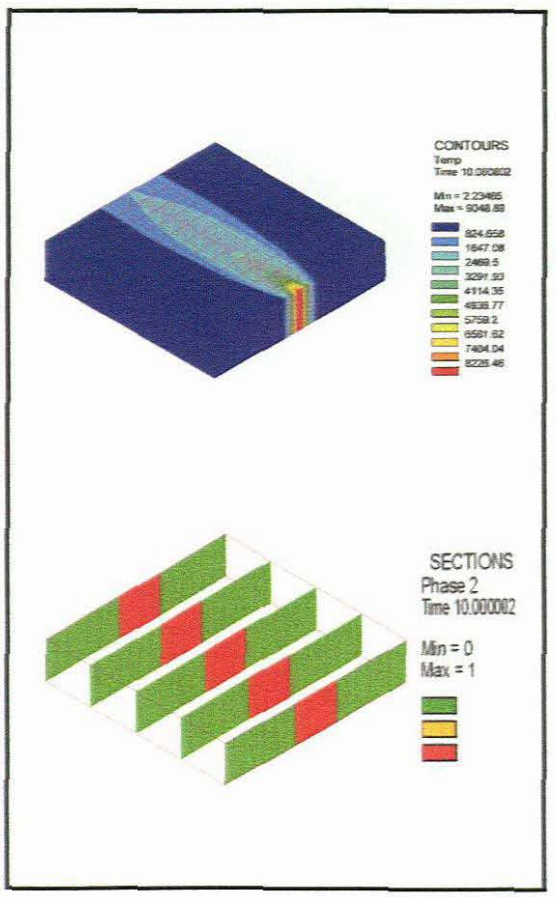

Figure A3.8 – HAZ and Kerf Width for the simulation of Plasma Arc Cuttting of a 10mm plate with the following cutting parameters

Efficiency = 80%
Voltage = 110V
Current = 90
Velocity = 10

Results
1) Thermal Analysis (Top Left)
Max Temperature = 9048.89

2) Thermo-Metallurgical Analysis (Bottom Left)
Kerf Width = 22.9mm

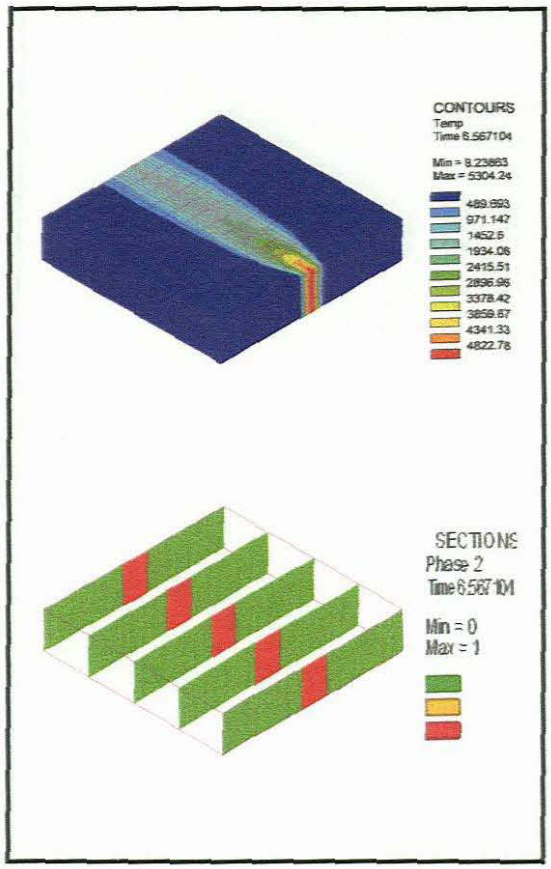

Figure A3.9 – HAZ and Kerf Width for the simulation of Plasma Arc Cuttting of a 10mm plate with the following cutting parameters

Efficiency = 80%
Voltage = 110V
Current = 90
Velocity = 15

Results
1) Thermal Analysis (Top Left)
Max Temperature = 5304.24

2) Thermo-Metallurgical Analysis (Bottom Left)
Kerf Width = 16 mm

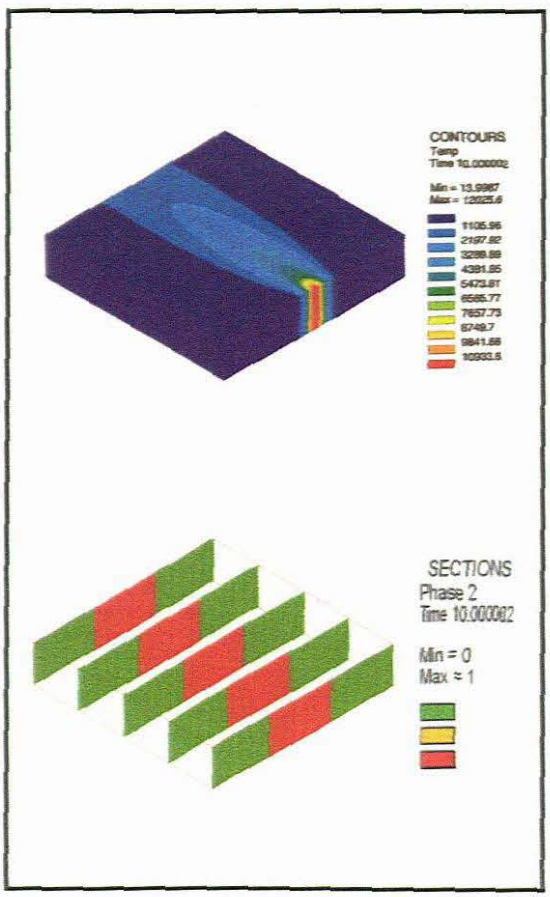

Figure 3.10 – HAZ and Kerf Width for the simulation of Plasma Arc Cuttting of a 10mm plate with the following cutting parameters

Efficiency = 80%
Voltage = 110V
Current = 120
Velocity = 10

Results
1) Thermal Analysis (Top Left)
Max Temperature = 12025.6

2) Thermo-Metallurgical Analysis (Bottom Left)
Kerf Width =34.1mm

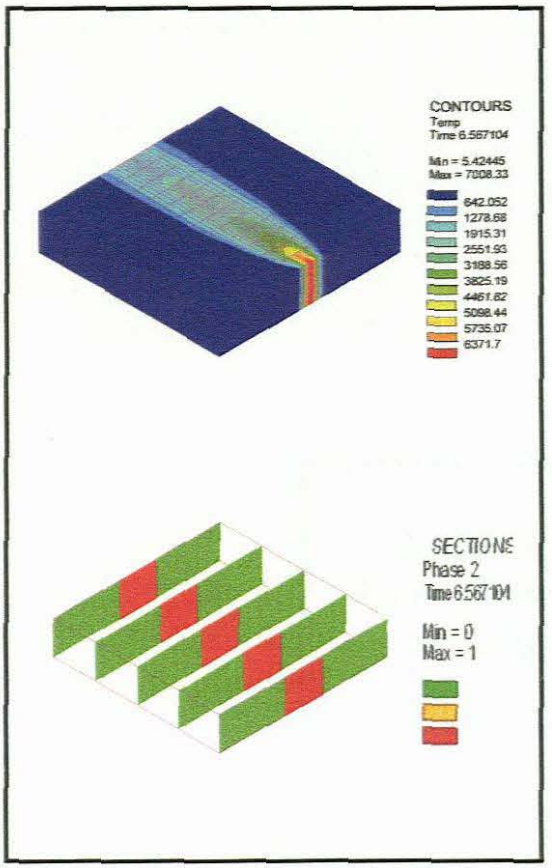

Figure A3.11 – HAZ and Kerf Width for the simulation of Plasma Arc Cuttting of a 10mm plate with the following cutting parameters

Efficiency = 80%
Voltage = 110V
Current = 120
Velocity = 15

Results
1) Thermal Analysis (Top Left)
Max Temperature = 7008.33

2) Thermo-Metallurgical Analysis (Bottom Left)
Kerf Width = 22.2mm

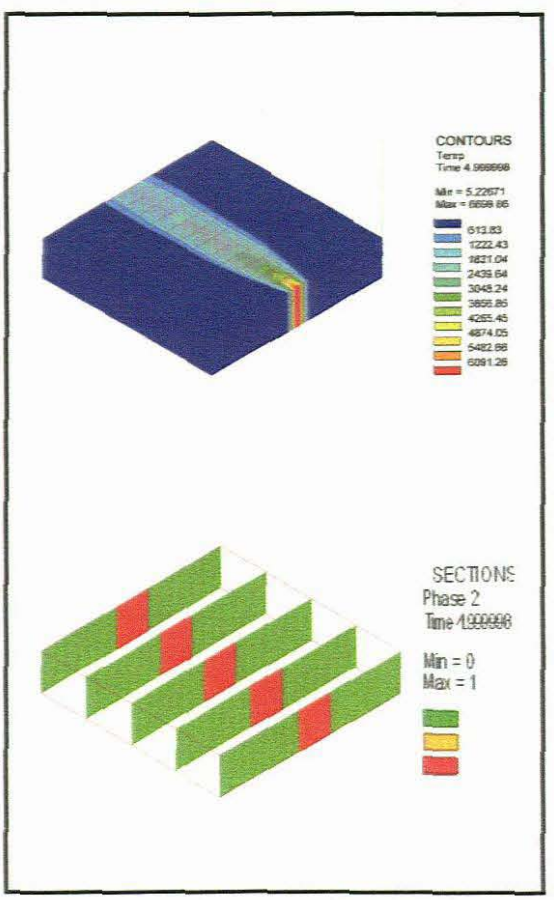

Figure A3.12 – HAZ and Kerf Width for the simulation of Plasma Arc Cuttting of a 10mm plate with the following cutting parameters

Efficiency = 80%
Voltage = 110V
Current = 120
Velocity = 20

Results
1) Thermal Analysis (Top Left)
Max Temperature = 6699.86

2) Thermo-Metallurgical Analysis (Bottom Left)
Kerf Width = 16.8mm

Appendix B: Graphical Representation of Simulation Outputs (10mm)

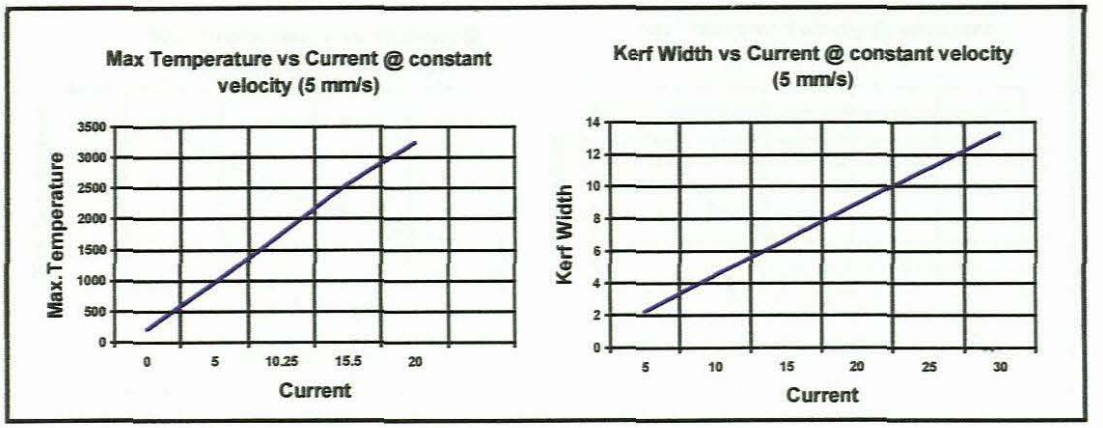

Figure B.1

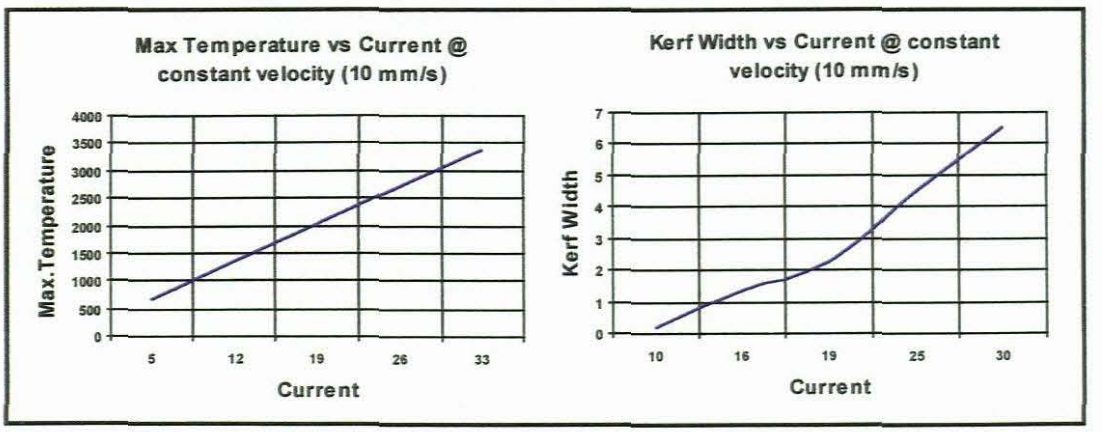

Figure B.2

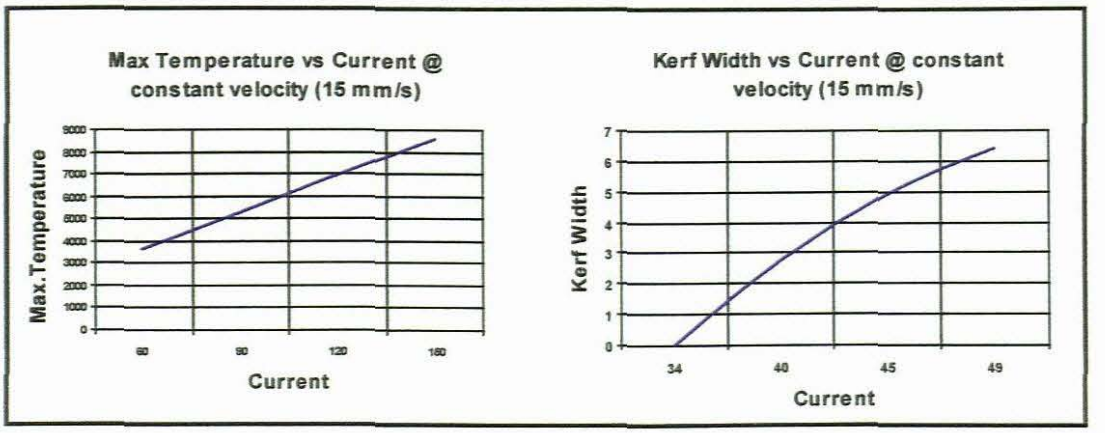

Figure B.3

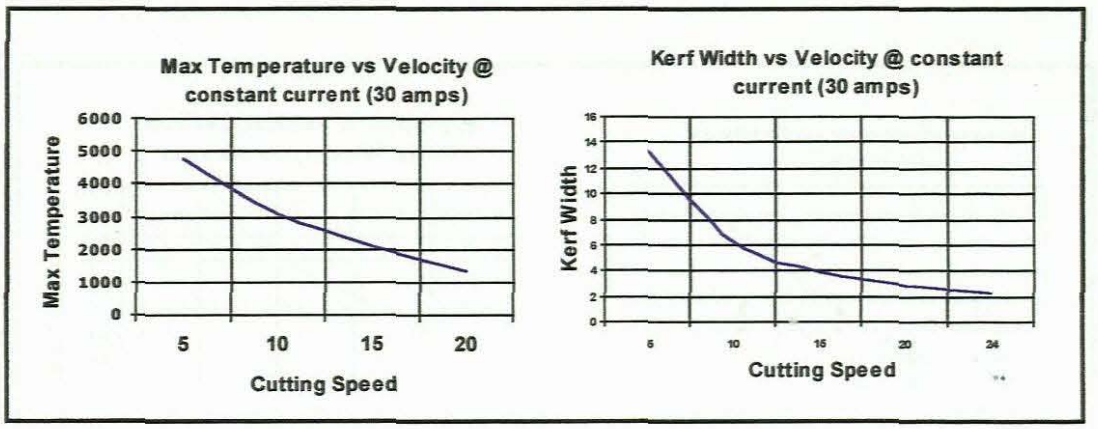

Figure B.4

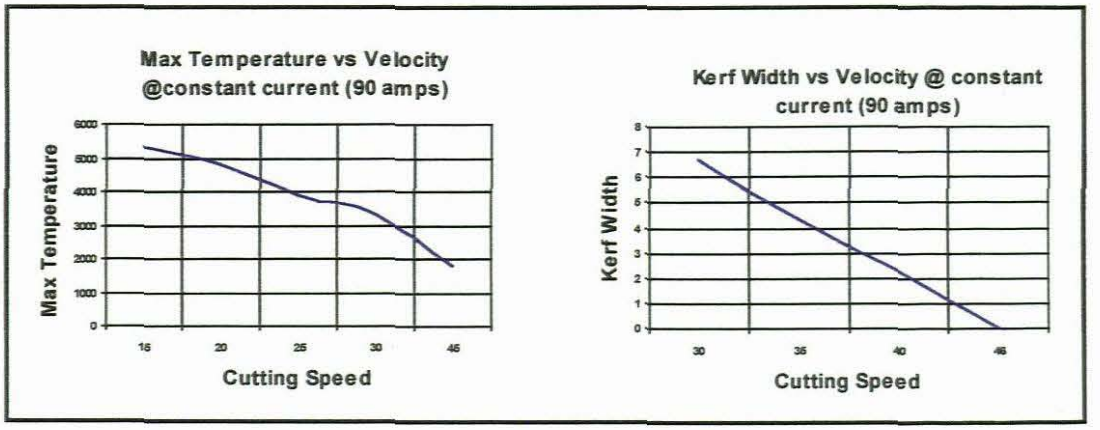

Figure B.5

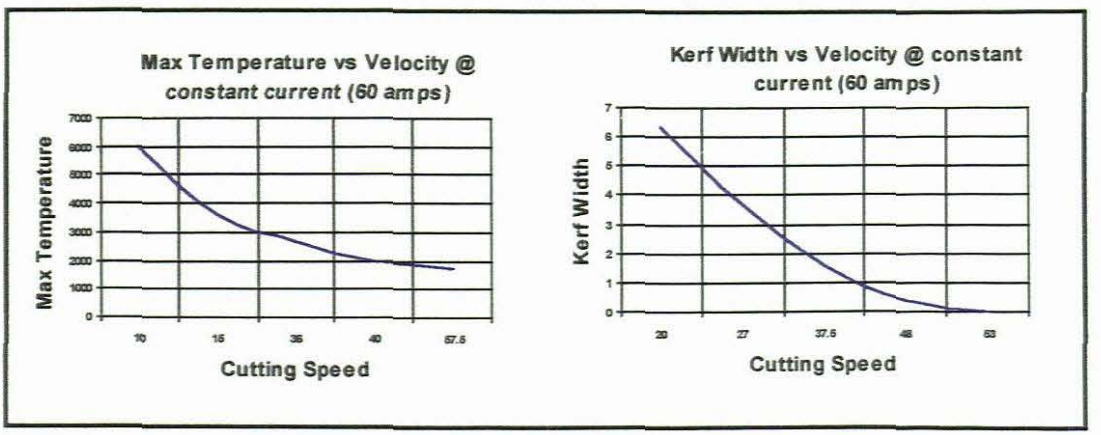

Figure B.6

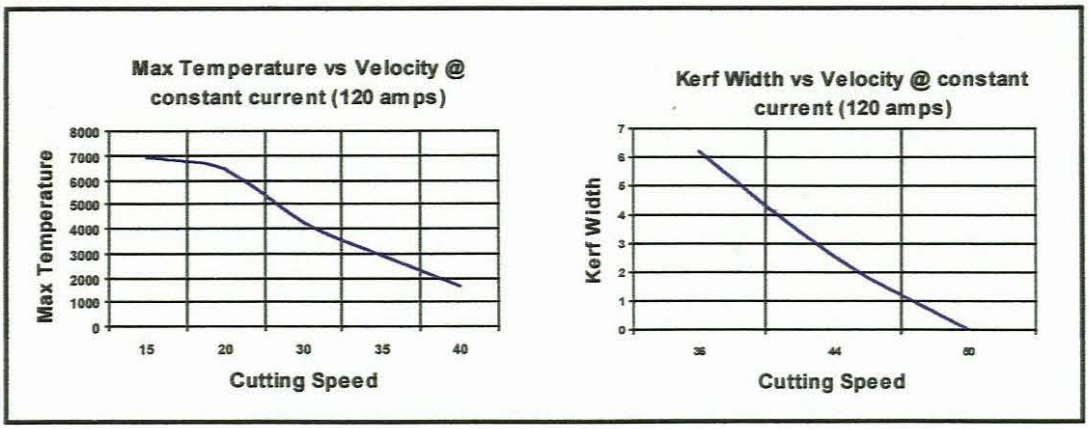
Max Temperature vs Velocity @ constant current (120 amps)
Max Temperature
8000
7000
6000
5000
4000
3000
2000
1000
0
15
20
30
35
40
Cutting Speed
Kerf Width vs Velocity @ constant current (120 amps)
Kerf Width
7
6
5
4
3
2
1
0
36
44
60
Cutting Speed

Figure B.7

Appendix C: Material Data

Chemical composition of material 1

	C	Mn	Si	S	P	Al	Mo	B
Material 1	0.18	1.39	0.37	0.011	0.022	0.052	-	-

Table C1 **Chemical composition of material**

Thermal properties for Material 1

TEMPERATURE (^{0}C)	0	50	700	900	1100	1300	1500	1800
CONDUCTIVITY (J/mm.s.^{0}C)	0.046	0.046	0.033	0.029		0.035	0.055	0.100

TEMPERATURE (^{0}C)	0	400	600	1500
SPECIFIC HEAT (J/Kg.^{0}C)	470	600	700	700

TEMPERATURE (^{0}C)	0	700	900	1500
DENSITY (Kg/mm^3)	7.8E-6	7.6E-6	7.6E-6	7.3E-6

Appendix D: Input Files for SYSTUS

```
SEARCH DATA 5
MODE BATCH
DEFINITION
 PLASMA ARC CUT2
OPTION THERMAL METALLURGICAL SPATIAL
RESTART GEOMETRY
MATERIAL PROPERTIES
 e 3601 to 9000 / KX KY KZ -1 C -2 RHO -3 MATERIAL 1
CONSTRAINTS
; CONVECTION FROM THE TOP SURFACE
 e 901 to 1800 2701 to 3600 / KT 1.*-3
LOADS
1 5mm plate
; AMBIENT TEMPERATURE
 e 901 to 1800 2701 to 3600 / TT 22
; HEAT FLUX
 e 3601 to 9000 / QR 1 VARI -4
TABLE
 1/1 0 0.046  50 0.046  700 0.033  900 0.029  1100 0.029
* 1300 0.035  1500 0.055  1800 0.100
; SPECIFIC HEAT
 2/1 0 465  400 600  600 700  1500 700
 3/1 0 7.8*-6  700 7.6*-6  900 7.6*-6  1500 7.3*-6
 4/          FORTRAN
             FUNCTION F(W)
             DIMENSION W(5)
C *** MODEL OF THE ARC ***
             X=W(1)
             Y=W(2)
             Z=W(3)
             S=W(4)
             T=W(5)

             VT=15
             I=90
             Z0=5
             V=110
             a=5
             b=4
             c=6
             P1=10.3923048454
             P2=5.56832799685
             X0=0
             Y0=VT*S
             X=X-X0
             Y=Y-Y0
             Z=Z-Z0
```

```
                R1=X*X
                R2=a*a
                R1=R1/R2
                R2=Y*Y
                R3=c*c
                R2=R2/R3
                R3=Z*Z
                R4=b*b
                R3=R3/R4
                R=R1+R2+R3
                R=3*R
                R=-(R)
                R5=P2*a
                R5=R5*b
                R5=R5*c
                P=V*I
                P=0.8*P
                P=P1*P
                P=P/R5
                F=exp(R)
                F=F*P
                CONTINUE
                RETURN
                END
RETURN
RENUMBER ITERATION 1
RETURN
SAVE DATA 2
MODE INTERACTIVE
TRANSIENT NON-LINEAR JOURNAL
BEHAVIOUR METALLURGY 2
METHOD DIRECT NONSYMMETRIC
ALGORITHM BFGS ITERATION 200
PRECISION ABSOLUTE DISPLACEMENT 0.01 FORCE 0.01
INITIAL CONDITIONS
 e/ P 1 0
 n/TT 22
TIME INITIAL 0.0
 10 STEP 0.1 / STORE 10
RETURN
SAVE DATA TRAN 1002
END
```

```
MATERIAL 1 PHASE 2
REACTION
 1 2 heating K table 1 KP table 2 F table 3 FP table 3
TABLE
 1/1 1549 0.9 1750 1
 2/1 1549 1 1750 0
 3/1 1 1 10 2 30 5 100 12
END
```